An Inverted Pressurized Water Reactor Design with Twisted-Tape Swirl Promoters

by

Nghia T. Nguyen

Submitted to the Department of Nuclear Science and Engineering
in partial fulfillment of the requirements for the degree of

Bachelor of Science in Nuclear Science and Engineering

at the

Massachusetts Institute of Technology

June 2014

Signature redacted

Author .....
Department of Nuclear Science and Engineering
May 9th, 2014

Signature redacted

Certified by .....
Neil E. Todreas
Professor of Nuclear Science and Engineering
Thesis Supervisor

Signature redacted

Accepted by .....
Richard K. Lester
Japan Steel Industry Professor and Head
Department of Nuclear Science and Engineering

An Inverted Pressurized Water Reactor Design with Twisted-Tape Swirl Promoters

by

Nghia T. Nguyen

Submitted to the Department of Nuclear Science and Engineering
on May 9th, 2014, in partial fulfillment of the
requirements for the degree of
Bachelor of Science in Nuclear Science and Engineering

Abstract

An Inverted Fuel Pressurized Water Reactor (IPWR) concept was previously investigated and developed by Paolo Ferroni at MIT with the effort to improve the power density and capacity of current PWRs by modifying the core geometry. A detailed study was performed to optimize the IPWR design considering mechanics, thermal hydraulics and neutronics design constraints from which it was concluded that the maximum achievable power for the IPWR design was 4078MW, 19 percent higher than the reference PWR (the Seabrook Power Station), limited simultaneously by the core pressure drop and steady state departure from nucleate boiling (DNB) constraints. While the thermal power is already higher than that of typical pressurized water reactors (PWRs), it is still possible to achieve higher power by improving the DNB performance of the design. Unlike the conventional pin geometry in current PWRs, the inverted geometry opens the possibility to improve the core DNB performance by using swirl flow promoters.

This thesis further takes advantage of the new core geometry to increase the core power density by using twisted tapes (TTs) as swirl flow promoters inside the IPWR cooling channels. The study focuses on optimizing the cooling channel design with twisted tapes to improve the DNB performance alongside using more powerful reactor coolant pumps to deliver higher core pressure drop limit. Four steady state design constraints, which are core pressure drop, DNB, peak fuel temperature and peak cladding temperature, are considered. As the core power rating is gradually increased from the reference value (3411 MWt), the steady state operating parameters can be calculated using Ferroni's IPWR analyzing tool and Arment's pressure drop and DNB correlations. The maximum achievable core power is determined when one of the design constraint reaches its limit value. Various options of IPWR cooling channel design, including the no TT (E-IPWR), full length TT (F-IPWR) and short length TT at a fixed location in the cooling channels (SF-IPWR), were investigated at different core inlet and outlet temperature conditions. Results show that the SF-IPWR design offers the best performance in all cases. When using Ferroni's selected assembly geometry and operating with the AP1000 enthalpy condition, the SF-IPWR

design can achieve the maximum core power of 4786 MWt, 140 percent of the reference core power, limited by the peak fuel temperature design constraint. By modifying the assembly geometry, higher power rating is achievable although more safety analyses would be needed to confirm the feasibility of operating at power rating higher than the reference plant full power value.

Thesis Supervisor: Neil E. Todreas
Title: Professor of Nuclear Science and Engineering

Acknowledgments

First and foremost, I would like to express my deepest appreciation and thanks to Professor Todreas for being not just my supervisor but also a life mentor, a dear friend who has put a tremendous amount of time and work to help me in all the time of research and writing of this thesis. Working with him in the past three years has been the greatest expericence I had at MIT. What I have learned from him is not just technical knowledge but also many life and research skills necessary for a successful graduate student and a research scientist in the future. His patience, enthusiasm, and immense knowledge have helped and motivated me to aim higher and try harder and for that I will be forever thankful.

Secondly, I wish to thank my family, especially my parents, who are always proud, encouraging and supporting. I could not be myself today without them.

I am greatful to Dr. Paolo Ferroni and Tyrel Arment for their beautiful works which gave me a project to start in the first place, for their research ideas and guidance which contributed a lot to the success of this project and for the time they spent to read and help me revise this thesis. I also want to thank Aditi Verma for her help during the time I just started working on this project. Her experience and advices made it easier for me to start a project which seemed very complicated at the time.

Finally, a special thank to my girlfriend Gemy for always being patience when I was working on this. She may not really know what I'm writing in this thesis but her mental support has been helping me to overcome every obstacle I had to face. This work is dedicated to you, my dear!

Contents

1 Introduction **23**

1.1 Motivations and objectives 23

1.2 Chapter organization 25

2 Background **27**

2.1 Conventional PWR power plant 27

2.1.1 System layout 27

2.1.2 Reactor coolant system 28

2.1.3 PWR core geometry 30

2.2 IPWR designs 31

2.2.1 IPWR core geometry 31

2.2.2 Twisted tapes 32

3 Methodology **35**

3.1 Analysis approach 35

3.2 Codes used 37

3.2.1 VIPRE-01 code for PWR evaluation 37

3.2.2 IPWR codes 38

4 Pressure drop correlations **39**

4.1 Ferroni's analysis methodology 39

4.1.1 Gravity pressure drop 40

4.1.2 Acceleration pressure drop 40

4.1.3 Friction pressure drop 41
4.1.4 Form losses 43
4.2 Arment's analysis methodology 44
4.2.1 Friction pressure drop 44
4.2.2 Form losses 45
4.3 Comparisons between Ferroni's and Arment's pressure drop correlations 47

5 DNB correlations **53**
5.1 Ferroni's calculation methodology 53
5.1.1 DNB in pure axial flow 53
5.1.2 DNB in swirl flow 54
5.2 Arment's DNB calculation methodology 57
5.2.1 DNB in pure axial flow 57
5.2.2 DNB in swirl flow 57
5.3 Comparisons between Ferroni's and Arment's DNB correlations. . . . 58

6 Reactor Coolant Pump **61**
6.1 Typical reactor coolant pumps. 61
6.2 High power RCPs 64

7 The Seabrook PWR design **67**
7.1 Thermal hydraulic design constraints 67
7.1.1 MDNBR limit 69
7.1.2 Pressure drop 69
7.1.3 Fuel temperature 70
7.2 Steady state safety analysis 71
7.3 Uprate analyses 73
7.3.1 Reference inlet temperature 73
7.3.2 Lower core inlet temperature 78

8 IPWR design choices **83**

8.1 Thermal hydraulic constraints 83

8.1.1 Core inlet temperature and coolant enthalpy rise 84

8.1.2 Pressure drop 84

8.1.3 Steady-state MDNBR 85

8.1.4 Fuel temperature and cladding temperature 85

8.2 Ferroni cooling channel designs 86

8.2.1 E-IPWR design 87

8.2.2 H-IPWR design 89

8.2.3 S-IPWR design 91

8.3 New cooling channel design choices 92

8.3.1 Normal enthalpy rise 92

8.3.2 High enthalpy rise 98

8.4 Twisted tape choices 104

8.4.1 SF-IPWR and MS-IPWR 104

8.4.2 F-IPWR 106

8.5 Summary: Design choices 108

9 IPWR design selection **111**

9.1 The reference condition 112

9.1.1 Pressure drop 114

9.1.2 MDNBR 115

9.1.3 Fuel temperature 115

9.1.4 Peak inside cladding temperature 117

9.1.5 Summary 117

9.2 The AP1000 condition 124

9.2.1 Pressure drop 124

9.2.2 MDNBR 125

9.2.3 Fuel temperature 127

9.2.4 Peak inside cladding temperature 127

9.2.5 Summary 129
9.3 Higher enthalpy rise condition 135
9.3.1 Pressure drop 135
9.3.2 MDNBR 136
9.3.3 Fuel temperature 136
9.3.4 Peak inside cladding temperature 139
9.3.5 Summary 139

10 Conclusions and future work **143**
10.1 Summary 143
10.1.1 PWR designs 143
10.1.2 IPWR designs 144
10.2 Conclusions 146
10.3 Future work 148
10.3.1 Pressure drop and DNB tests 148
10.3.2 Analyses 150

A Assessment of the difference between Ferroni's and Arment's pressure drop predictions **151**

B MATLAB Codes **157**

List of Figures

1-1 IPWR geometry vs. typical LWR geometry [1] 24

2-1 Simple system layout of a PWR power plant [2] 28
2-2 Reactor coolant system of a typical four-loop Westinghouse PWR [2] 29
2-3 Cross section of four fuel assemblies [2] 30
2-4 Comparison of Interior Unit Cells for the pin (left) and Inverted (right) Designs [3] 31
2-5 Inverted fuel assembly for the IPWR design [3] 32
2-6 Twisted-tape: key geometric parameters for two design example [3] . 33

4-1 Pressure losses across the channels predicted by the Ferroni and Arment correlations 48
4-2 Pressure loss terms predicted by the Ferroni and Arment correlations for the empty channels (note that the two gravity curves overlap) . . 49
4-3 Pressure loss terms predicted by the Ferroni and Arment correlations for the MSLTT channels (note that the two gravity curves overlap) . 49
4-4 Pressure loss terms predicted by the Ferroni and Arment correlations for the FLTT channels (note that the two gravity curves overlap) . . 50
4-5 Flow quality vs. axial location for all three cases of channel design at thermal power 4.0 GWt 50
4-6 Core pressure drop of the three Ferroni IPWR designs predicted by Ferroni's correlation vs. Arment's 52
4-7 The relative differences between the pressure drop predictions by the Ferroni and Arment correlations at various core thermal power levels 52

5-1 MDNBR predictions for the three Ferroni IPWR designs by Ferroni's correlation vs. Arment's 59

5-2 Relative differences of the two MDNBR predictions by Ferroni's and Arment's correlations at various core power levels. 59

6-1 Cutaway view of a reactor coolant pump [2] 62

6-2 Estimated performance characteristic curve of a typical Westinghouse RCP [4] 63

6-3 Characteristic curves of the RCP model at various power levels 65

6-4 Pumping power vs. flow rate for RCPs of various power levels (coolant at 295°C) 66

7-1 Core pressure drop compared to core pressure drop limits for various RCP power ratings 75

7-2 MDNBR results for the reference core by different correlations 76

7-3 Peak and average temperatures for the reference core at various power levels 77

7-4 Core pressure drop compared to core pressure drop limits for various RCP power ratings 80

7-5 MDNBR results for the reference core at new working conditions . . . 82

8-1 Power map and limiting parameter map for the E-IPWR with 1.5X RCPs 88

8-2 DNBR vs. location in a E-IPWR hot channel at 3953.1 MWt 89

8-3 Hot channel DNBR curve of the H-IPWR design 90

8-4 Hot channel DNBR curve of the S-IPWR design at 3953.1 MWt . . . 92

8-5 DNBR profile of the E-IPWR design at thermal power P=3500 MWt 93

8-6 DNBR profile of the E-IPWR design at thermal power P=4000 MWt 94

8-7 DNBR profile of the E-IPWR design at thermal power P=4500 MWt 94

8-8 DNBR profile of the E-IPWR design at thermal power P=5000 MWt 95

8-9 DNBR profile of the IPWR design at thermal power P=4500MWt with 1 TT at z=1.75m 95
8-10 DNBR profile of the IPWR design at thermal power P=5000MWt with 1 TT at z=1.5m 96
8-11 DNBR curves for the two designs: SO-IPWR and SF-IPWR 98
8-12 Pressure drop curves for the two designs: SO-IPWR and SF-IPWR . 99
8-13 DNBR curves of the E-IPWR design with different enthalpy rises for T_{inlet}=296.3°C 100
8-14 DNBR curves of the E-IPWR design with different inlet temperatures for Δh=195.2 kJ/kg 100
8-15 Core pressure drop vs. outlet temperature for the E-IPWR at 4000 MWt and T_{inlet}=280.4°C 102
8-16 MDNBR vs. outlet temperature for the E-IPWR at 4000 MWt and T_{inlet}=280.4°C 102
8-17 DNBR profile for the SF-IPWR at new outlet condition of 326.8°C, P=4500 MWt 104
8-18 Core pressure drop of the SF-IPWR at the reference temperature conditons 105
8-19 MDNBR of the SF-IPWR at the reference temperature conditons . . 105
8-20 DNBR curves for the SF-IPWR different twist ratios at 5000 Mwt . . 106
8-21 MDNBR of the SF-IPWR with the AP1000 temperature conditions . 107
8-22 MDNBR of the SF-IPWR with T_{in}=280.4°C, T_{out}=326.8°C 107
8-23 Pressure drop curves for the F-IPWR with various twist ratio values . 108
8-24 MDNBR curves for the F-IPWR design with various twist ratio values 109

9-1 Pressure drop of various designs compared to the core pressure drop limits for various RCP power ratings 115
9-2 MDNBR for the designs at different power levels 116
9-3 Peak fuel temperature at different core thermal power levels 118

9-4 Steady state peak inside cladding temperature for the designs at different corepower levels 119
9-5 Maximum core power for the E-IPWR design for each type of RCP . 120
9-6 Maximum core power for the F-IPWR design for each type of RCP . 121
9-7 Maximum core power for the SF-IPWR design for each type of RCP . 121
9-8 Maximum uprate levels (%) limiting by each constraint for the designs 123
9-9 Pressure drop of various designs compared to the core pressure drop limits for various RCP power ratings for the AP 1000 core enthalpy rise condition 126
9-10 MDNBR curves for the designs in the AP1000 condition 127
9-11 Peak fuel temperature at different core power levels in the AP1000 condition 128
9-12 Maximum inside cladding temperature for the designs in the AP1000 condition 130
9-13 Maximum E-IPWR core thermal power in the AP1000 condition . . . 130
9-14 Maximum F-IPWR core thermal power in the AP1000 condition . . . 131
9-15 Maximum SF-IPWR core thermal power in the AP1000 condition . . 132
9-16 Maximum uprate levels for the designs, limited by each design constraint in the AP1000 condition 134
9-17 Pressure drop of various designs compared to the core pressure drop limits for various RCP power ratings with enthalpy rise 261.2 kJ/kg . 137
9-18 MDNBR for the designs with enthalpy rise 261.2 kJ/kg 138
9-19 Peak fuel temperature for the designs with enthalpy rise 261.2 kJ/kg 139
9-20 Maximum inside cladding temperature for the design with enthalpy rise 261.2 kJ/kg 140

10-1 Core power map for the SF-IPWR using 3.0x RCPs at the AP1000 enthalpy conditions 147
10-2 Limiting constraint map for the SF-IPWR using 3.0x RCPs at the AP1000 enthalpy conditions 148

A-1 Equilibrium quality in a hot channel with D_{ci}=10.79mm, flow rate 0.648 kg/s and core power 4.0GW 152
A-2 Pressure drop predictions by Ferroni's and Arment's correlations for the channel with D_{ci}=10.79mm, flow rate 0.648 kg/s and core power 4.0GW (gravity loss curves overlap) 153
A-3 Equilibrium quality in a hot channel with D_{ci}=10.79mm, flow rate 0.648 kg/s and core power 1.0GW 153
A-4 Pressure drop predictions by Ferroni's and Arment's correlations for the channel with D_{ci}=10.79mm, flow rate 0.648 kg/s and core power 1.0GW (gravity loss curves overlap) 154
A-5 Equilibrium quality in a hot channel with D_{ci}=10.79mm, flow rate 0.648 kg/s and core power 6.0GW 155
A-6 Pressure drop predictions by Ferroni's and Arment's correlations for the channel with D_{ci}=10.79mm, flow rate 0.648 kg/s and core power 6.0GW (gravity loss curves overlap) 155

List of Tables

4.1 Multipliers used for friction + form loss factor calculation for channels with MSLTT 42

7.1 Comparison table for the reference core and the Seabrook Uprate [4] . 68

7.2 Pressure drop coefficients of the Reference core [5] 70

7.3 Key characteristics used in the steady state safety analysis of the Reference core [1] 72

7.4 Key results of the reference core steady-state safety analysis 72

7.5 Power levels and coolant flow rates at various uprate levels 73

7.6 Pressure drop of the reference core compared to the core pressure drop limits for various RCP power ratings 74

7.7 MDNBR results for reference PWR 75

7.8 Peak and average fuel temperatures for the reference core at various power levels 77

7.9 The reference core with different operating conditions 79

7.10 Pressure drop of the reference core compared to the core pressure drop limits for various RCP power ratings 80

7.11 MDNBR results for the reference core at new working conditions . . . 81

7.12 Maximum peak and average fuel temperatures of the reference core at new working conditions 82

8.1 Assembly geometry of the Ferroni IPWR design 87

8.2 IPWR design choices for each temperature condition 109

9.1 Maximum achievable core power (%) for the designs 112
9.2 Geometry and operating parameters of the selected SF-IPWR design 113
9.3 Core power and coolant flow rate at different uprate levels 113
9.4 Core pressure drop compared to pressure drop limits (kPa) at various RCP power ratings 114
9.5 Maximum core power levels limited by pressure drop for each design at each RCP power level 114
9.6 MDNBR for the designs at different core power levels 116
9.7 Peak fuel temperature (°C) at different core thermal power levels . . 117
9.8 Steady state peak inside cladding temperature (°C) for the designs at different core power levels 118
9.9 Maximum increased core power (uprate level) limiting by each constraint for the designs 122
9.10 Core power levels and the required flow rates to be considered in the AP1000 condition 124
9.11 Core pressure drop and pressure drop limits (kPa) at different core power levels in the AP1000 condition 125
9.12 Maximum core power (MWt) for the designs limiting by pressure drop in the AP1000 condition 125
9.13 MDNBR values for the designs in the AP1000 condition 126
9.14 Peak fuel temperature (°C) at different core power levels in the AP1000 condition 128
9.15 Maximum inside cladding temperature (°C) for the designs in the AP1000 condition 129
9.16 Maximum core power increase (%) for the designs, limited by each design constraint in the AP1000 condition 133
9.17 Required flow rate at different core power levels with enthalpy rise 262.1 kJ/kg 135
9.18 Core pressure drop and the core pressure drop limits (kPa) for the designs with enthalpy rise 261.2 kJ/kg 136

9.19 MDNBR for the designs with enthalpy rise 261.2 kJ/kg 137
9.20 Peak fuel temperature (°C) for the designs with enthalpy rise 261.2 kJ/kg 138
9.21 Maximum inside cladding temperature (°C) for the design with enthalpy rise 261.2 kJ/kg 140

10.1 IPWR design choices investigated in Chapter 8 144

Nomenclature

BOWR The Bowring DNB correlation

BW-2 The Babcock and Wilcox 2 DNB correlation

CE-1 The Combustion Engineering DNB correlation

CHF Critical Heat Flux

DNB Departure from Nucleate Boiling

E-IPWR IPWR design in which the cooling channels are empty tubes, i.e. tubes not provided with turbulence promoters

EPRI EPRI-01 DNB correlation

GROE The Groeneveld DNB correlation

H-IPWR IPWR design in which a long twisted tape (TT) is located in the top 1.6 m of each cooling channel

LOCA Loss Of Coolant Accident

MDNBR Minimum Departure from Nucleate Boiling Ratio

Nturns Number of 360o rotations of the twisted-tape

PWR Pressurized Water Reactor

RCP Reactor Coolant Pump

RCS Reactor Coolant System

S-IPWR IPWR design in which multiple short-length twisted tapes are located in the top half of each cooling channel

SF-IPWR IPWR design in which a short twisted tape is located at z=1.5m in each cooling channel

SO-IPWR IPWR design in which a short twisted tape is located at its optimal position in each cooling channel

W-3S The Westinghouse DNB correlation with S-grid factor

WEC Westinghouse Electric Corporation

Chapter 1

Introduction

This chapter, introducing the study and the structure of this thesis, consists of two sections:

- Motivations and objectives: Section 1.1
- Chapter organization: Section 1.2

1.1 Motivations and objectives

The Inverted Pressurized Water Reactor (IPWR) is a new reactor concept that has been investigated recently with the goal of increasing the power density above current PWRs. Increasing power density allows more power to be generated in the same vessel size as an existing standard PWR thus allowing the capital cost ,measured in $/KW-hr electricity, to be reduced. Such a reduction is exactly the step needed to make nuclear power more economically viable thus addressing a key problem in the deployment of greater nuclear capacity with its attendant benefit to climate change mitigation.

The IPWR concept was initially explored by Malen et al. in 2009 [6]. An IPWR design was then completed by Paolo Ferroni at MIT in his Ph.D thesis [1] in which the IPWR core was designed to operate at thermal power 4078MW, 19% higher than typical Westinghouse PWRs (the Seabrook Power Station core with thermal power

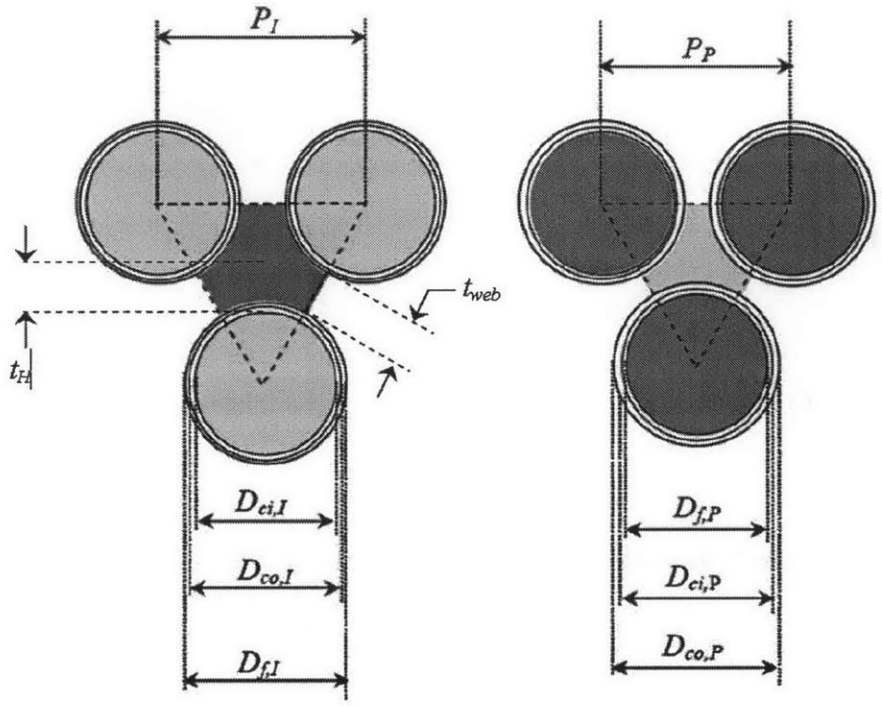

Figure 1-1: IPWR geometry vs. typical LWR geometry [1]

3411 MW was used as the reference core) with the power limited simultaneously by the pressure drop and departure from nucleate boiling (DNB) constraints. The Ferroni IPWR was designed to replace PWR cores in current PWR power plants. The power enhancement was achieved thanks to the new configuration of the fuel bundle of the IPWR design. The difference between the IPWR fuel bundle and typical LWR fuel bundles is expressed visually in Figure 1-1.

As shown in Figure 1-1, in PWR cores, the coolant flows in a continuous medium surrounding the fuel rods. This geometry gives no practical option to improve the DNB performance when the needed heat removal rate is increased which is necessary to achieve higher power rating. Hence when the thermal power is limited by the DNB constraint, the core cannot be uprated to higher power. In the IPWR core, the geometry is inverted to have the fuel as the continuous medium and the coolant flowing in different tubes (cooling channels). By inserting twisted tapes as swirl flow promoters in the cooling channels, the DNB performance of the core can be improved

and higher core thermal power can be achieved. TT insertions, however, would also increase the pressure drop across the core and make the pressure drop more limiting. Considering a trade-off between the DNB improvement and the pressure drop increase alongside other design constraints can lead to the identification of the best IPWR design.

In his IPWR concept, Ferroni did initial research on the option of using twisted tape to increase the core power of the design but the study was not conclusive due to the lack of twisted tape pressure drop and DNB correlations. After Ferroni's work another study was performed at MIT by Tyrell Arment [7] to devise a set of twisted tapes pressure drop and DNB correlations. In this project, starting from the empty cooling channel IPWR design by Ferroni (2010), the Arment correlations will be used to investigate the effect of twisted tapes insertion in cooling channels and from that finding select the best IPWR design which offers the highest achievable power. The main objectives of this study are:

- Comparing the differences between the pressure drop and DNB correlation sets selected and developed by Arment (2012) and those by Ferroni (2010).
- Evaluating the option of uprating the current PWR design by using more powerful reactor coolant pumps (RCPs).
- Further exploring the potential of the IPWR deisgn by using twist tapes as swirl flow promoters in association with higher power RCPs.

Comparing the performance of the best taped IPWR design vs. the uprated PWR design will give designers a better idea of which core design to use in the next generation of nuclear power plants.

1.2 Chapter organization

Whith those three main objectives in mind, this thesis is organized as follow:

- Chapter 1: Introduction of the study and the thesis

- Chapter 2: Background information relevant to the current PWR design and the IPWR design
- Chapter 3: The analysis and computing methodologies used in this study
- Chapter 4: The pressure drop correlations chosen by Arment (2012) and Ferroni (2010) and their differences
- Chapter 5: The DNB correlations chosen by Arment (2012) and Ferroni (2010) and their differences
- Chapter 6: Reactor coolant pump characteristics
- Chapter 7: Uprating options for current PWR design
- Chapter 8: IPWR design choices
- Chapter 9: IPWR design selection
- Chapter 10: Conclusions and future work

Chapter 2

Background

This chapter reviews basic concepts of the current PWR design (generation III) and summarizes the differences between the typical PWR core and the IPWR core design. It is presented in the following order:

- PWR power plant overview: Section 2.1
- IPWR core and twisted tape designs: Section 2.2

2.1 Conventional PWR power plant

PWR is the most common reactor type used in commercial nuclear power plants. Main design components and basic operation of typical PWR power plants are summarized in this section.

2.1.1 System layout

A simple block diagram of the system and the flow of energy in a PWR power plant are described in Figure 2-1 below:

The system consists of two loops in which the main components are:

- Reactor core (contained inside the reactor vessel): Thermal energy produced by fission chain reactions in the core is used to heat water (the primary coolant)and is carried away to the steam generator.

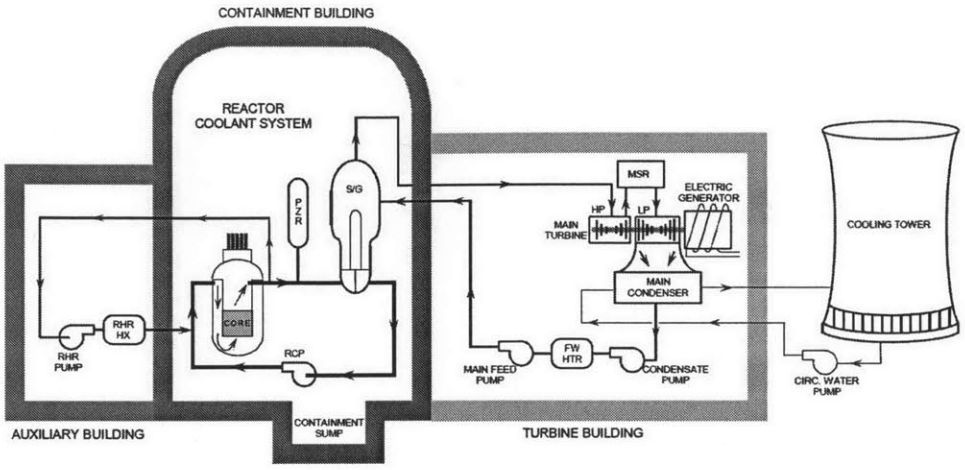

Figure 2-1: Simple system layout of a PWR power plant [2]

- Steam generator: transferring the heat from the core to the power cycle by boiling the water in the secondary loop (the secondary coolant).
- Turbines (and the whole power cycle in general): converting the heat to mechanical energy which is used to operate the electric generator.
- Electric generator: converting the mechanical energy from the steam turbines to electrical energy.

Beside these main components, many other minor components, control and support systems are used in order for the primary and secondary systems to perform their functions.

2.1.2 Reactor coolant system

The Reactor Coolant System (RCS - also known as the primary system) consists of the reactor coolant pumps (RCP), the reactor vessel (which contains the core and other control and support system), a pressurizer, the steam generators and the connecting piping. Similar to other light water reactor designs, light water is used as moderator as well as coolant in both the primary and secondary loop. RCPs produce work to

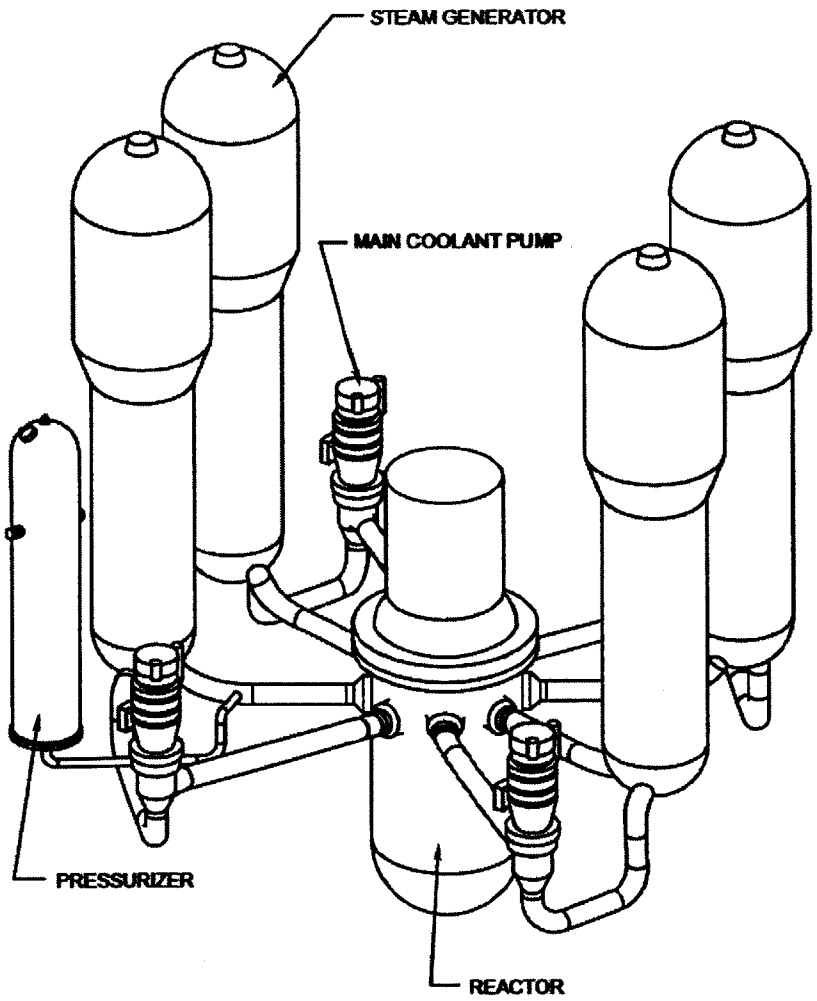

Figure 2-2: Reactor coolant system of a typical four-loop Westinghouse PWR [2]

circulate the primary coolant around the primary reactor coolant loop to transfer the heat from the core to the steam generators. Depending on the power rating , a plant can be built with two, three or four (primary) loops. Figure 2-2 shows the layout of the reactor coolant system of a typical four-loop Westinghouse PWR plant which has four reactor coolant pumps, four steam generators and a pressurizer connected to the primary system hot leg piping.

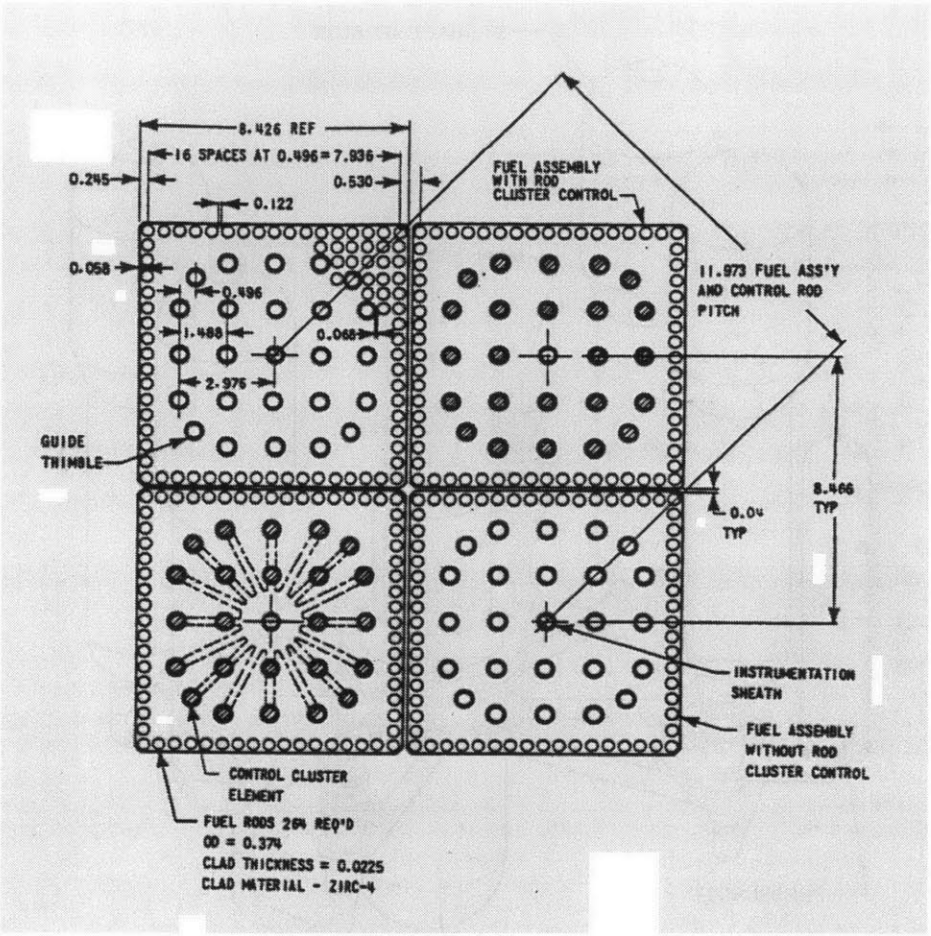

Figure 2-3: Cross section of four fuel assemblies [2]

2.1.3 PWR core geometry

Similar to other light water reactors, PWRs use uranium dioxide (UO_2) as the fuel. Slightly enriched UO_2 (~4%) is manufactured into small right cylindrical ceramic fuel pellets. The fuel pellets are then stacked in hermetically sealed zirconium alloy tubing to create fuel rods. The core consists of multiple fuel assemblies containing multiple fuel rods. The fuel rods in each assembly are supported and held apart, surrounded by the coolant, by spacer grids. Typical 4-loop Westinghouse PWR core designs have 193 fuel assemblies per core, 264 fuel rods per assembly (50952 fuel rods in total) [2]. Figure 2-3 shows the cross section of four 17x17 fuel assemblies:

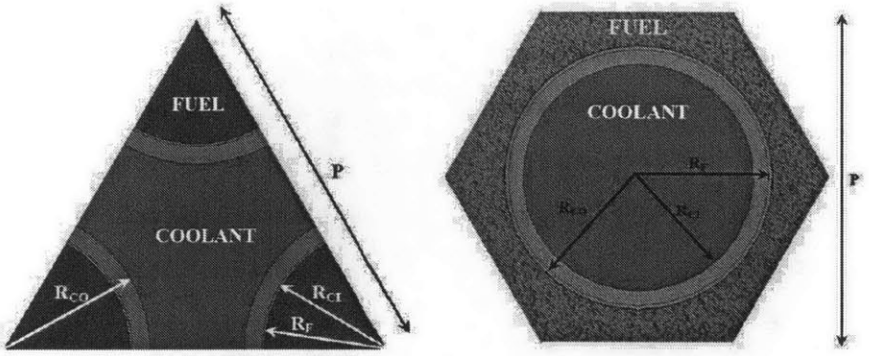

Figure 2-4: Comparison of Interior Unit Cells for the pin (left) and Inverted (right) Designs [3]

2.2 IPWR designs

The IPWR core was designed to replace PWR core in current PWR power plants. Therefore, one can expect IPWR systems to be the same as PWR systems except for the core. The core geometry of the Ferroni IPWR design is reviewed in this section. After that, key properties of twisted tapes to be used as swirl flow promoters in the IPWR design will also be summarized.

2.2.1 IPWR core geometry

Unlike typical light water reactors, the IPWR uses enriched uranium hydride (about 20% enrichment) as its fuel (U-$ZrH_{1.6}$-ThH_2 [3]). As referred to by the term "inverted", the IPWR fuel assembly has the fuel as a continuous region while the coolant (also moderator) flowing in cooling channels, in contrast with the pin design in PWRs in which the coolant is the continuous region. This difference is showed explicitly in Figure 2-4.

An IPWR core consists of many hexagonal fuel assemblies. Each assembly has multiple cylindrical cooling channels whose wall is made of Zircaloy. The channels can be empty or can be provided with twisted tapes as swirl flow promoters to enhance critical heat flux performance. The cladding walls of the cooling channels are separated from the fuel by liquid-metal (LM) eutectic bond of lead-tin-bismuth. The

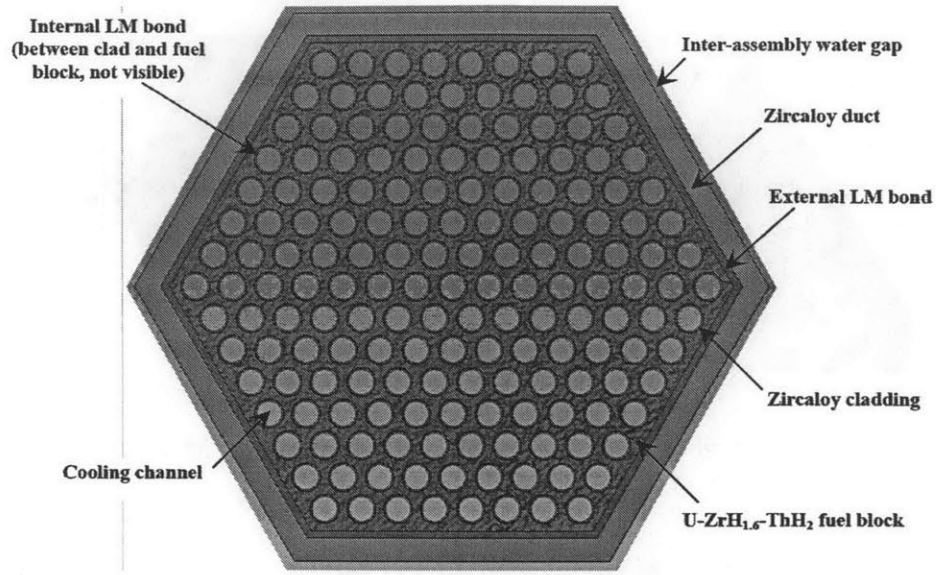

Figure 2-5: Inverted fuel assembly for the IPWR design [3]

cross section of a hexagonal fuel assembly is shown in Figure 2-5.

2.2.2 Twisted tapes

Twisted tapes can be inserted in IPWR cooling channels to be used as swirl flow (turbulence) promoters to enhance the critical heat flux performance of the flow. The two key parameters of a twisted-tape design are: the twist ratio (y) and the number of 360°-revolutions made around its axis (N_{rev}). The twist ratio is defined as the ratio between half pitch (P_{180} in Figure 2-6) and the channel diameter. To maximize the heat transfer and CHF performance, the TTs are designed to fit snuggly into the channels. The thickness also needs to be chosen carefully to ensure mechanical stability while minimizing the pressure losses caused by the TTs. Figure 2-6 shows two different twisted tape geometries.

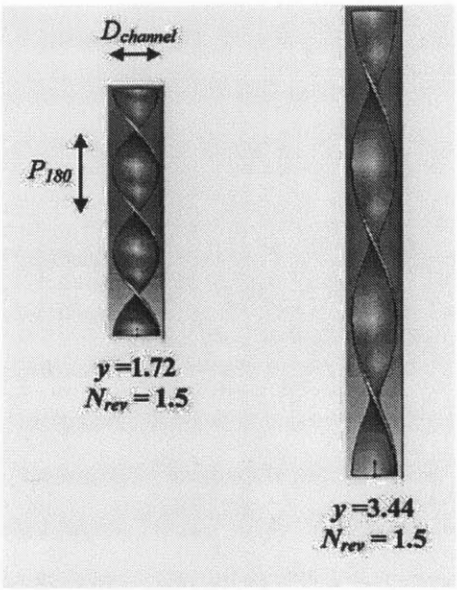

Figure 2-6: Twisted-tape: key geometric parameters for two design example [3]

Chapter 3

Methodology

This chapter presents the methodology (Section 3.1) and the computing tools (Section 3.2) used in this study to evaluate the pressure drop and DNB correlations as well as the PWR and IPWR designs.

3.1 Analysis approach

Recall from Section 1.1 that the three major objectives of this study are:

1. Comparing the differences between the pressure drop and DNB correlation sets selected and developed by Arment (2012) and Ferroni (2010).
2. Evaluating the option of uprating the current PWR design by using more powerful reactor coolant pumps (RCPs).
3. Further exploring the potential of the IPWR design by using twist tapes as swirl flow promoters in association with higher power RCPs.

The tasks for objective 1 are straightforward: the two correlation sets are used to predict the core pressure drop and the MDNBR using real operating conditions from the Ferroni IPWR design. The results will then be used to compare the two correlation sets.

For objectives 2 and 3: As stated earlier, twisted tapes could be inserted in cooling channels as swirl flow promoters to enhance the critical heat flux performance of

the core. Beside the heat transfer and critical heat flux performance enhancement, inserting twisted tapes in IPWR cooling channels would also increase the pressure loss across the core. In additional, if the core were to be operated at a higher power rating, the coolant flow rate would be higher and thus the core pressure drop would be further increased. Ultimately, the total reactor coolant pressure loss for the taped IPWR design will be significantly higher. Therefore, more powerful reactor coolant pumps (RCPs) would be required for the uprated cores. The first step of objective 2 of the study is to investigate the characteristics of typical reactor coolant pumps. As higher power RCPs are not available at the time of this study (due to technology limits or due to the lack of demand), assumption need to be made for their modeling. These powerful RCPs can be used with both PWR cores and IPWR cores.

The Seabrook PWR will be used as the reference core for comparisons with the uprated IPWR designs. The second step of objective 2 is to study the option of uprating the reference core using higher power RCPs. For each level of RCP power, the core pressure drop limit is computed. Other thermal hydraulic constraints, such as: MDNBR, fuel temperature, inside cladding temperature will also be evaluated. The core will then be modeled and the thermal hydraulic properties at steady state for each core thermal power level will be calculated using the VIPRE-01 code [8]. The maximum power is determined when one of the constraints reaches its limit value. The maximum power of the reference core for each type of RCP is thus determined. This fulfills objective #2.

The next step of the project is to investigate the IPWR and new cooling channel designs using different codes: the Ferroni code, the Arment code and other necessary codes to be written during the study. Firstly, the IPWR cooling channel designs with twisted tapes inserted by Ferroni (2010) are reviewed. After that, new cooling channel designs using twisted tapes are proposed based on the DNB performance across the channels at each power rating level. The Ferroni designs and the new designs of this thesis (Nguyen's) will then undergo the first round of design choices selections. Impractical or inefficient designs will be eliminated. The selected designs will be fully evaluated to determine the maximum achievable power rating of each

design using each RCP type. As for the design constraints, similar to the method for the reference core, the core pressure drop limit for the IPWR design will be computed for each RCP power level. The DNB limit is set to be the DNB value in the reference core at its reference condition. Other core design constraints (fuel temperature, inside cladding temperature) will also be applied. Using these constraints and the operating parameters calculated by the code, the maximum power for the IPWR design will be determined.. This is objective #3.

The results from the achievement of these three objectives can be used to select the optimal IPWR design, which is the ultimate goal of this research.

3.2 Codes used

The analyses and calculations in this study are conducted using various computer code and computing tools:

- Objective 1: The MATLAB code provided by Ferroni will be updated to evaluate the Ferroni pressure drop and DNB correlations. The MATLAB code by Arment will be used in association with the Ferroni code to evaluate the Arment correlations.

- Objective 2: All calculations and evaluations for the reference PWR will be performed using the VIPRE-01 code

- Objective 3: The updated Ferroni code, Arment code and other supplement codes will be used.

3.2.1 VIPRE-01 code for PWR evaluation

The VIPRE-01 code [8] is a computer program that can be used to perform detailed nuclear reactor core thermal-hydraulic calculations to obtain MDNBR, pressure drop and other operating parameters for steady-state conditions. It has been used widely by the nuclear industry to support plant operation and reactor design. In this study,

the VIPRE-01 code will be used to perform steady-state safety analyses for the reference PWR core at various operating conditions. . Some of the analyses of the reference PWR were performed by Ferroni (2010) [1]. Those analyses will be replicated using the VIPRE input settings as used by Ferroni (2010). The parameters in the input file can also be changed for further analyses at new operating conditions when needed. More information about the code and the input file is available in the VIPRE-01 manual [8] and the Ferroni Ph.D thesis [1].

3.2.2 IPWR codes

The calculations for IPWR designs are performed by using a MATLAB code set prepared from the codes written by Ferroni [1] and Arment [7].

The Ferroni code, used as the backbone of the computing tool, is a set of Matlab scripts that can be used to compute the power map and other operating parameters of an IPWR given the geometric parameters of the core and its operating conditions. The code was originally written by Ferroni using MATLAB R12 (2000) and can only be run in that or older MATLAB versions. The code was updated by the author of this thesis in order to reduce the run time and and enhance the convenience of future research. The updated Ferroni code is compatible with the latest MATLAB version (R2013b) that can be installed on both Windows and Macintosh computers. More details about the code can be found in the Ferroni thesis [1]. The Arment code,a set of Matlab scripts written by Arment (2012), containing his pressure drop and DNB correlations, will be used to update the pressure drop and DNB correlations in the Ferroni codes. Using both these codes, a new integrated tool to investigate IPWR cores with updated pressure drop and DNB correlations was completed, namely the IPWR code. Updates of the IPWR code from the Ferroni codes are presented in Appendix A.

Chapter 4

Pressure drop correlations

During the development of his IPWR concept, Ferroni selected a set of pressure drop and DNB correlations to predict the core steady state operating parameters. The selected correlations performed well in the case of empty cooling channel design but due to the lack of swirl flow experimental data at the time, they had several limitations when being used with twisted tape designs. To resolve these limitations, which includes: very limited choice for twisted tape location and spacing in each channel, limited applicability range and allow further evaluation and development of the IPWR concept, Arment (2012) derived a new analysis methodology with new pressure drop and DNB correlations. This chapter summarizes the pressure drop correlations selected by Ferroni (2010) and Arment (2012). These correlation sets are then used to predict the core pressure drop of typical IPWR design cases. The prediction results are used to compare and verify the two correlation sets.

4.1 Ferroni's analysis methodology

To compute the total pressure drop through a IPWR cooling channel, each channel is divided into small axial zones, each having a differential length of dz . The total pressure drop across a generic i-th zone, which consists of four terms: gravity, acceleration, friction and form losses, is calcualted by:

$$(dp)_i = (dp_g)_i + (dp_a)_i + (dp_f)_i + (dp_F)_i \tag{4.1}$$

where the subscripts g, a, f and F identify gravity, acceleration, friction and form respectively[1].

4.1.1 Gravity pressure drop

The term for gravity pressure drop in Eq. 4.1 is computed as:

$$(dp_g)_i = (\rho_c)_i \times g \times dz \tag{4.2}$$

where g is the gravitational acceleration, dz is the length and ρ_c is the bulk coolant density in zone i.

In single-phase regions, ρ_c is the density of the subcooled liquid while in the two-phase region it equals the mixture density and is calculated as:

$$(\rho_c)_i = \alpha_i \rho_g + (1 - \alpha_i)\rho_l \tag{4.3}$$

where α_i is the void fraction in zone i,ρ_l is the liquid bulk density.

4.1.2 Acceleration pressure drop

The acceleration pressure drop term due to coolant density variation is calculated as:

$$(dp_a)_i = (G^2)_i \left[\frac{1}{(\rho_c)_i} - \frac{1}{(\rho_c)_{i-1}}\right] \tag{4.4}$$

where G is the mass flux in zone i.

The acceleration pressure drops/gains due to flow area changes are calculated only at the core inlet and outlet zones:

$$(\Delta p_a)_{areachange} = (\Delta p_a)_{inlet} + (\Delta p_a)_{outlet} = \left(\frac{G^2}{2\rho_c}\right)_{i=1} - \left(\frac{G^2}{2\rho_c}\right)_{i=N} \tag{4.5}$$

4.1.3 Friction pressure drop

The fiction pressure drop across zone i is computed as:

$$(dp_f)_i = \begin{cases} (f \times V_{visc})_i \frac{dz}{D_{ci}} \frac{G^2_{empty}}{2(\rho_l)_i} & if\ z_i \leq z_{ONB} \\ (f)_i \frac{dz}{D_{ci}} \frac{G^2_{empty}}{2(\rho_c)_i} & if\ z_{ONB} < z_i < z_{OSB} \\ (f \times V_{visc})_i \frac{dz}{D_{ci}} \frac{G^2_{empty}}{2\rho_f} (\Phi^2_{lo})_i & if\ z_i \geq z_{OSB} \end{cases} \tag{4.6}$$

where:

- f_i is the isothermal liquid-only Darcy's friction factor at axial location i,
- V_{visc} is the coolant viscosity correction factor, which accounts for the coolant viscosity difference between the heated walls and the bulk, given by:

$$V_{visc} = K \left(\frac{\mu_w}{\mu_b} \right)^{n\left(\frac{D_e}{D_{ci}}\right)} \tag{4.7}$$

  with $K = 1$, μ_w and μ_b are the coolant dynamic viscosities at the wall and bulk temperature, respectively; D_e and D_{ci} are the equivalent and tube inside diameter. The exponent n is set to 0.28 for empty tube (where twisted tapes are not present) and 0.35 where TTs are present [9].

- G_{empty} is the coolant mass flux in the channel assumed to be TT-free
- z_{ONB} and z_{OSB} are the Onset of Nucleate Boiling and Onset of Saturated Boiling axial location, respectively.
- Φ^2_{lo} is the liquid-only two-phase multiplier, calculated using the EPRI-Columbia correlation [10]

Isothermal liquid-only friction factor calculation

The isothermal liquid-only friction factor is defined for each of the three geometries: TT-free, long twisted tape and multiple short length TTs (MSLTT)

Table 4.1: Multipliers used for friction + form loss factor calculation for channels with MSLTT

s	y						
	1.5	2.0	2.5	3.0	4.0	5.0	6.0
30	3.3	2.55	2.28	2.04	1.92	1.90	1.92
40	2.83	2.30	2.14	1.87	1.83	1.79	1.68
50	2.66	1.86	1.85	1.69	1.50	1.58	1.58

- For TT-free regions (no twisted tape inserted), the friction factor is given by the Churchill equation [11]:

$$f_i = \frac{8}{6.0516}\left\{ln\left[\frac{1}{3.7}\frac{\lambda}{D_{ci}} + \left(\frac{7}{Re_{empty,lo}}\right)^{0.9}\right]\right\}^{-2} \tag{4.8}$$

where: λ, depth of the cavities on the inside surface of the tubes, is set equal to $1.5 \times 10^{-6}m$, $Re_{empty,lo}$ is the liquid-only Reynolds number of the empty tube at zone i.

- For axial zones provided with a long TT the friction factor is given by the Manglik-Bergles correlation [12]:

$$f_i = \frac{0.3164}{Re^{0.25}_{empty,lo}}\left(1 + \frac{2.752}{y^{1.29}}\right)\left(\frac{\pi}{\pi - \frac{4t_{TT}}{D_{ci}}}\right)^{1.75}\left(\frac{\pi + 2 - \frac{2t_{TT}}{D_{ci}}}{\pi - \frac{4t_{TT}}{D_{ci}}}\right)^{1.25} \tag{4.9}$$

with t_{TT} is the twisted tape thickness, y is the TT twist ratio.

- For MSLTT-provided channels, the friction factor calculated by Eqn. 4.8 is used for the TT-free region upstream of the first TT (where the flow is purely axial). Downstream of the first TT, the friction factor is calculated as the empty tube firction factor multiplied by a coefficent, which was determined experimentally by Ferroni (2010) [1]. The value of this coefficient for each TT property combination is listed in Table 4.1, in which s is the spacing between successive TTs .

Two-phase multiplier

The liquid-only two-phase multiplier, is calculated using the EPRI-Columbia correlation[10]:

$$\Phi_{lo}^2 = 1 + x_{eq}\left(\frac{\rho_f}{\rho_g} - 1\right)C \tag{4.10}$$

where x_{eq} is the equilibrium quality, ρ_f and ρ_g are the saturated liquid and steam densities, C is a parameter to be computed as:

$$C = \begin{cases} 0.357\left(1 + 10\frac{p}{p_{cr}}\right)x_{eq}^{-0.175}(7.373257 \times 10^{-4}G)^{-0.45} & for\ 2.07 \leq p \leq 4.14MPa \\ 1.02 \times x_{eq}^{-0.175}(7.373257 \times 10^{-4}G)^{-0.45} & for\ p \geq 4.14MPa \end{cases} \tag{4.11}$$

where p is the operating pressure, p_{cr} is the coolant critical pressure and G is the mass flux in kg/m^2s

4.1.4 Form losses

Form pressure drop across an obstacle located at zone i is computed as:

$$\Delta p_{form} = \begin{cases} K\frac{G_{empty}^2}{2(\rho_l)_i} & if\ z_i \leq z_{OSV} \\ K\frac{G_{empty}^2}{2\rho_f}(\Phi_{lo}^2)_i & if\ z_i > z_{OSV} \end{cases} \tag{4.12}$$

where K is the form loss coefficient, $G_{empty}$is the mass flux in the empty channel. Three form losses are considered:

- abrupt flow area contraction: $K = 0.5$ [13]
- abrupt flow area expansion: $K = 1$ [13]
- form loss due to swirl formation at the entrance of long TTs is calculated using the Gambill equation [14]:

$$K = \frac{1}{8}\left(\frac{\pi}{y}\right)^2 \frac{A_{empty}}{A_{with-TT}} = \frac{1}{8}\left(\frac{\pi}{y}\right)^2 \left(\frac{0.25\pi D_{ci}^2}{0.25\pi D_{ci}^2 - t_{TT}D_{ci}}\right)^2 \tag{4.13}$$

The form loss factor caused by short length twisted tapes is included in the multipliers as listed in Table 4.1.

4.2 Arment's analysis methodology

Arment[7] used the same method as Ferroni did to calculate the pressure drop through IPWR cooling channels, i.e. each channel was divided to small axial zones with the total pressure drop across a certain zone i was calculated as the sum of four term: gravity, acceleration, friction and form losses. The gravity and acceleration pressure drops were computed using the same equations as presented in Section 4.1 while correlations for fiction pressure drop and form losses were updated.

4.2.1 Friction pressure drop

The fiction pressure drop was calculated by the same equation as used by Ferroni (2010) (Eqn. 4.6) except that the friction factor for each region was updated. For single phase axial flow (liquid-only ($z_i < z_{ONB}$) or vapor-only regions), the friction factor is calculated by:

$$f_{jo} = \begin{cases} \frac{64}{Re_j} & if\ Re_j \leq 1187 \\ \frac{0.316}{Re_j^{0.25}} & if\ Re_j > 1187 \end{cases} \tag{4.14}$$

where the subscript j is either liquid (l) or vapor (v) and Re_j is the Reynolds number.

For two-phase regions in axial flow[15]:

$$\left(\frac{dp_f}{dz}\right)_{tp} = \beta(1 - x_{eq})^{1/3} + Bx_{eq}^3 \tag{4.15}$$

where:

$$\beta = A + 2(B - A)x$$

$$A = \left(\frac{dp_f}{dz}\right)_l = f_{lo}\frac{G^2_{empty}}{2\rho_l D_e}$$

$$B = \left(\frac{dp_f}{dz}\right)_g = f_{vo}\frac{G^2_{empty}}{2\rho_g D_e}$$

From this, the two-phase (tp) friction factor can be calculated as:

$$f_{tp} = \left(\frac{dp_{fric}}{dz}\right)_{tp,p}\frac{2\rho_c D_e}{G^2_{empty}} \tag{4.16}$$

For swirl flow, the friction factor is calculated using Eqn. 4.17 [15] with the corresponding axial flow friction factor f_{empty} is calculated either by Eqn. 4.14 (if single phase) or Eqn. 4.16 (two-phase):

$$\frac{f_{sw}}{f_{empty}} = (1 + 2y^{-0.4}Fr_h^{-0.1})^{1.5} \tag{4.17}$$

where:

$$Fr_h = \frac{G^2_{empty}}{gD_e\rho_c^2}$$

4.2.2 Form losses

The form loss term is calculated by:

$$(\Delta p_F)_i = \begin{cases} K_i\frac{G^2_{empty}}{2(\rho_l)_i} & if\ z_i \le z_{OSV} \\ K_i\frac{G^2_{empty}}{2\rho_f}(\Phi^2_{lo})_i & if\ z_i > z_{OSV} \end{cases} \tag{4.18}$$

where K the form loss coefficient. $K = 0.5$ for abrupt constriction, $K = 1$ for abrupt expansion. For the case of long TTs or at the entrance of each short TT, the form loss coefficient is[14]:

$$K_{TT} = \frac{1}{8}\left(\frac{\pi}{y}\right)^2\left(\frac{0.25\pi D_{ci}^2}{0.25\pi D_{ci}^2 - t_{TT}D_{ci}}\right)$$

The two-phase multiplier for axial flow:

$$\Phi_{lo}^2 = \frac{\left(\frac{dp}{dz}\right)_{tp}}{\left(\frac{dp}{dz}\right)_{lo}} = \frac{\beta(1-x)^{1/3} + Bx^3}{A} \tag{4.19}$$

where A and B are calculated using saturated liquid and steam conditions.

At the entrance of SLTTs where swirl flow exists, a correction factor is added to account for the swirl flow:

$$\Phi_{lo}^2 = \frac{\beta(1-x)^{1/3} + Bx^3}{A} \left(\frac{1 + 2y_{eff}^{-0.4} Fr_h^{-0.1}}{1 + 2y_{eff}^{-0.4} Fr_{l,sat}^{-0.1}} \right)^{1.5} \tag{4.20}$$

with y_{eff} is the effective twist ratio, calculated by the Wu model[16]:

$$y_{eff} = \frac{\pi}{2z} \tag{4.21}$$

with:

$$ln\left(\frac{6 + 2z^2 + 2\sqrt{3}\sqrt{z^4 + 3z^2 + 3}}{2\sqrt{3} + 2\sqrt{3}z^2 - 2\sqrt{z^4 + 3z^2 + 3}} \right) = 2\sqrt{3}f\left[\bar{x} - 6exp\left(-0.25\bar{x}\right) + 6\right] + C_0$$

in which:

$$\bar{x} = \frac{L_h}{D}$$

$$f = \begin{cases} \frac{0.3164}{Re^{0.25}} & if\ smooth \\ 0.0096 + \sqrt{\frac{\varepsilon}{D}} + \sqrt{\frac{2.88}{Re}} & with\ roughness\ \varepsilon \end{cases}$$

$$C_0 = ln\left(\frac{6 + 2z_0^2 + 2\sqrt{3}\sqrt{z_0^4 + 3z_0^2 + 3}}{2\sqrt{3} + 2\sqrt{3}z_0^2 - 2\sqrt{z_0^4 + 3z_0^2 + 3}} \right)$$

where z_0 is the ratio of tangential to axial velocity at the exit of the swirl promoter, L_h is the heated length.

4.3 Comparisons between Ferroni's and Arment's pressure drop correlations

This section presents a comparison between the Ferroni's pressure drop correlation and Arment's as they are used to predict the core pressure drop of the three different Ferroni IPWR designs, namely E-IPWR, S-IPWR and F-IPWR [1]. The E-IPWR design uses empty cooling channels (no twisted tape), the S-IPWR design uses multiple short length twisted tapes per cooling channel (in this case, 3 twisted tapes with y=2.5, N_{rev}=1.5 at 1.83, 2.46 and 3.08m) while the F-IPWR uses one full length twisted tape (y=2.5) for each channel. The calculations were performed using the core geometry Ferroni selected for his E-IPWR design, listed in Table XI- 4, Ferroni thesis [1] with the two key parameters being the inside cooling channel diameter D_{ci}=10.79mm and the fuel web thickness t_{web}=2.89mm (see Figure 1-1).

Firstly, the core thermal power is fixed at 4.0GW (nearly the maximum achievable power of the Ferroni E-IPWR design [1]). The pressure losses along the channels of each design predicted by the two correlations are calculated and plotted in Figure 4-1.

The results show that the values predicted by Ferroni's correlation are always higher than those by Arment's, which can be explained given the differences between the two correlations. More specifically, Ferroni and Arment used the same formulas for the acceleration,gravity and entrance/exit form losses while the formula for the friction loss and the two-phase multiplier are different. They also use different approaches to account for the presence of twisted-tapes. Ferroni used a base friction factor correlation for the bare tube case and a modified version of that correlation for the case with full length twisted tapes. For the short length twisted tapes (MSLTT) case, he used experimental multipliers for friction factor calculations due to the lack of short TTs data and correlation, which can lead to more accurate predictions. Arment, on the other hand, used the same base friction factor correlation (Kanizawa at al. [15]) for all three cases. The special treatment Ferroni used for the MSLTT case can explain why the pressure drop prediction curves for Ferroni's and Arment's

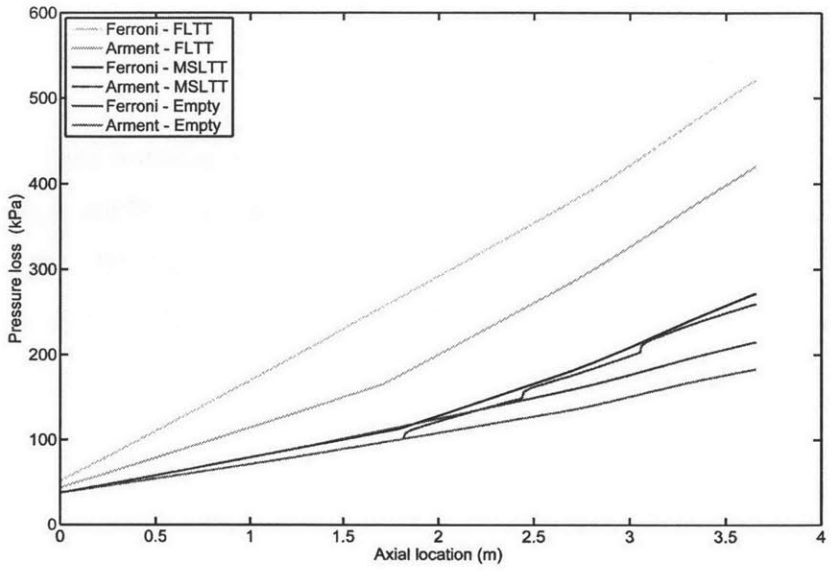

Figure 4-1: Pressure losses across the channels predicted by the Ferroni and Arment correlations

correlations are much closer for this case than for the empty tube and FLTT cases. The predicted accumulated acceleration loss, gravity loss and friction+form loss by the two correlation are plotted in Figures 4-2, 4-3 and 4-4 for the empty channel, MSLTT channel and FLTT channel, respectively. The flow quality vs. axial location plot for all three cases is shown in Figure 4-5.

Figure 4-5 shows that for all three cases, the flow in the channels can be considered mostly single phase. For the empty channels, the predictions for the gravity loss by the two correlations are identical and the difference between the acceleration loss predictions is insignificant (the two acceleration are identical in the single phase region). As the two correlations use the same formula for these two terms, these expected results confirm the consistency and the correctness of the calculation codes used for the two correlations. The entrance and exit form losses predicted by the two correlations are also the same. The significant difference between the two correlations is expressed by the friction loss term, mainly caused by the different formulas used by Ferroni (2010) (Eqn. 4.8 which includes the channel roughness) and Arment (2012) (Eqn. 4.14). More details on this can be found in Appendix A

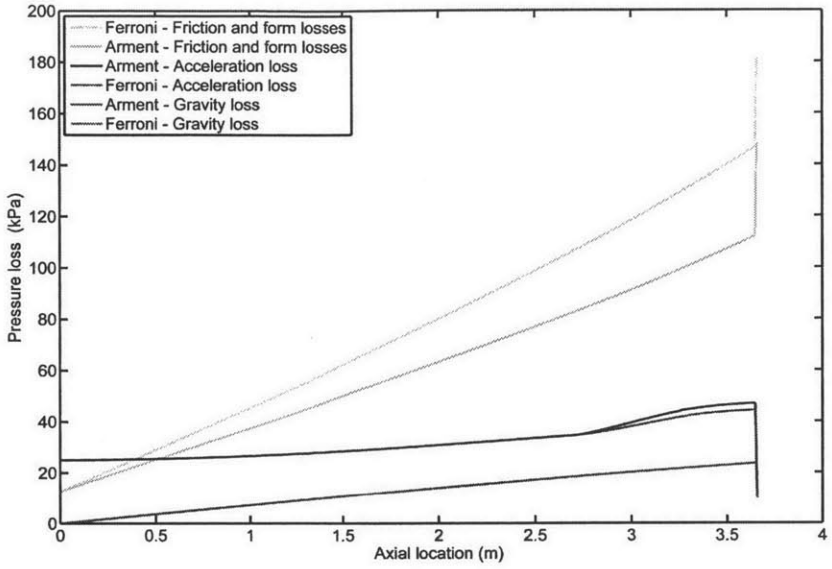

Figure 4-2: Pressure loss terms predicted by the Ferroni and Arment correlations for the empty channels (note that the two gravity curves overlap)

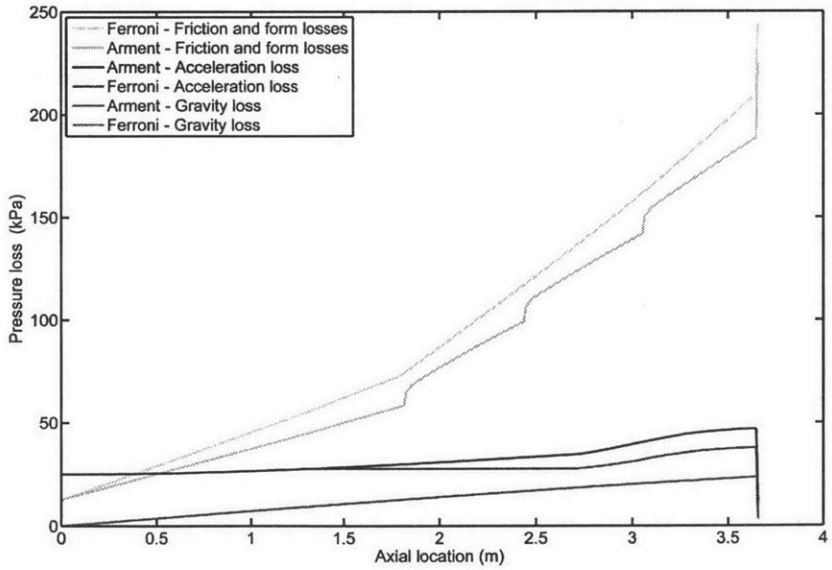

Figure 4-3: Pressure loss terms predicted by the Ferroni and Arment correlations for the MSLTT channels (note that the two gravity curves overlap)

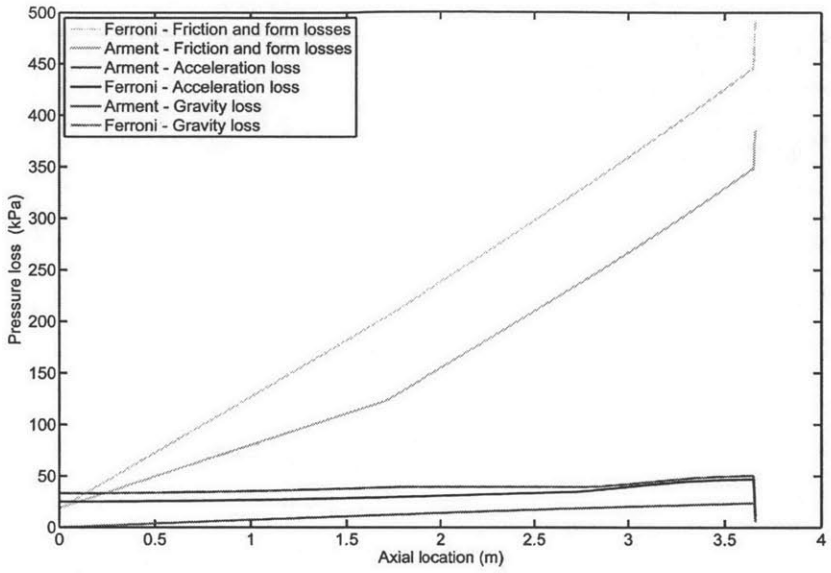

Figure 4-4: Pressure loss terms predicted by the Ferroni and Arment correlations for the FLTT channels (note that the two gravity curves overlap)

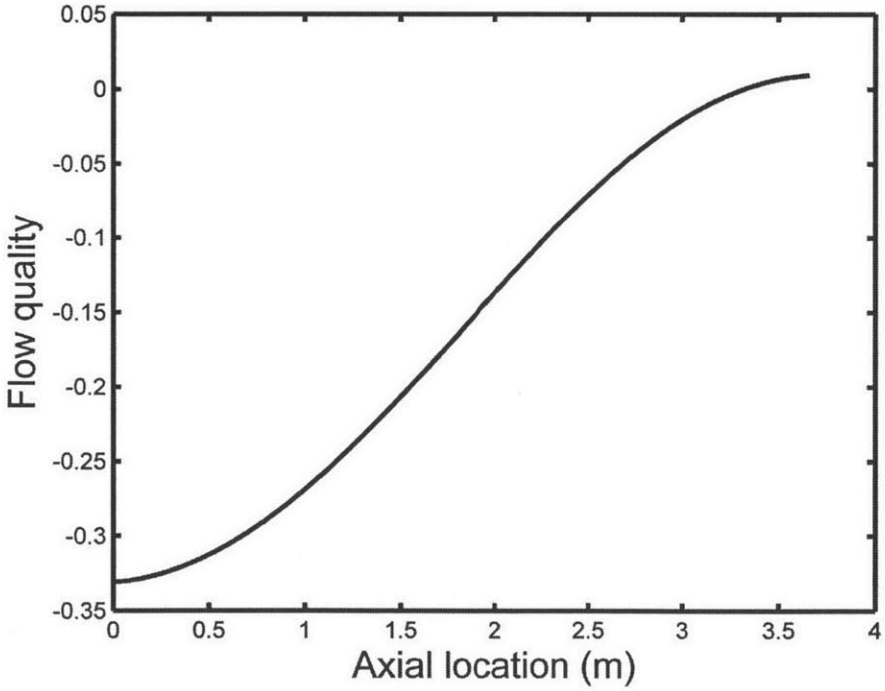

Figure 4-5: Flow quality vs. axial location for all three cases of channel design at thermal power 4.0 GWt

For the MSLTT channels, as shown in Figure 4-3, the difference between the friction losses are less significant. The distance between the two curves increases in the single phase axial flow (no TT) region and varies very little after the region with short length TTs (the distance between the two curves at 1.8m (location of the first TT) and 3.6m (the end of the region) are almost the same). The distance does vary locally in that region with short length TTs because Ferroni used experimental multipliers to globally account for the effect of those short TTs, not locally as Arment did with his correlation. The same reason leads to the difference between the acceleration loss predictions in that region.

For the FLTT channels, the difference between the two predictions by Ferroni's and Arment's correlations is also caused by the different formula used for friction factor calculations. As show in Figure 4-4, the prediction difference increases in the first half of the channel and keeps almost the same in the upper half which implies that the difference is caused by the single phase friction factor formulas.

As the core thermal power varying from 3.0 GW to 5 GW, the core pressure drop of each design at each power rating is predicted by each of the two correlations. The predictions by the two correlations are shown in Figure 4-6:

The pressure drop values predicted by Ferroni's correlation are higher than those by Arment's and the differences increase as the core power increase (or more specially as the coolant flow rate increases). The relative differences, defined as the ratio of the absolute differences and the corresponding Arment's predicted values, are shown in Figure 4-7 for various core power levels. From the figure, the difference between the two correlation is quite significant at low core power (low coolant flow rate) and becomes even more significant at higher core power levels.

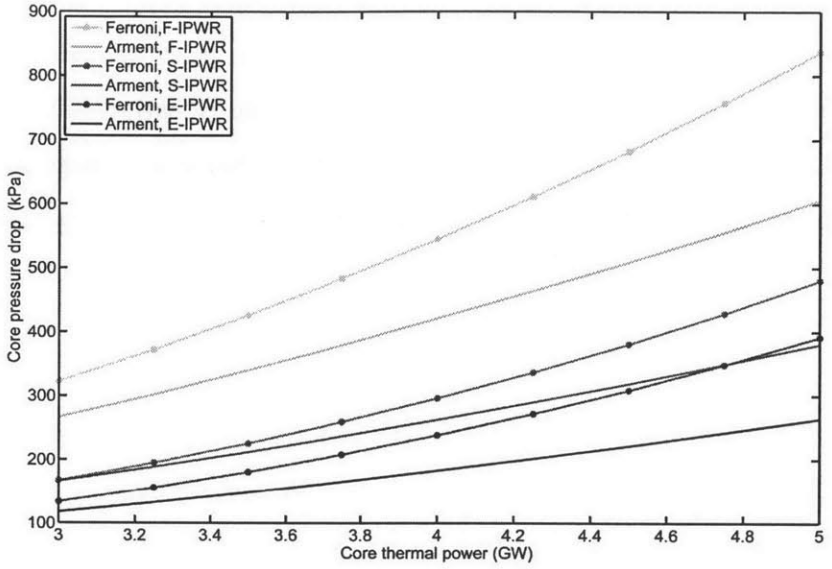

Figure 4-6: Core pressure drop of the three Ferroni IPWR designs predicted by Ferroni's correlation vs. Arment's

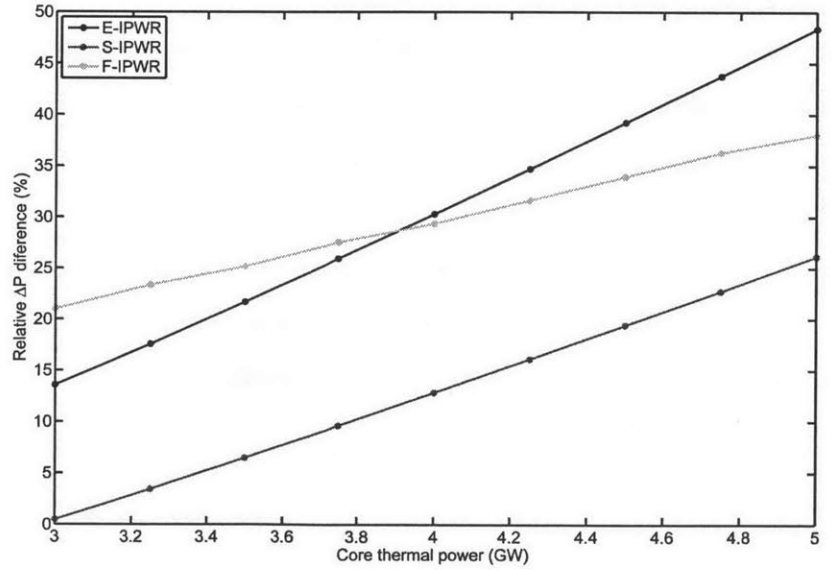

Figure 4-7: The relative differences between the pressure drop predictions by the Ferroni and Arment correlations at various core thermal power levels

Chapter 5

DNB correlations

As a complement to Chapter 4, this chapter summarizes and compares the DNB correlations selected by Ferroni (2010) and developed by Arment (2012).

5.1 Ferroni's calculation methodology

5.1.1 DNB in pure axial flow

Ferroni used the 2006 Groeneveld look-up tables [17] to calculated critical heat flux (CHF) in pure axial flow. The Groeneveld look-up tables contain CHF values ($(q"_{CHF})_{LUT}$) of a pure axial flow in a 8 mm diameter tube given the pressure, the mass flux and the equilibrium quality of the flow. The CHF of a pure axial flow in a general tube is given by:

$$q"_{CHF} = (q"_{CHF})_{LUT} K_D K_F \tag{5.1}$$

where $(q"_{CHF})_{LUT}$ is the CHF from the look-up tables. K_D, the diameter correction factor, is given by [17]:

$$K_D = \left(\frac{8}{D_{eq}}\right)^{0.5} \tag{5.2}$$

where D_{eq} is the equivalent diameter of the tube in mm. K_F is the heat flux

distribution correction factor, given by [17]:

$$K_F = \begin{cases} \frac{q"}{q"_{BLA}} & if\ x_{eq} > 0 \\ 1 & otherwise \end{cases} \tag{5.3}$$

where $q"_{BLA}$ is the average heat flux from the Onset of Saturated Boiling to the location of interest, $q"$ is the heat flux at the location of interest and x_{eq} is the steam equilibrium quality at the location of interest

5.1.2 DNB in swirl flow

Given the same pressure, mass flux and equilibrium quality, the CHF in a swirl flow is typically higher than that in a pure axial flow. That enhancement is expressed by the ratio, TTCHFR, between the swirl flow CHF and the pure axial flow CHF:

$$TTCHFR = \frac{q"_{CHF,TT}}{q"_{CHF,empty}} \tag{5.4}$$

where $q"_{CHF,TT}$ is the CHF of the flow in a tube with presence of twisted tapes (swirl flow) and $q"_{CHF,empty}$ is the CHF of the flow in the tube without twisted tapes (pure axial flow).

CHF calculation method in presence of long TTs

Ferroni used the Jensen correlation [18] to calculate CHF in swirl flow generated by long twisted tapes. The modified Jensen correlation is expressed by:

$$TTCHFR = \frac{q"_{CHF,FLTT}}{q"_{CHF,empty}} = \begin{cases} A & if\ A > 1\ and\ y \leq y_{crit} \\ 1 & if\ A < 1\ and\ y \leq y_{crit} \end{cases} \tag{5.5}$$

whereas for $y > y_{crit}$ the correlation is not applicable. In the above equation:$q"_{CHF,FLTT}$ is the CHF at the taped axial location of interest; $q"_{CHF,empty}$is the CHF at the same location of an empty tube (no TT), calculated by the Katto correlation [19]; and:

$$A = \left(4.597 + 0.09254y + 0.004154y^2\right)\left(\frac{\rho_g}{\rho_f}\right)^{0.7012} + 0.09012ln\left(\frac{a}{g}\right) \tag{5.6}$$

$$y_{crit} = \begin{cases} 23.023p^{-0.4114} & if\ 0.1 \leq p \leq 3\ MPa \\ -5.6794ln(p) + 20.134 & if\ 3 < p \leq 21\ MPa \end{cases} \tag{5.7}$$

with y is the twist ratio of the TTs, ρ_g and ρ_f are the saturated steam and liquid densities, g is the gravitational acceleration and:

$$\frac{a}{g} = \frac{2}{gD_{ci}}\left(\frac{V_{ax,TT}\pi}{2y}\right)^2 \tag{5.8}$$

where D_{ci} is the tube inside diameter, $V_{ax,TT}$ is the axial velocity in presence of the tape:

$$V_{ax,TT} = \frac{G_{TT}}{\alpha\rho_g + (1-\alpha)\rho_f} \tag{5.9}$$

G_{TT} is mass flux in presence of the tape and α is the homogeneous void fraction:

$$\alpha = \frac{1}{1 + \frac{\rho_g}{\rho_f}\frac{1-x}{x}} \tag{5.10}$$

CHF calculation method in decaying swirl flow (short length TTs)

For swirl flow in presence of multiple short length twisted-tapes (SLTTs), the CHF correlation is given by:

$$TTCHFR = \frac{q"_{CHF,SLTT}}{q"_{CHF,empty}} = 1 + \left(\frac{q"_{CHF,FLTT}}{q"_{CHF,empty}} - 1\right)S_f \tag{5.11}$$

in which the ratio $\frac{q"_{CHF,FLTT}}{q"_{CHF,empty}}$ is calculated using the modified Jenson correlation, i.e. Eqn. 5.5. The swirl fraction S_f, proportional to an angular velocity fraction, is computed as suggested by Kreith and Sonju (1965) [20]:

$$S_f(z_T) = \sqrt{\frac{\int_0^{R_{ci}} [W(r, z_T)]^2 r dr}{\int_0^{R_{ci}} [W(r, 0)]^2 r dr}} \tag{5.12}$$

where R_{ci} is the tube inner radius, z_T is the distance of the axial location of interest from the TT exit while W, a dimensionless velocity defined as the ratio between the tangential velocity and the axial velocity (the latter being the same for axial and swirl flow), is is calculated using results from Algifri and Bhardwaj (1985) [21] as:

$$\begin{aligned}
W(r, z_T) \quad = \quad & \frac{7.73}{4y} J_1\left(7.664 \frac{r}{D_{ci}}\right) exp\left[-\frac{29.368(1+\varepsilon_d)}{N_R} \frac{z_T}{D_{ci}}\right] + \\
- \quad & \frac{5.26}{4y} J_1\left(14.032 \frac{r}{D_{ci}}\right) exp\left[-\frac{98.448\,(1+\varepsilon_d)}{N_R} \frac{z_T}{D_{ci}}\right] + \\
+ \quad & \frac{4.04}{4y} J_1\left(20.346 \frac{r}{D_{ci}}\right) exp\left[-\frac{206.98\,(1+\varepsilon_d)}{N_R} \frac{z_T}{D_{ci}}\right] + \\
- \quad & \frac{3.38}{4y} J_1\left(26.648 \frac{r}{D_{ci}}\right) exp\left[-\frac{355.06\,(1+\varepsilon_d)}{N_R} \frac{z_T}{D_{ci}}\right] + \\
+ \quad & \frac{3.00}{4y} J_1\left(32.928 \frac{r}{D_{ci}}\right) exp\left[-\frac{542.12\,(1+\varepsilon_d)}{N_R} \frac{z_T}{D_{ci}}\right] + \\
- \quad & \frac{3.06}{4y} J_1\left(39.232 \frac{r}{D_{ci}}\right) exp\left[-\frac{769.58\,(1+\varepsilon_d)}{N_R} \frac{z_T}{D_{ci}}\right] +
\end{aligned}$$

$$+ \quad \frac{3.33}{4y} J_1\left(45.520\frac{r}{D_{ci}}\right) exp\left[-\frac{1036.04\,(1+\varepsilon_d)}{N_R}\frac{z_T}{D_{ci}}\right] +$$

$$- \quad \frac{5.43}{4y} J_1\left(50.612\frac{r}{D_{ci}}\right) exp\left[-\frac{1280.8\,(1+\varepsilon_d)}{N_R}\frac{z_T}{D_{ci}}\right] \quad (5.13)$$

where:

y= twist ratio of the SLTT generating the swirl;

J_1: Bessel function of order 1;

D_{ci}= tube inner diameter;

$N_R = Re_{empty}/2$;

ε_d=dimensionless eddy diffusivity $=4.15 \times 10^{-3} N_R^{0.86}$

5.2 Arment's DNB calculation methodology

5.2.1 DNB in pure axial flow

Similar to Ferroni's method, Arment also chose the 2006 Groeneveld look-up table as the base correlation to calculate the pure axial flow CHF. The correlation was presented previously in Section 5.1.1.

5.2.2 DNB in swirl flow

The DNB correlation developed by Arment is given by:

$$TTCHFR = \frac{q"_{CHF,sw}}{q"_{CHF,empty}} = \left(1 + 0.7\theta exp\left[-0.09\left(\frac{\rho_f}{\rho_g}\right)\right]\right)^{0.14}$$

where:

$$\theta = \frac{\pi^2 V_{ax}^2}{2y_{eff}^2 D_{ci} g}$$

g=gravitational acceleration, 9.81 $[m/s^2]$

D_{ci}=tube inner diameter $[m]$

V_{ax}= axial velocity of the coolant $[m/s]$=$\frac{G}{\rho_m}$

$\rho_m = \left(\frac{x}{\rho_g} + \frac{1-x}{\rho_l}\right)^{-1}$

y_{eff} = effective twist ratio, calculated by the Wu model[16] as presented by Eqn. 4.21

5.3 Comparisons between Ferroni's and Arment's DNB correlations.

Similar to the comparisions of pressure drop correlations performed in Section 4.3, the comparisions between Ferroni's DNB correlation and Arment's are presented in this section. The geometric parameters of the IPWR designs are the same as presented in Section 4.3. As the core thermal power varying from 3.0 GW to 5.0 GW, the predicted MDNBR of each IPWR design by each correlation is shown in Figure 5-1:

For the E-IPWR design, the flow in each cooling channel is purely axial, both Ferroni's and Arment's correlations use the same base correlation (Groeneveld look up tables [17]). The prediction results by these two correlations shown in Figure 5-1 are identical, as expected. For the F-IPWR and S-IPWR, the flow is swirl, the MDNBR values predicted by Arment's correlation are slightly higher.

The relative differences between the two predictions, defined as the absolute differences divided by the Ferroni predictions, are shown in Figure 5-2. For the E-IPWR design, the two predictions are identical as illustrated by the 0% relative differneces. For the S-IPWR design, the difference is kept small at around 3% while for the F_IPWR design, the difference increases from 1% at 3.0 GW power to 11% at 5.0 GW power. Overall, the difference between the two correlations is minor and can be considered insignificant at low core power or for design with empty channels and channels with short length twisted tapes.

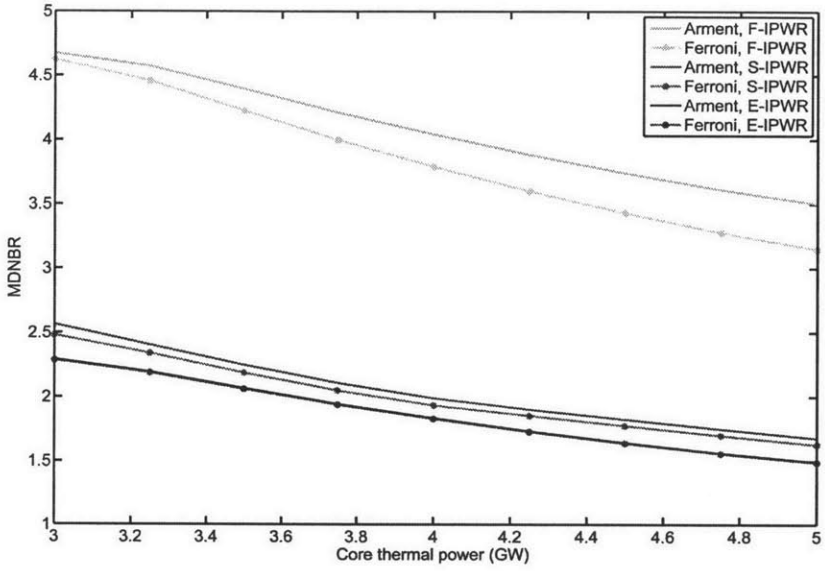

Figure 5-1: MDNBR predictions for the three Ferroni IPWR designs by Ferroni's correlation vs. Arment's

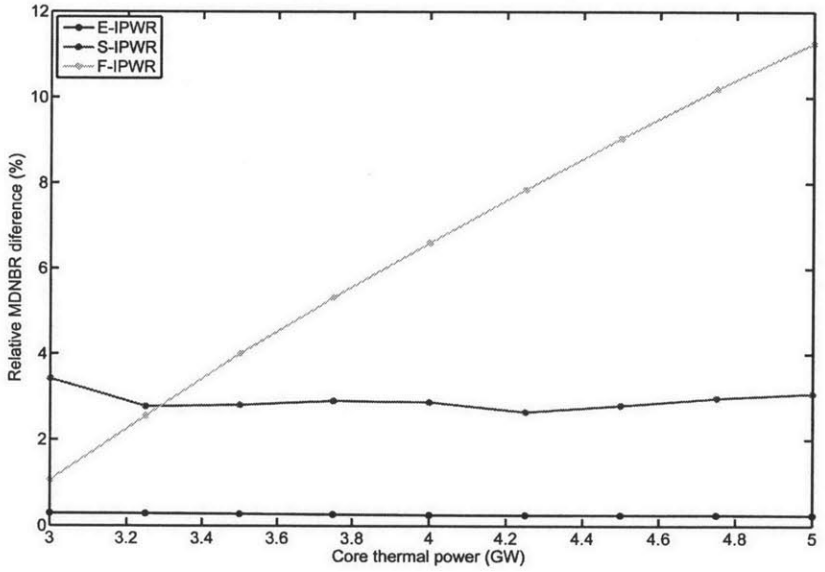

Figure 5-2: Relative differences of the two MDNBR predictions by Ferroni's and Arment's correlations at various core power levels.

Chapter 6

Reactor Coolant Pump

This chapter presents characteristics of typical reactor coolant pumps (RCPs). Also, as required by the uprated reactors (higher power rating PWR and IPWR cores), assumptions are made to regarding the characteristics of more powerful reactor coolant pumps.

6.1 Typical reactor coolant pumps.

Reactor coolant pumps are used to circulate the primary coolant in the reactor coolant systems to transfer the heat produced by the reactor core to the steam generator. The Seabrook PWR and other typical Westinghouse designed PWRs use single speed centrifugal pumps as main reactor coolant pumps . A cutaway view of these typical RCPs is shown in Figure 6-1.

The major components of a reactor coolant pump are the electric motor, the hydraulic section and the seal package. The reactor coolant enters the suction side of the RCP from the outlet of the steam generator. Across the pump, the coolant is accelerated to increase its velocity and energy. The velocity increase is then converted to pressure increase in the discharge volute[2]. This pressure increase (total head) must be enough to compensate for the pressure loss around the reactor coolant system. The total head vs. coolant flow rate relation of a typical Westinghouse pump is illustrated in Figure 6-2. The characteristic curve for the typical RCP is expressed in

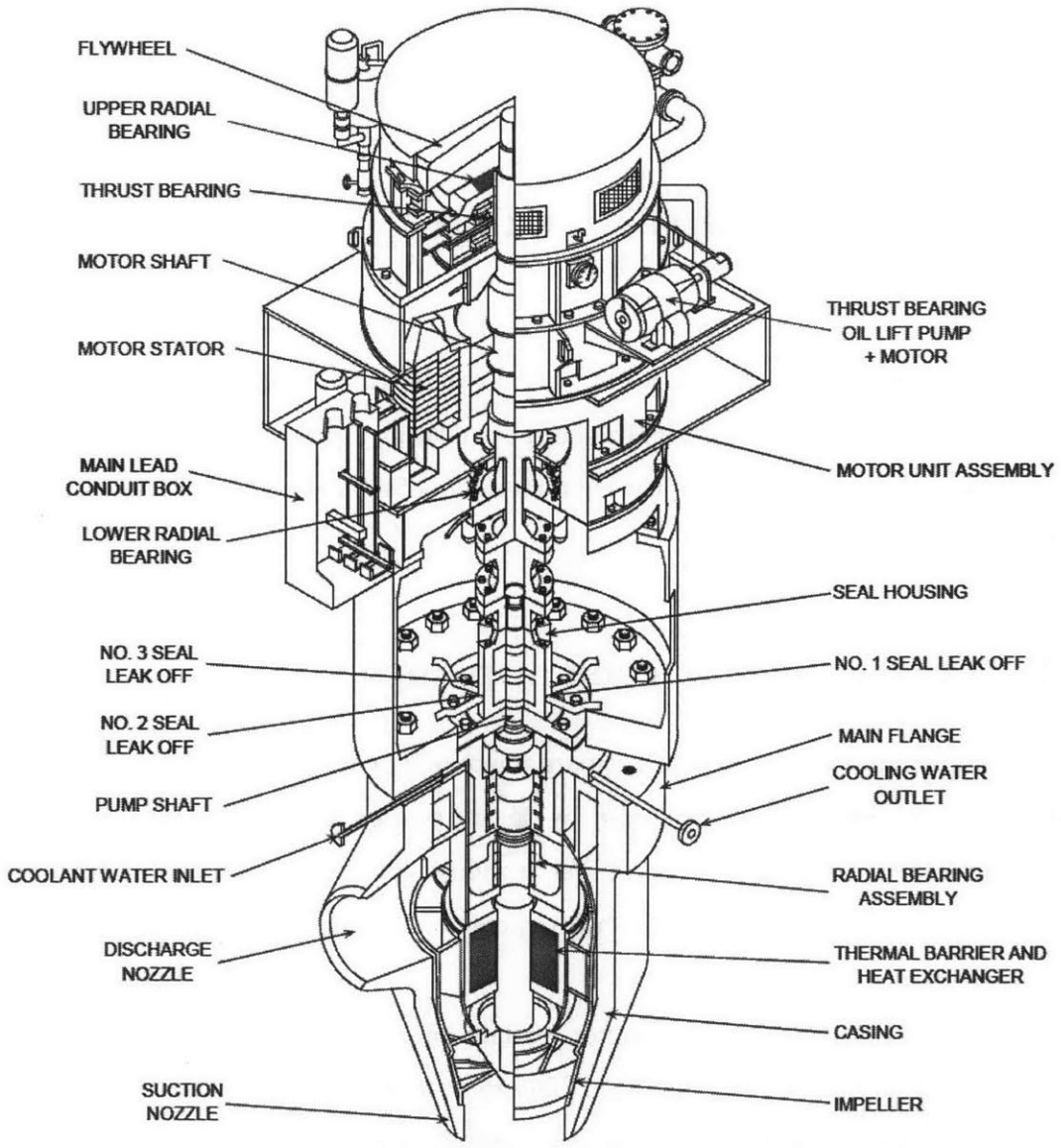

Figure 6-1: Cutaway view of a reactor coolant pump [2]

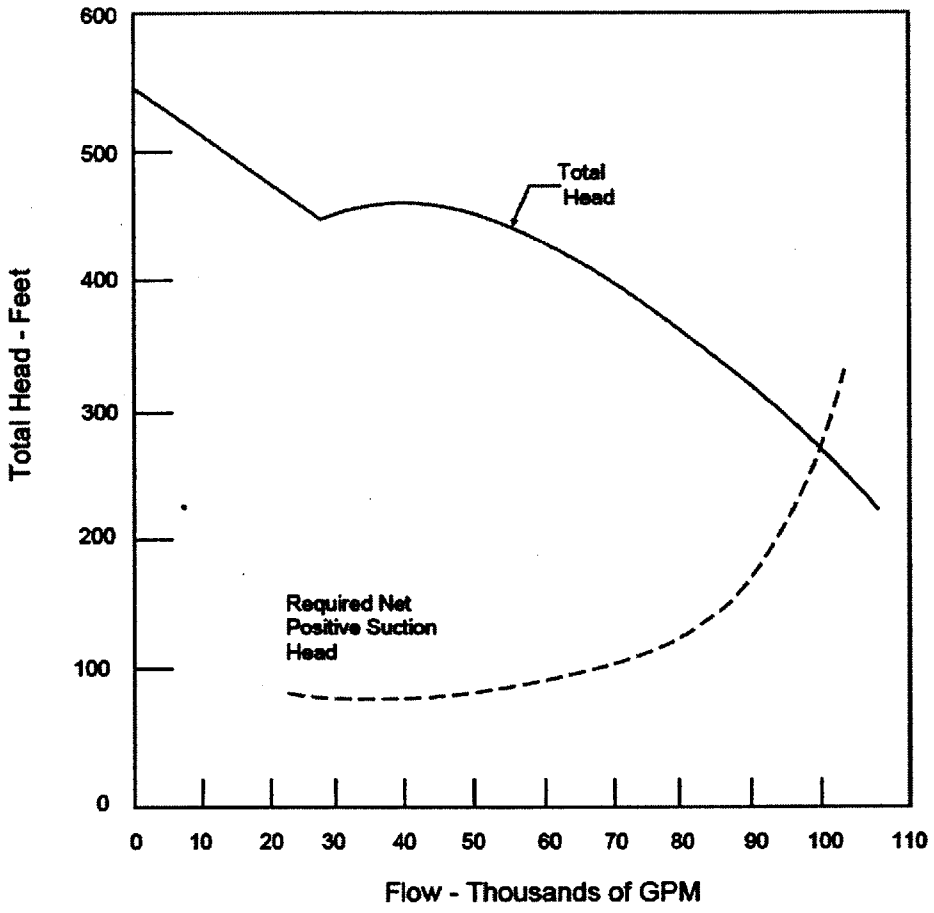

Figure 6-2: Estimated performance characteristic curve of a typical Westinghouse RCP [4]

Eqn. 6.1 [5]

$$\Delta h(Q) = 0.8174.Q^3 - 18.676.Q^2 + 113.46.Q - 92.004 \tag{6.1}$$

in which Δh is the total head in m and Q is the volumetric coolant flow rate in m^3/s. The valid range for Q is 5-8.5 m^3/s.

The pump power can be expressed as:

$$\dot{W}_p = \frac{\dot{m}\Delta P}{\rho} = Q\Delta P = Q\rho g\Delta h(Q) \tag{6.2}$$

where ΔP is the pressure rise due to the pump, ρ is the coolant density and g is the gravitational acceleration.

6.2 High power RCPs

Typical flow in current PWRs is about 100,000 gpm (or 6.3 m^3/s) per loop which is nearly the maximum flow rate deliverable by a typical pump in the primary circuit of a Westinghouse 4-loop PWR, and the total head provided by the pumps decreases rapidly in this flow rate range. As analyzed in Section 3.1, the use of twisted tapes in IPWR coolant channels and the higher coolant flow rate required by uprated reactors will both increase the pressure loss in the reactor coolant systems. More powerful RCPs than the typical power rating are required to operate the reactors in these condition. The development of higher power pumps is, however, still underway. In the near future one can expect higher power pumps compared to these typical RCPs which were designed and built a long time ago when the reactors were constructed (in the period 1976-1986 for the Seabrook PWR).

In this study, five pump power levels are considered: 1.0x (typical RCP), 1.5x power, 2.0x power, 2.5x power and 3.0x power. The pump power is proportional to the product of total head and flow rate. These more powerful pumps are defined as:

- 1.5x power: can deliver 1.5x flow rate at the same total head
- 2.0x power: 1.333x total head at 1.5x flow rate
- 2.5x power: 1.667x total head at 1.5x flow rate
- 3.0x power: 2.0 total head at 1.5x flow rate

Starting from the characteristic equation (Eqn. 6.1) and the power equation (Eqn. 6.2) of the typical pump with the assumption that the higher power pumps are to use similar technology (with higher flow capacity and higher power motors), the characteristic curves of more powerful pumps are calculated and plotted in Figure 6-3

.

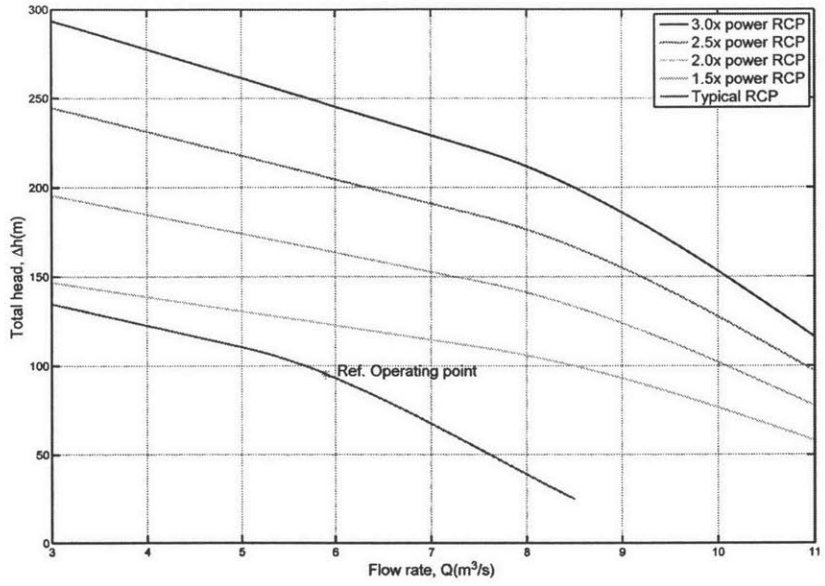

Figure 6-3: Characteristic curves of the RCP model at various power levels

Note that since Eqn. 6.1 is valid for flow rate in range of 5-8.5 m^3/s, the curves in Figure 6-3 were constructed using linear interpolation to cover a flow rate range to 3 m^3/s. With the pumping power defined in Eqn. 6.2 as the product of total pressure rise and volumetric flow rate, the pumping power curves were calculated and showed in Figure 6-4 (the water coolant was at 295°C).

From Figure 6-4, it can be observed that each pump has a specific flow rate range in which it can operate at nearly maximum power, and this range would shift to higher flow rates as the pump power increases. Optimally, the RCP should be operated in its maximum power region to achieve the highest efficiency. In this study, the reactor power is expected to be uprated to around 50%, therefore a 1.5x flow rate was applied for the higher power RCPs at all power levels (from 1.5x to 3.0x). When the coolant flow rates required by the reactors at the same power rating are the same, the higher power RCPs are used for core designs that have higher core pressure drop.

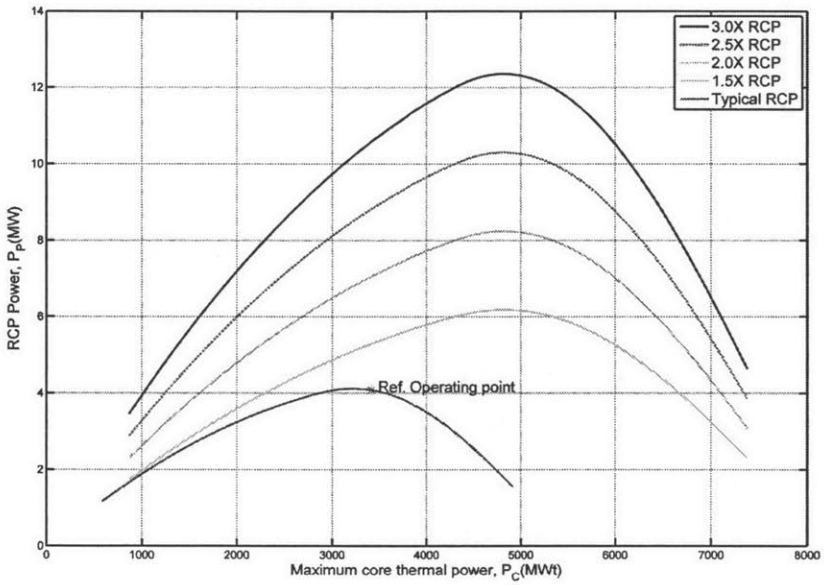

Figure 6-4: Pumping power vs. flow rate for RCPs of various power levels (coolant at 295°C)

Chapter 7

The Seabrook PWR design

The Seabrook Nuclear Power Plant, a nuclear power plant located in Seabrook, New Hampshire, United States, is used as the reference PWR plant in this study in order to make the comparisons of design options more meaningful. The plant was constructed during the period 1976 - 1986 using the design that was considered the "standard" Westinghouse 4-loop PWR plant (as described in Section 2.1). Although the reactor has undergone minor uprates to increase the thermal power from 3411MWt to 3659MWt [4], its original operating conditions at 3411MWt will still be used in this study as reference conditions. The reference operating conditions of the core are listed in Table 7.1 [4]. Operating conditions of the uprated Seabrook are also included for later use.

7.1 Thermal hydraulic design constraints

Many material and thermal hydraulic constraints are applied in the design of nuclear reactors to meet safety requirements and to ensure the design operates properly. In this study, however, only three of the most limiting thermal hydraulic constraints on core thermal power of PWRs are considered, namely: MDNBR, pressure drop and fuel temperature.

Table 7.1: Comparison table for the reference core and the Seabrook Uprate [4]

Thermal hydraulic design parameters	Reference Core	Seabrook Uprate
Reactor core heat ouput (MWt)	3411	3659
System pressure (MPa)	15.51	15.51
COOLANT FLOW		
Total thermal flow rate (kg/s)	18358	17896
Effective flow rate for heat transfer (kg/s)	17476	16758
Effective flow area for heat transfer (m^2)	4.77	4.75
COOLANT TEMPERATURE		
Nominal inlet (^oC)	293.1	291.9
Average rise in vessel (^oC)	32.2	35.1
Average rise in core (^oC)	33.7	37.3
Average in core (^oC)	310.8	311.7
Average in vessel (^oC)	309.2	309.5
HEAT TRANSFER		
Active heat transfer surface area (m^2)	5546.3	5546.3
Average heat flux (kW/m^2)	598.7	642.0
Peak heat flux for normal operation (kW/m^2)	1496.9	1605.1
Average linear power (kW/m)	17.86	19.16
Peak linear power for normal operation (kW/m)	44.62	47.90
PRESSURE DROP		
Across core (kPa)	196.5±19.65	197.2
Across vessel, including nozzle (kPa)	335.8±50	335.8

7.1.1 MDNBR limit

Departure from nucleate boiling (DNB) is a flow boiling crisis that occurs when the heat flux of a system exceeds its critical heat flux (CHF) , the heat flux being high enough to build up a vapor blanket that prevents the fluid from reaching the heated surface, which decreases the heat transfer coefficient significantly and can cause localized overheating of the heating surface. Therefore during DNB, the fuel cladding temperature can increase substantially above the bulk fluid temperature which can damage the fuel. To prevent possible DNB system failures, a limit value is imposed for the MDNBR of the design, which is the minimum ratio of the critical heat flux to the maximum localized heat flux in the core.

The steady state DNB is considered in this study. The MDNBR results are calculated using the Groeneveld correlation [17] with the flow properties provided by the VIPRE-01 code [8]. The MDNBR limit will be set to be the MDNBR value of the reference core at its steady state operation to ensure that all new designs will demonstrate the same steady-state DNB margin as the reference core.

7.1.2 Pressure drop

The coolant is circulated in the primary loop by the reactor coolant pumps (RCPs). The total pressure drop in each loop is balanced by the head provided by the RCP. The total RCS (Reactor Coolant System) pressure drop in a primary loop can be estimated using Eqn. 7.1 [5]:

$$\Delta P_{RCS} = \sum \Delta P_i = \Delta P_{CL} + \Delta P_{HL} + \Delta P_{CO} + \Delta P_{RV} + \Delta P_{SG} \qquad (7.1)$$

where:

ΔP_{CL}: Cold leg pressure drop, nozzles, down-comer, etc.

ΔP_{HL}: Hot leg pressure drop

ΔP_{CO}: Core pressure drop

ΔP_{RV}: Reactor vessel pressure drop

ΔP_{SG}: Steam generator pressure drop

The pressure drop in each component is estimated as:

$$\Delta P_i = \frac{1}{2} k_i \frac{\dot{m}_i^2}{\rho_i} \tag{7.2}$$

with k_i a pressure drop coefficient, ρ_i is the coolant density and $\dot{m}_i$ is the mass flow rate in the component.

For the reference core at its operating conditions, the pressure drop coefficients were estimated and listed in Table 7.2[5]

Table 7.2: Pressure drop coefficients of the Reference core [5]

Component	Friction factor	Value(m^{-4})
Steam Generator	k_{SG}	0.939498
Cold Leg	k_{CL}	0.330773
Reactor Vessel	k_{RV}	0.548069
Hot Leg	k_{HL}	0.059101

Finally, the core pressure drop limit can be estimated approximately as:

$$\Delta P_{CO} = \Delta P_{pump} - \sum_{i \neq core} \Delta P_i = \rho_{cold} g \Delta h - \frac{1}{2} \dot{m}_{RCS}^2 \sum_{i \neq core} \frac{k_i}{\rho_i} \tag{7.3}$$

As the reactor coolant flow rate changes, the friction factor may be changing as well. However, Eqn. 7.3 can still be used as an estimation for the core pressure drop limit.

7.1.3 Fuel temperature

Conventional PWRs use UO_2 fuel which has the melting point at 2800^oC. Therefore, the fuel will be damaged if at any point in the core, the fuel temperature exceeds this value. The limit for maximum fuel temperature is set at 2800^oC. Further, during the reactor operation, UO_2 fuel can release fission gas. The amount of fission gas, which increases with the fuel temperature, can over-pressurize the fuel pin leading to

its failure. The limit for average fuel temperature is set at 1400^oC to keep the fission gas release fraction below 5%.

7.2 Steady state safety analysis

A steady state analysis for the Seabrook PWR using the VIPRE-01 code [8] was performed by Ferroni in his Ph. D. thesis [1]. The core was modeled at the plant's operating conditions (the reference conditions) except for the core power and core inlet temperature which were conservatively increased in accordance with the common practice in safety analyses. Specifically, the thermal power was increased 2% from 3411.0 MWt to 3479.2 MWt and the inlet temperature was increased by 3.2°C from 193.1°C to 196.3°C. In this study, the model provided by Ferroni in form of a VIPRE input file was used perform a reverse engineering analysis to calculate key thermal hydraulic properties (MDNBR, pressure drop and fuel temperatures) of the reference core. Geometry and key characteristics of the core used in the analysis are summarized in Table 7.3 .

The VIPRE-01 code has five options for DNB correlations: Babcock & Wilcox, W3-S, Combustion Engineering, Bowring and EPRI-1. However, in this study, the Groeneveld correlation (the Groeneveld look-up tables with correction factors[17]), which was also used in IPWR analyses, was used as the main DNB correlation to make the results comparable with DNB results in the IPWR core. Six parameters are required for the Groeneveld correlation: three main inputs (equilibrium quality, mass flux and system pressure) for the look-up tables and other three inputs (channel equivalent diameter, flow quality and axial power distribution) for the correction factors. In his study, Ferroni calculated a core average channel equivalent diameter and used that value in DNB calculations for every channel. In this study, however, the exact equivalent diamter for the hot channel , which was given in the VIPRE output file, was used. Therefore the result was expected to be slightly different compared to Ferroni's although the same correlation was used. Finally, key results of the analysis is listed in Table 7.4

Table 7.3: Key characteristics used in the steady state safety analysis of the Reference core [1]

OPERATING CONDITIONS	
Core inlet temperature (^{o}C)	296.3
Average core outlet temperature (^{o}C)	329.1
Core thermal power (MW)	3479.2
Hot assembly radial peaking factor	1.515
Axial peaking factor	1.515
Axial power profile	Chopped cosine
Hot pin radial peaking factor	1.089
Effective coolant flow rate through the core (kg/s)	17476
Percentage of coolant flowing through guide thimbles	2
Coolant enthalpy rise across the core (kJ/kg)	195.2
GEOMETRY	
Number of assemblies	193
Assembly lattice	17x17
Number of fuel rods per assembly	264
Number of guide thimbles per assembly	24
Number of instrumentation tubes per assembly	1
Total assembly height (m)	4.063
Active assembly height (m)	3.658
Assembly pitch (mm)	215.04
Fuel rod pitch (mm)	12.6
Cladding outside diameter (mm)	9.5
Cladding inside diameter (mm)	8.3566
Fuel pellet diameter (mm)	8.1915
Guide thimble inner/outer diameter (mm)	11.430/12.243
Instrumentation tube inner/outer diameter (mm)	11.379/12.294
Number of grids per assembly (including Intermediate Flow Mixers, IFM)	8
Number of IFMs per assembly	3

Table 7.4: Key results of the reference core steady-state safety analysis

Parameter	Unit	Value
MDNBR	-	1.85
Core pressure drop	kPa	144.8
Maximum fuel temperature	^{o}C	2069.6
Maximum average fuel temperature	^{o}C	1321.5

Table 7.5: Power levels and coolant flow rates at various uprate levels

Uprate*	Thermal Power (MW)	Flow rate (kg/s)
102%	3479.2	17476
105%	3581.6	18350
110%	3752.1	19224
115%	3922.7	20097
120%	4093.2	20971
125%	4263.8	21845
130%	4434.3	22718
135%	4604.9	23593
140%	4775.4	24466
145%	4946.0	25340
150%	5116.5	26214

*: The power values in this column are the real power rating + plus 2% increase for safety analysis.

7.3 Uprate analyses

This section presents possible uprate analyses for the reference core with the use of higher power reactor coolant pumps with 5 pump power levels: 1.0x (typical WEC RCP), 1.5x, 2.0x, 2.5x and 3.0x. Two cases will be considered: In the first case, the inlet temperature is kept the same as the reference value while in the second case, the temperature is lowered to 280^oC as used in new PWR design (AP1000 by Westinghouse). The analyses were performed by using the VIPRE code starting from the model as used in the steady state analysis.

7.3.1 Reference inlet temperature

To keep the inlet and outlet coolant temperature constant, as the power increased, the coolant flow rate was increased by the same percentage. Uprates up to 50% thermal power were considered. The power level and the effective coolant flow rate at each power are summarized in Table 7.5

Steady state analysis for each uprate level was performed by the VIPRE code. The results are presented below.

Table 7.6: Pressure drop of the reference core compared to the core pressure drop limits for various RCP power ratings

Uprate level	Pressure drop (kPa)	Core pressure drop limits				
		1.0x RCP	1.5x RCP	2.0x RCP	2.5x RCP	3.0x RCP
102%	144.8	223.0	447.8	710.9	1032.9	1325.0
105%	155.8	166.6	411.7	671.8	989.9	1278.5
110%	168.2	67.5	350.0	604.9	916.7	1199.5
115%	180.6	-	286.3	535.9	841.3	1118.4
120%	194.4	-	220.5	464.9	764.0	1035.3
125%	207.5	-	152.6	391.8	684.5	950.1
130%	222.0	-	-	314.7	600.5	859.8
135%	237.2	-	-	231.1	508.7	760.6
140%	252.3	-	-	141.4	409.7	653.1
145%	268.2	-	-	-	303.8	537.8
150%	284.1	-	-	-	191.6	415.4

Pressure drop

Results of the pressure drop analysis are presented in Table 7.6 . The values in the second column are the pressure drop of the core at each flow rate level while columns 3-7 contain the pressure drop limits imposed by the RCPs (as described by Eqn. 7.3).

In term of pressure drop limit, it is shown in Figure 7-1 that without replacing RCPs, the reference core can be uprated to 105% power. With 1.5x power RCPs, the uprate power is bounded at 120%.

DNB

The Groeneveld correlation was used as the main DNB correlation although it was not included in the VIPRE code. Table 7.7 contains the MDNBR results calculated by the Groneveld correlation (using flow properties provided in the VIPRE output file) and other correlations which were included in the code.

The Groeneveld MDNBR at the reference conditions was used as the MDNBR limit. The results in Table 7.7 and in Figure 7-2 show that the MDNBR values strictly decreased as the power increased. The thermal power of the reference core is limited by MDNBR and cannot be uprated beyond the 100% level.

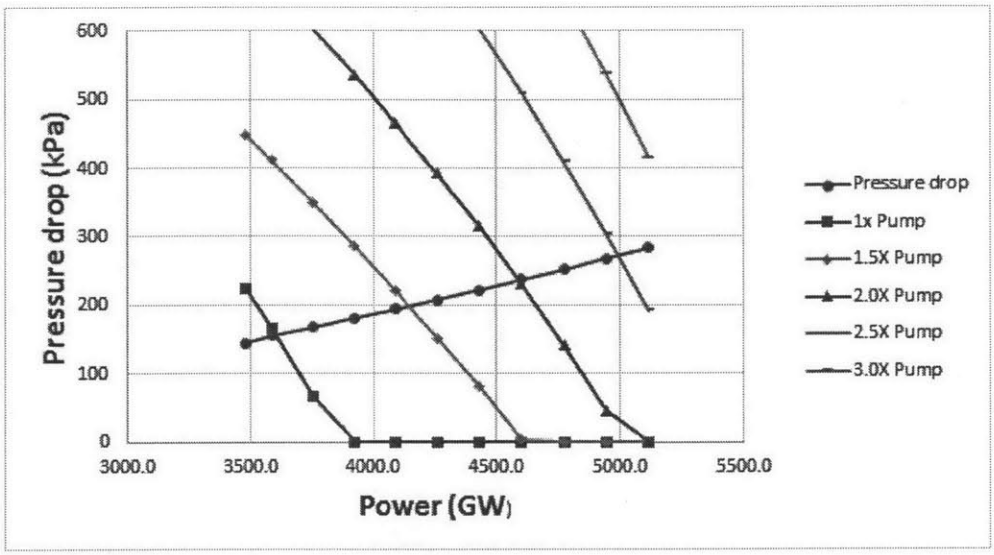

Figure 7-1: Core pressure drop compared to core pressure drop limits for various RCP power ratings

Table 7.7: MDNBR results for reference PWR

Uprate	GROE	EPRI	W-3S	BW-2	BOWR	CE-1
102%	1.85	1.40	2.06	2.45	1.59	1.83
105%	1.82	1.41	2.07	2.43	1.60	1.85
110%	1.73	1.39	2.01	2.34	1.57	1.82
115%	1.65	1.37	1.96	2.26	1.54	1.79
120%	1.58	1.35	1.91	2.19	1.51	1.76
125%	1.51	1.34	1.87	2.12	1.49	1.74
130%	1.45	1.32	1.82	2.06	1.46	1.72
135%	1.40	1.31	1.78	2.00	1.44	1.70
140%	1.34	1.30	1.75	1.94	1.42	1.69
145%	1.30	1.28	1.71	1.89	1.39	1.68
150%	1.25	1.27	1.68	1.84	1.37	1.67

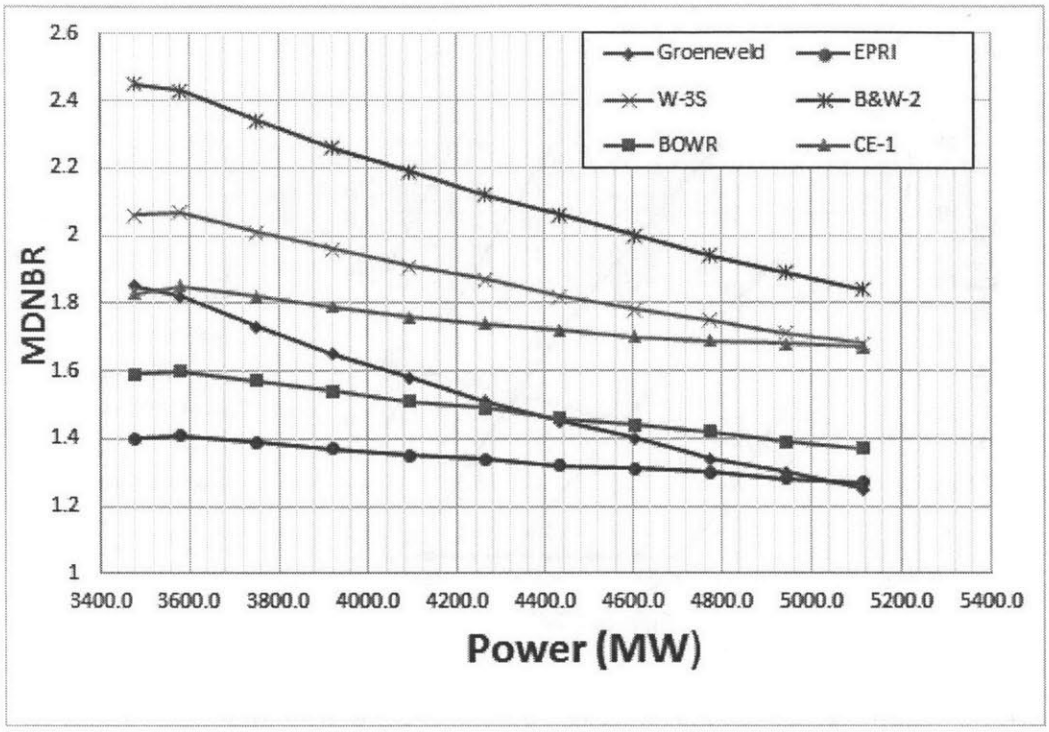

Figure 7-2: MDNBR results for the reference core by different correlations

Fuel temperature

The maximum peak and average fuel temperature were calculated by the VIPRE code and are illustrated in Table 7.8 and Figure 7-3

With the peak and average temperature limits set at $1400°C$ and $2800°C$, respectively, it can be observed that the power is firstly limited by the average temperature constraint at 109% and would be limited by the peak temperature constraint at over 150%.

Overall, considering all three design constraints, the power of the reference core is limited at its reference conditions by the MDNBR and cannot be uprated. Replacing RCPs would not help in this case. To increase the core power, a method to improve the MDNBR performance in the core is required.

Table 7.8: Peak and average fuel temperatures for the reference core at various power levels

Uprate	$T_{avg}(^oC)$	$T_{peak}(^oC)$
102%	1322	2070
105%	1356	2124
110	1415	2214
115	1473	2302
120	1528	2380
125	1581	2452
130	1634	2522
135	1686	2589
140	1737	2653
145	1789	2714
150	1838	2773

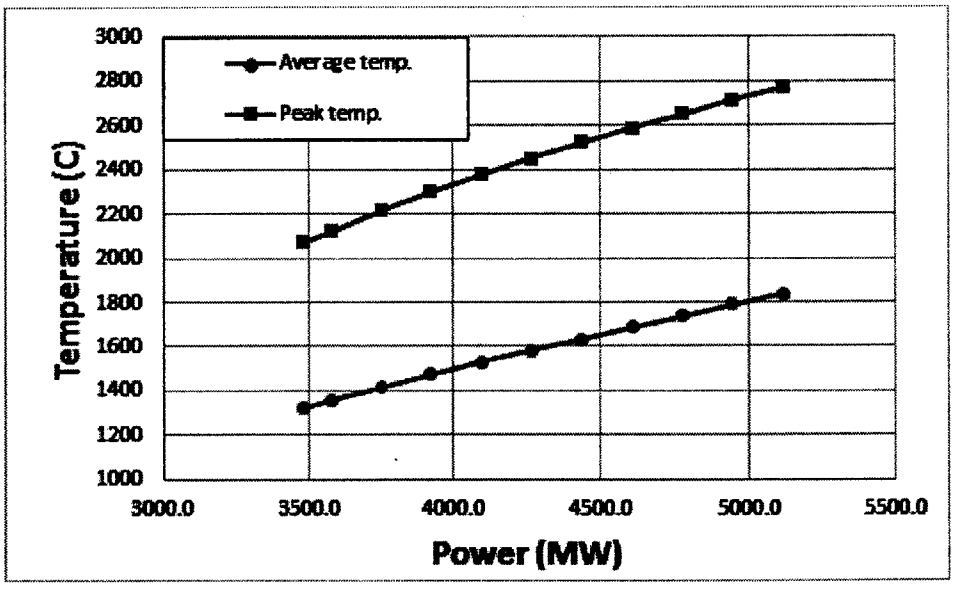

Figure 7-3: Peak and average temperatures for the reference core at various power levels

7.3.2 Lower core inlet temperature

This section presents the results of the analyses for the reference core with lower coolant inlet temperature. A lower inlet temperature offers several advantages to improve the reactor performance:

- If the outlet temperature were kept the same or decreased by a smaller amount: The enthalpy rise across the core would be higher, thus the required coolant flow rate would be lower. Less pumping power is needed (lower pressure drop across the core).

- If the outlet temperature were decreased by a significant amount: The average bulk temperature is lower compared to the reference condition, therefore the fuel temperatures are lowered and the MDNBR profile may be improved. Also, a lower core output temperature would cause less corrosion/fouling issues in the steam generators.

Beside these advantages, lower inlet temperature also brings up some problems:

- If the outlet temperature were kept the same: at the same core thermal power, the coolant flow rate would be lower, therefore the MDNBR is expected to be lower. Since the thermal power of the reference core at its reference operating conditions was limited by MDNBR, this is not a possible option. A lower inlet temperature requires lower outlet temperature.

- Lowering the outlet temperature in the primary loop may limit the maximum temperature of the working fluid in the secondary loop which would decrease the thermal efficiency of the thermal power cycle.

Therefore, to improve the performance of PWRs by lowering the inlet temperature, a trade-off between these advantages and disadvantages needs to be considered. Here, the inlet and outlet temperature of the new Westinghouse AP1000 PWR [22] are used as the new inlet and outlet temperature of the reference core. Table 7.9 shows the comparison of these two working conditions:

Table 7.9: The reference core with different operating conditions

Parameter	Reference conditions	New inlet and outlet T
Core thermal power (MWt)	3411	3411
System pressure (MPa)	15.51	15.51
COOLANT TEMPERATURE		
Nominal inlet (^oC)	293.1	280.4
Core outlet temperature (^oC)	326.8	321.3
Average rise in core (^oC)	33.7	40.9
COOLANT FLOW		
Enthalpy rise (kJ/kg)	195.4	226.2
Total thermal flow rate (kg/s)	18358	15852
Effective flow rate for heat transfer (kg/s)	17476	15091

The system was considered the same (the reactor was assumed to operate at these new conditions without any change to the reactor coolant system components), the new flow rates were calculated as product the old flow rates and the ratio of the old enthalpy rise/the new one.

Applying these new conditions to the VIPRE code, the analyses for the reference core were performed. Note that a 3.2°C (5 F) conservative increase in core inlet temperature was still applied in the safety analyses (the standard procedure in steady state safety analysis).

Pressure drop

The core pressure drop at each uprate level and the pressure drop limits provided by RCPs were calculated and are listed in Table 7.10 and Figure 7-4

It can be observed in Figure 7-4 that the core pressure drop decreased significantly compared to the core at reference conditions, shown in Figure 7-1. A 1x pump now allows the core to operate at ~127% power. Thus when the power is limited by pressure drop, lowering the inlet temperature (to reduce the required flow rate) is a solution.

Table 7.10: Pressure drop of the reference core compared to the core pressure drop limits for various RCP power ratings

Uprate	Pressure drop (kPa)	1.0x RCP	1.5x RCP	2.0x RCP	2.5x RCP	3.0x RCP
102%	113.1	520.7	670.5	993.7	1317.8	1641.0
105%	122.0	488.4	643.8	964.0	1285.2	1605.5
110%	130.3	429.2	598.1	913.5	1229.8	1545.1
115%	140.0	363.7	551.0	861.4	1172.8	1483.3
120%	149.6	292.4	502.4	808.0	1114.5	1420.0
125%	159.3	215.9	452.4	753.1	1054.7	1355.3
130%	169.6	134.7	401.0	696.7	993.4	1289.2
135%	180.6	-	348.1	639.0	930.7	1221.6
140%	191.7	-	293.7	579.7	866.6	1152.6
145%	202.7	-	238.0	519.1	801.0	1082.1
150%	215.1	-	180.7	457.0	734.0	1010.2

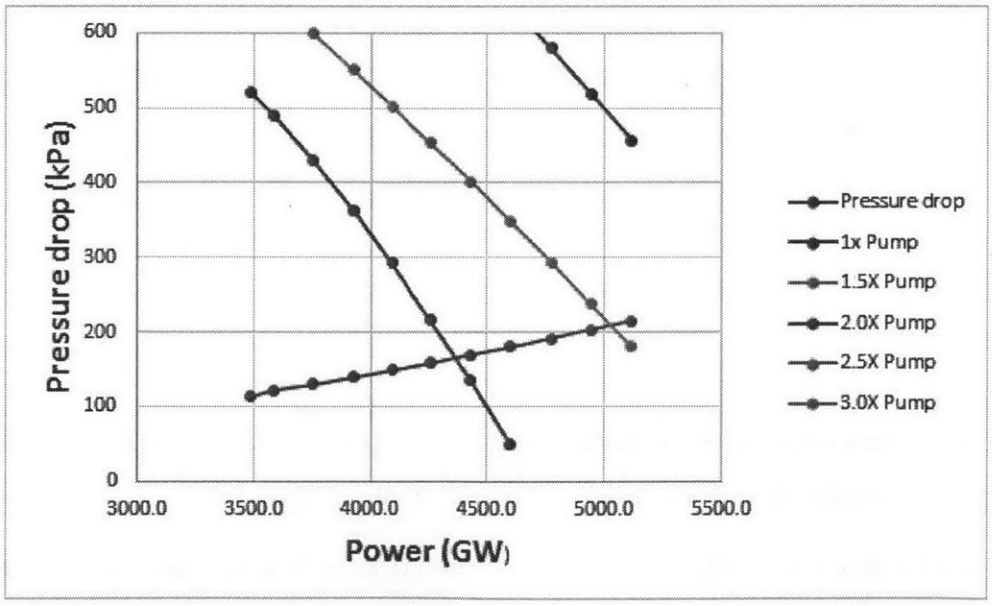

Figure 7-4: Core pressure drop compared to core pressure drop limits for various RCP power ratings

Table 7.11: MDNBR results for the reference core at new working conditions

Uprate	GROE	EPRI	W-3S	BW-2	BOWR	CE-1
102%	1.92	1.39	2.16	2.56	1.60	1.83
105%	1.88	1.40	2.17	2.54	1.61	1.84
110%	1.79	1.38	2.11	2.45	1.58	1.80
115%	1.71	1.36	2.05	2.37	1.56	1.76
120%	1.64	1.35	2.01	2.29	1.53	1.73
125%	1.56	1.33	1.96	2.22	1.51	1.70
130%	1.51	1.32	1.92	2.16	1.49	1.68
135%	1.45	1.31	1.88	2.09	1.47	1.65
140%	1.38	1.29	1.84	2.03	1.45	1.63
145%	1.34	1.28	1.80	1.98	1.43	1.62
150%	1.29	1.27	1.77	1.93	1.41	1.60

DNB

Table 7.11 listed the MDNBR results for the reference core at different uprate levels with the new inlet and outlet temperatures.

By lowering the inlet temperature, the MDNBR profile was slightly improved. The Groeneveld MDNBR at 102% power is now 1.92, larger than the limit 1.85. The maximum thermal power, limiting by MDNBR, is now ~107%.

Fuel temperature

The maximum peak and average fuel temperatures are listed in Table 7.12. While inlet fuel temperature was lowered from 296.2 ^oC to 283.7 ^oC (both included the 3.2^oC conservative increase), the peak and average fuel temperature only decreased by about 0.4^oC, which is negligible. The thermal power is still limitted by the average fuel temperature constraint at 1400^oC.

Overall, by lowering the inlet temperature, the core pressure drop significantly decreased while the MDNBR slightly improved. The maximum achievable power is now 107% the reference power, still limited by the DMNBR constraint. If core thermal power were limited by pressure drop, lowering the inlet temperature could be a promising method to increase the power. Taking into account the +2% power increased for the safety analysis, the maximum uprated power is 105%.

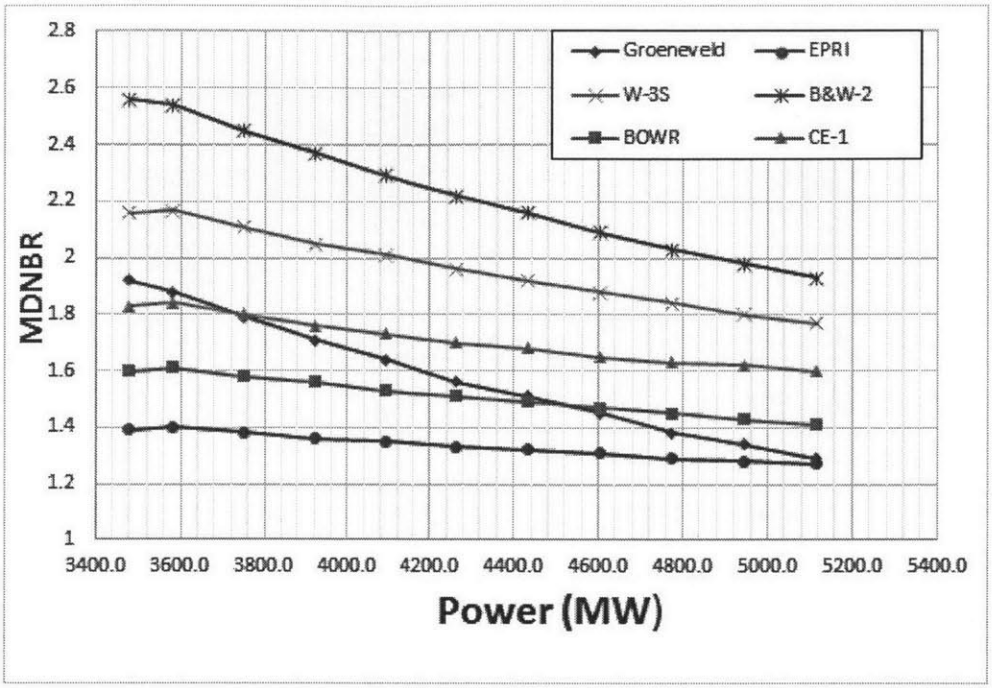

Figure 7-5: MDNBR results for the reference core at new working conditions

Table 7.12: Maximum peak and average fuel temperatures of the reference core at new working conditions

Uprate	$T_{avg}(^oC)$	$T_{peak}(^oC)$
102%	1321	2069
105%	1356	2124
110%	1414	2214
115%	1473	2301
120%	1527	2379
125%	1580	2452
130%	1633	2521
135%	1685	2588
140%	1737	2652
145%	1788	2714
150%	1838	2772

Chapter 8

IPWR design choices

This chapter investigates various options for the IPWR cooling channel designs operating at different temperature and enthalpy conditions. Starting from the Ferroni IPWR concept with six thermal hydraulic design constraints, three Ferroni designs (E-IPWR, S-IPWR and H-IPWR) and newly proposed designs are evaluated for the reference inlet/outlet temperature condition as well as for higher core enthalpy rise conditions. After going through a first round comparison of potential design configurations, the best performing designs will be evaluated in the next chapter to select a preferred design configuration.

For the reference and the AP1000 temperature conditions, three designs are selected after the first round: E-IPWR, SF-IPWR and F-IPWR while the MS-IPWR is introduced for evaluation alongside with those three design in a very high enthalpy rise case.

8.1 Thermal hydraulic constraints

In his IPWR concept, Ferroni used six thermal hydraulic constraints[1]:

1. Core inlet temperature and coolant enthalpy rise
2. Core pressure drop
3. Steady-state MDNBR

4. Steady-state peak fuel temperature

5. Steady-state peak inside cladding temperature

6. Peak cladding temperature and oxidation thickness during a LOCA

The first five constraints apply for steady-state operation of the reactor while only the last one is for the transient safety requirement in case a LOCA occurs. In the framework of this study, the five steady-state constraints are considered.

8.1.1 Core inlet temperature and coolant enthalpy rise

In his IPWR design, Ferroni used the same core inlet temperature and enthalpy rise as in the reference core to ensure that it can be used to replace the core in current PWR power plants. A high enough core outlet temperature is needed to maintain a high thermal efficiency of the power cycle while too high enthalpy rise across the core is not allowable due to mechanical safety requirements. Thus the inlet temperature cannot be set too low. Two values of inlet temperature are considered here:

- The reference core inlet temperature: 293.1°C, plus 3.2°C for safety analyses
- A new inlet temperature as used in the new advanced PWR (AP1000 by WEC [22]): 280.4°C, plus 3.2°C for safety analyses

8.1.2 Pressure drop

In his design, Ferroni used three limit values for the core pressure drop: 1.0x, 1.5x and 2.0x the reference core pressure drop (150kPa, 225kPa and 300kPa respectively). While these limit values provided good estimations for the pressure drop constraint, they didn't totally solve the design problem. As the core power increases, the coolant flow rate must be increased by the same percentage (to keep the enthalpy rise across the core unchanged) which will increase the pressure drop across every RCS component (including the core) and therefore increase the total RCS pressure loss. This

results in the decrease of the allowed value for the core pressure drop (the core pressure drop limit), i.e. the core pressure drop limit will decrease as the coolant flow rate increases.

As assumed in the Ferroni IPWR concept, the IPWR is to be used to replace PWRs in current power plants. Therefore the core pressure drop analysis presented in Section 7.1.2 can be applied for IPWRs. Given the total head Δh of RCPs, the core pressure drop limit is given by Eqn. 7.3:

$$\Delta P_{CO} = \rho_{cold} g \Delta h - \frac{1}{2} \dot{m}_{RCS}^2 \sum_{i \neq core} \frac{k_i}{\rho_i}$$

these parameters are defined in Section 7.1.2.

The typical WEC RCP used in the reference core is used as the reference RCP (1.0x); 4 higher power pumps: 1.5x, 2.0x, 2.5x and 3.0x will also be considered. The head characteristic curves of these pumps are given in Chapter 6.

8.1.3 Steady-state MDNBR

The MDNBR values of IPWR designs in this study are calculated using the DNB correlation developed by Arment [7], which was developed from the Groeneveld DNB correlation. The MDNBR of the reference core at its reference condition calculated by the Groeneveld (1.85) will be used as the MDNBR limit for IPWR designs.

8.1.4 Fuel temperature and cladding temperature

The IPWR uses hydride fuel ($UTh_{0.5}Zr_{2.25}H_{5.625}$) instead of uranium dioxide (UO_2) as in conventional PWRs but similar problems with fuel temperatures as in PWRs still apply. The fuel temperature must be maintained within limits to prevent the excessive release of fission and hydrogen gas. Another phenomenon that must be considered for hydride fuel is irradiation-induced fuel swelling, which in fact limits the fuel temperature even more than does the fuel melting temperature, as stated in the Ferroni thesis [1]. The peak fuel temperature limit is set at 650°C, as used by Ferroni (2010).

Beside the fuel temperature, a temperature limit is also set for the inside cladding temperature. The limit on maximum (peak) cladding temperature is set to 370°C to limit the oxidation of the cladding materials, as used by Ferroni.[1]

8.2 Ferroni cooling channel designs

As stated before, this study focuses on thermal hydraulic constraints to improve the Ferroni IPWR concept by modifying the cooling channel design while keeping all other design components the same.

Ferroni considered three different designs[1]:

- E-IPWR: IPWR design in which the cooling channels are empty tubes, i.e. tubes not provided with turbulence promoters.
- H-IPWR: IPWR design in which a long twisted tape (TT) is located in the top 1.6 m of each cooling channel.
- S-IPWR: IPWR design in which multiple short-length twisted tapes (MSLTTs) are located in the top half of each cooling channel (geometric details are given later).

Ferroni conducted a parametric study using the aforementioned parameters to find the optimum design. He concluded that the E-IPWR was the best design and using the empty tube approach selected an assembly geometry which is summarized in Table 8.1

The goal of inserting twisted-tapes as swirl flow promoters in cooling channels is to improve the critical heat flux in the PWR subcooled boiling flow region, thus increasing the MDNBR in cooling channels. However, the existence of twisted-tapes would also increase the pressure loss across the cooling channels. In this section, the three Ferroni cooling channel designs are re-investigated using the pressure drop and DNB correlations developed by Arment[7] with the selected assembly geometry given in Table 8.1.

Table 8.1: Assembly geometry of the Ferroni IPWR design

Characteristic	Unit	Value
Heated length	m	3.67
Upper plenum height	m	0.1
Total height	m	3.8
Duct outer flat-to-flat distance	mm	228
Duct wall thickness	mm	9.8
Fuel prism flat-to-flat distance	mm	208
Cooling channel inner diameter	mm	10.79
Cladding thickness	mm	0.67
Clad-fuel gap width	mm	0.3
Fuel hole diameter	mm	12.74
Cooling channel pitch	mm	15.63
Fuel web thickness	mm	2.9
Number of fuel cells per assembly	-	169
Fuel volume fraction (unit-cell level)	-	0.397
Coolant volume fraction (unit-cell level)	-	0.432
Clad volume fraction (unit-cell level)	-	0.113

8.2.1 E-IPWR design

Considering the selected E-IPWR with the new MDNBR limit 1.85 (instead of 1.79 as used by Ferroni[1]) and the new pressure drop (as described in Section 8.1.2), the new power map and limiting parameter map are showed in Figure 8-1 for the case with 1.5x RCPs.

At the selected geometry ($D_{ci} = 10.79\ mm$,$t_{web} = 2.9\ mm$), the maximum achievable power is now 3953.1 MWt, limited by MDNBR. The DNBR values in the channel are illustrated in Figure 8-2

As showed in Figure 8-2, the DNBR curve hits the limit value (1.85) at $z = 2.44\ m$. The pressure drop accros the channel is 154.01 kPa while the core pressure drop limit at this flow rate is 289.2 kPa. To achieve higher power, it is required that the DNBR values must be increased, at least at $z = 2.44\ m$ (where DNBR=MDNBR) and the region around that point.

Ferroni considered two solutions to this problem: the H-IPWR and S-IPWR

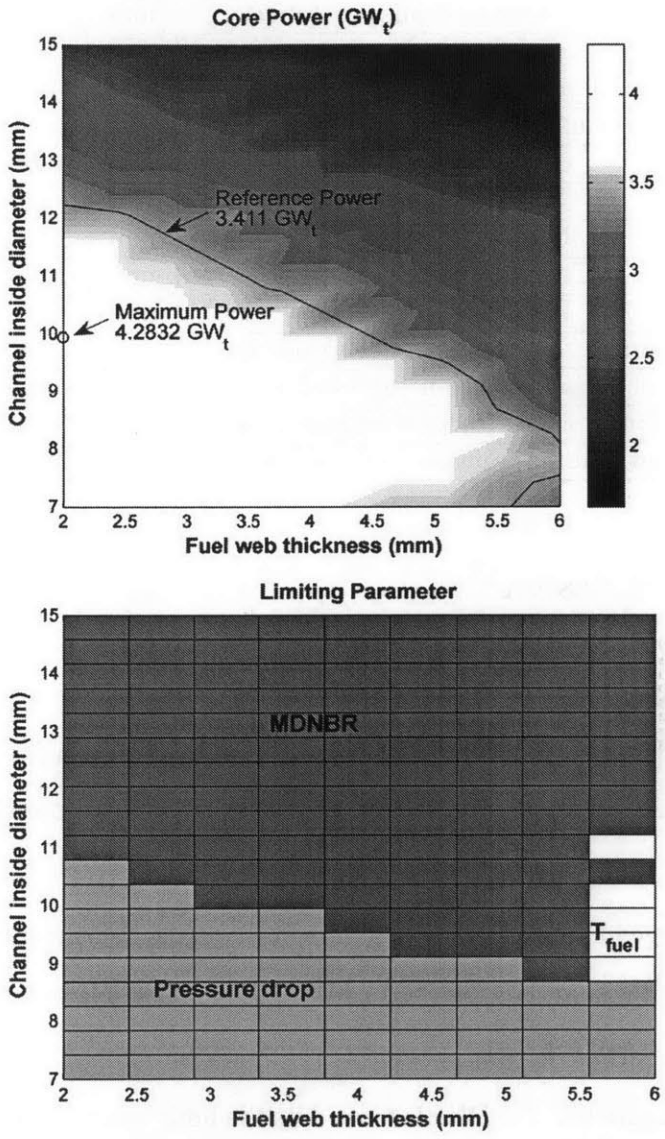

Figure 8-1: Power map and limiting parameter map for the E-IPWR with 1.5X RCPs

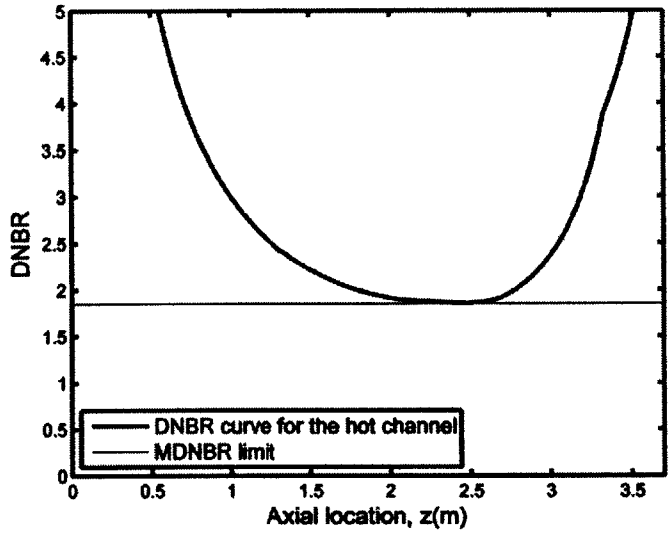

Figure 8-2: DNBR vs. location in a E-IPWR hot channel at 3953.1 MWt

8.2.2 H-IPWR design

For the IPWR design, a long twisted tape is inserted in the top 1.6m of the cooling channel, i.e. from $z = 2.07\ m$ to $z = 3.67\ m$. While this design should increase the DNBR in that region and therefore increase the maximum achievable power, three issues need to be considered:

- At the given power level (3953.1 MWt) the DNB value at $z = 2.07\ m$ is already very close to the limit value (the exact value is 1.89 with the limit is 1.85) and since the twisted tape doesn't affect the DNBR upstream it may increase the maximum power but the increase is not much. The DNBR value at $z = 2.07\ m$ and locations before that will soon hit the limit value as the power increase. To achieve significantly higher power, the twisted tape should be relocated in the channel toward the core inlet

- It can be observed in Figure 8-2 that the DNBR curve increases after hitting the MDNBR. This is because the heat flux is decreasing in the upper half of the channel (the axial power profile of the core was assumed to be chopped cosine). A long twisted tape extending to the end of the channel is therefore

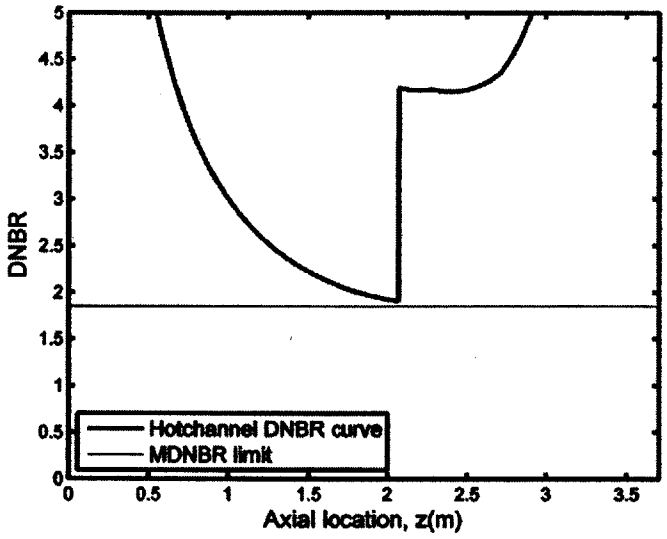

Figure 8-3: Hot channel DNBR curve of the H-IPWR design

unnecessary.

- The pressure drop increase due to the twisted tape may be too high and can exceed the pressure drop limit value ($289.2kPa$ at $3953.1MW$ power). To reduce the pressure drop, the unnecessary parts need to be removed.

Figure 8-3 shows the DNBR profile for the H-IPWR hot channel (the twist ratio of the TT is y=2.5 as used by Ferroni (2010)). At $z = 2.07\,m$ where the twisted-tape starts, the DNBR goes up to 4.1 and for larger z locations is kept higher than that value because of the existence of the TT. From $z = 2.7m$ onward, the DNBR is much higher than 4.1 due to the decrease of heat flux. This part of the TT is not necessary. On the other hand, the pressure drop through the channel in this case is $313.4kPa$, higher than the limit $289.2kPa$. The twisted-tape does help to increase the DNBR but it significantly increase the pressure drop as well. The core pressure drop constraint now limits the core power and the maximum achievable power decreases to lower than that of the E-IPWR. This make the H-IPWR a poorer design than the E-IPWR. To improve this, unnecessary portions of the long twisted-tape need to be removed.

8.2.3 S-IPWR design

The S-IPWR was designed to improve the DNBR profile while keeping the pressure drop lower than the limit value by using multiple short length twisted tapes instead of one long twisted-tape as in the H-IPWR. The characteristics of the S-IPWR design:

- Multiple short twisted tapes with $y = 2.5$ and $N_{turns} = 1.5$, yielding a tape length of 80.9 mm
- First twisted tape starts at $z = 2.0\ m$
- Spacing between successive TTs: $\Delta z = 50 \times D_{ci}$

For the selected geometry ($D_{ci} = 10.79\,mm$, $\Delta z = 0.54\,m$), 3 TTs are inserted in each S-IPWR channel at $z = 2.0\,m$, $2.54\,m$ and $3.08\,m$. Before presenting the detailed performance of the design, it can be noticed that:

- The first issue with the H-IPWR design still remains here: The twisted tape at $z = 2.0m$ and those after that do not affect the DNBR curve in the region$z < 2.0m$. Therefore the power increase, if there is any, is not much.
- The last TT at $3.62m$ may be unnecessary

Figure 8-4 shows the DNBR profile for the S-IPWR design at 3953.1 MWt and confirms these two conclusions. The last TT is unnecessary and the DNBR values for $z < 2m$ are very close to the limit. The pressure drop in this case is $248.5kPa$. Notice that in the selected design, Ferroni considered 225kPa (1.5 times the reference core pressure drop) as the core pressure drop limit, which is lower than 248.5kPa. For that case, the S-IPWR was a poor design because the maximum achievable power was lower than the E-IPWR power, limiting by pressure drop. Here in this current analysis, a 1.5x power pump is considered and the core pressure drop limit is 289.2 kPa higher than the S-IPWR design value of 248.5 kPa. Nevertheless the MDNBR and pressure drop are close to their limits and soon will hit the limits as the power increases.

The S-IPWR design is better than H-IPWR but it still can be improved: unnecessary TTs need to be removed and the locations of the TTs can be optimized.

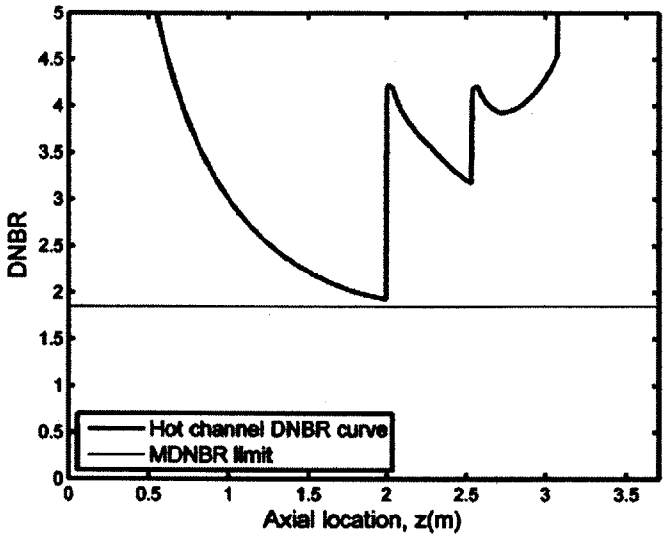

Figure 8-4: Hot channel DNBR curve of the S-IPWR design at 3953.1 MWt

8.3 New cooling channel design choices

In this section, new cooling channel designs with short length twisted tapes are considered along with the empty channel design, E-IPWR, to select candidates for the best IPWR design. As stated in Section 8.1.1, two different core inlet temperature conditions are to be considered for the IPWR design because those conditions affect the DNBR profile in cooling channels. The properties of TTs in this section: $y = 2.5$, $N_{turns} = 1.5$ (the length for each TT is $2N_{turns}yD_{ci}$)

8.3.1 Normal enthalpy rise

The cooling channel designs in this Section are applied for IPWR designs with core inlet temperature and enthalpy rise as used in the reference core: $T_{in} = 293.1^oC$ and $\Delta h = 195.2\ kJ/kg$.

In Section 8.2, three cooling designs were considered in a system using 1.5x RCPs. The S-IPWR appeared to be the best design but its pressure drop was close to the limit. Therefore for systems with low pressure pumps (1.0x as in the reference core), the E-IPWR may be better.The E-IPWR is selected as the first design to be evaluated

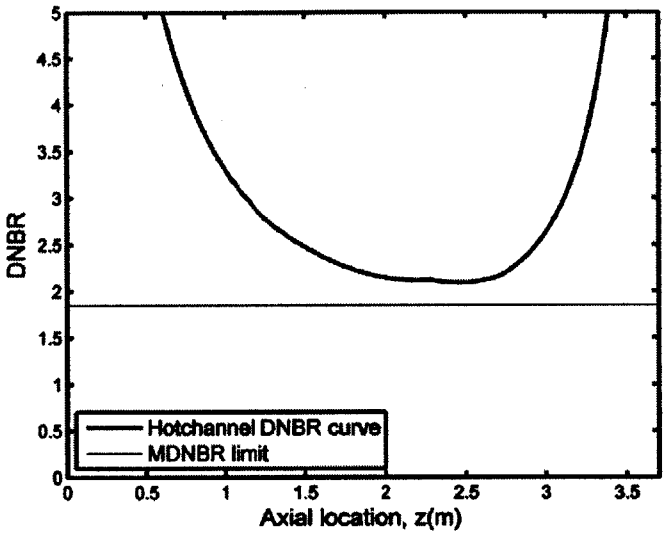

Figure 8-5: DNBR profile of the E-IPWR design at thermal power P=3500 MWt

In systems with high pressure drop limits (high power RCPs), the powers are limited by MDNBR and therefore designs with TTs insertions could be better. In this section, effects of TTs insertions on the DNBR profile are investigated while the pressure drop limit is temporarily removed.

Consider the IPWR at power levels of 3500 MWt, 4000 MWt, 4500 MWt and 5000 MWt. The DNBR profiles at these power are showed in Figure 8-5-8-8, respectively, for the E-IPWR design and in Figure 8-9 and 8-10 for designs with twisted tapes.

At $P = 3500\ MWt$, the MDNBR is higher than the limit 1.85, no TT is needed.

At $P = 4000\ MWt$, MDNBR= 1.85 at $z = 2.43\ m$, the MDNBR approaches its limit but the system can still be considered operable. No TT needed.

At $P = 4500\ MWt$, MDNBR= 1.66 at $z = 2.43\ m$. The DNBR is below the limit starting at $z = 1.75\ m$ and goes back beyond the limit at $z = 2.83\ m$. Since MDNBR is lower than the limit, the system in this case is unoperable. TT insertions are required to increase the DNBR. For insertion of a TT at z=1.75m, the new DNBR profile is showed in Figure 8-9. Now MDNBR= 1.85 at $z = 1.75\ m$ and after that DNBR is larger than 1.85. A second TT is not necessary.

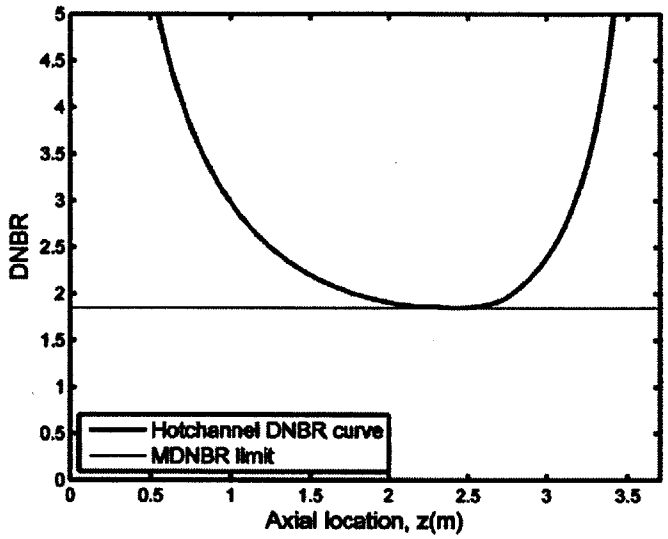

Figure 8-6: DNBR profile of the E-IPWR design at thermal power P=4000 MWt

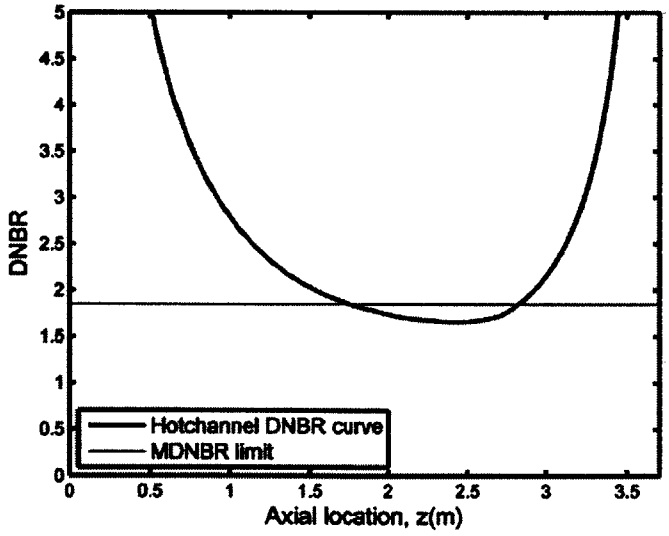

Figure 8-7: DNBR profile of the E-IPWR design at thermal power P=4500 MWt

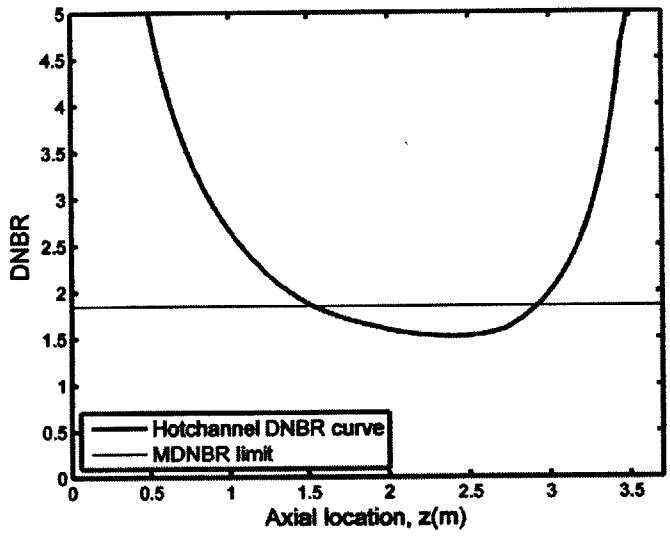

Figure 8-8: DNBR profile of the E-IPWR design at thermal power P=5000 MWt

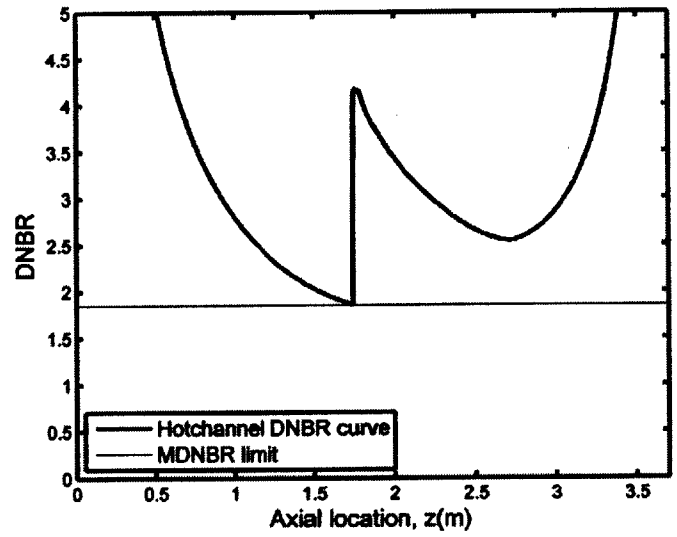

Figure 8-9: DNBR profile of the IPWR design at thermal power P=4500MWt with 1 TT at z=1.75m

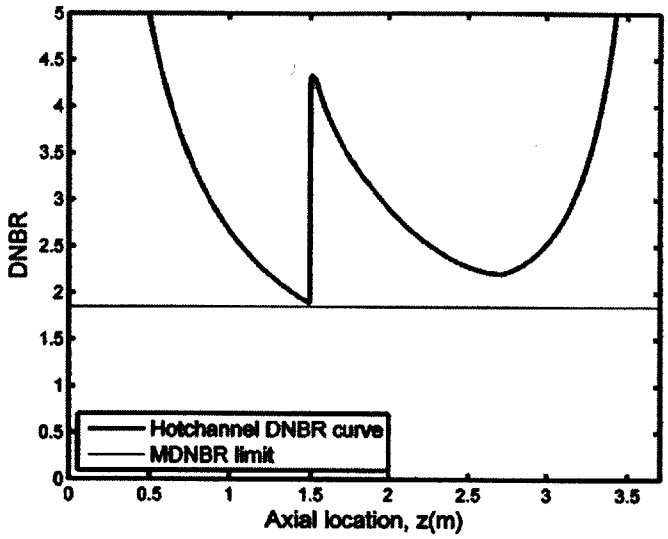

Figure 8-10: DNBR profile of the IPWR design at thermal power P=5000MWt with 1 TT at z=1.5m

Similarly at $P = 5000\ MWt$, MDNBR= 1.52 at $z = 2.40\ m$. The DNBR is below the limit starting at $z = 1.52\ m$ and goes back beyond the limit at $z = 2.93\ m$. Since MDNBR is lower than the limit, the system in this case is inoperable. TT insertions are required to increase the DNBR. Inserting a TT at $z = 1.52m$, the new DNBR profile is showed in Figure 8-10. A second TT is not needed.

From these analyses, it is showed that:

- For $P < 4000\ MWt$, no TT insertion is needed
- For $P > 4000\ MWt$: Only 1 TT is required for each channel to maintain the DNBR above the MDNBR limit and there exists an optimal location for the TT: Moving the TT upstream would decrease the MDNBR while moving the TT downsteam would increase the pressure drop through the channel since the TT would be moved into the subcooled boiling region.

For $P > 5200\ MWt$, the coolant mass flux is out of the Groeneveld LUT range. However, it will be showed later in this study that the maximum achievable power for this enthalpy rise condition is lower than 5200 $MW\ t$ and therefore considering powers larger than 5200 MWt is unnecessary.

For the given geometry, the E-IPWR already gives the maximum power of 4000 MWt. For expected power $> 4000\ MWt$, the design with 1 TT at its optimal position for each channel is the best design (compared to long twisted-tape or multiple twisted-tapes). Two issues may occur with this design:

- Across the core, the heating power is different for each channel and therefore the optimal TT position in each channel is different. Manufacturing an IPWR core with TTs inserted at different locations in cooling channels is complicated and unfavorable.

- The TT is located at the position where the DNBR first reaches the limit 1.85 so that the MDNBR for the system at that power is 1.85. If the core power increases or the coolant flow rate decreases, the DNBR values at locations before the TT will go below the limit, which may lead to system failure.

A possible solution for both these problems is to fixed the TT at a location that covers the core power range: $4000MWt$ to $> 5000MWt$. Considering now a design in which a TT is inserted in each cooling channel at a fixed location $z = 1.5m$ - the optimal position for TTs in cooling channel with core power slightly larger than 5000 MWt. For convenience, the acronyms used for these two designs are:

- SO-IPWR: IPWR design in which a short twisted tape is located at its optimal position in each cooling channel

- SF-IPWR: IPWR design in which a short twisted tape is located at $z = 1.5\ m$ in each cooling channel

Figure 8-11 shows the DNBR curves for the two designs. The MDNBR in the SO-IPWR is kept close to 1.85 as expected while that value for the SF-IPWR decreases from 2.21 at $P = 4000\ MWt$ to 1.85 at $P > 5100\ MWt$. This will solve the two issues of the SO-IPWR design. Considering this aspect, the SF-IPWR is the better design.

On the other hand, in the SF-IPWR design because the TTs are moved downsteam from their optimal locations, the pressure drop across the channel is expected to

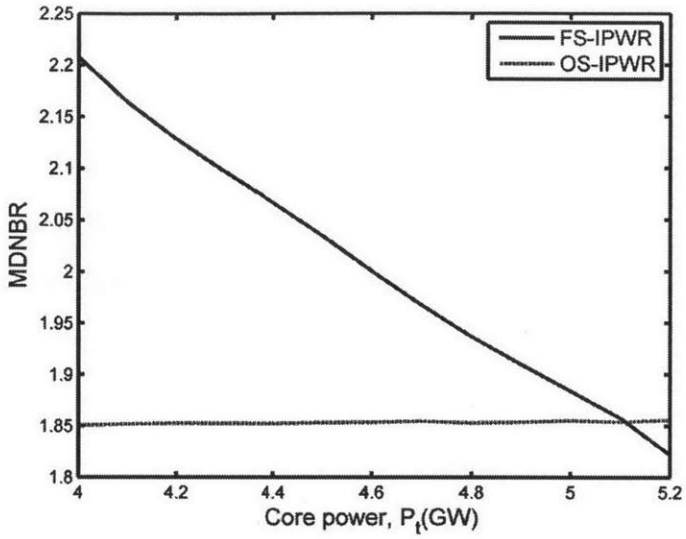

Figure 8-11: DNBR curves for the two designs: SO-IPWR and SF-IPWR

be higher than that in the SO-IPWR design. Figure 8-12 shows the core pressure curves for these two design as the core power varies from $4000MWt$ to $5200MWt$. As expected, the pressure drop is lower for the SO-IPWR design and the different decreases as the core power increase (because the optimal location for the TT is closer to the fixed location z=1.5m). However, the pressure drop different is small (the maximum value is only $8kPa$ 4% at $P = 4000MWt$) and is negligible.

Considered both the DNBR and the pressure drop performance of the two design, it can be concluded that the SF-IPWR is the better design.

However, manufacturing the fuel assembly for the SF-IPWR may be still challenging (although it's easier compared to the SO-IPWR design). A design with a full length twisted tape inserted to each cooling channel will also be considered.

Finally, for this normal enthalpy rise case, three designs are selected for further evaluation in Chapter 9: E-IPWR, SF-IPWR and F-IPWR

8.3.2 High enthalpy rise

In this section, the inlet temperature and enthalpy rise conditions of the new PWR AP1000[22] are used. These condition were listed in Table7.9.

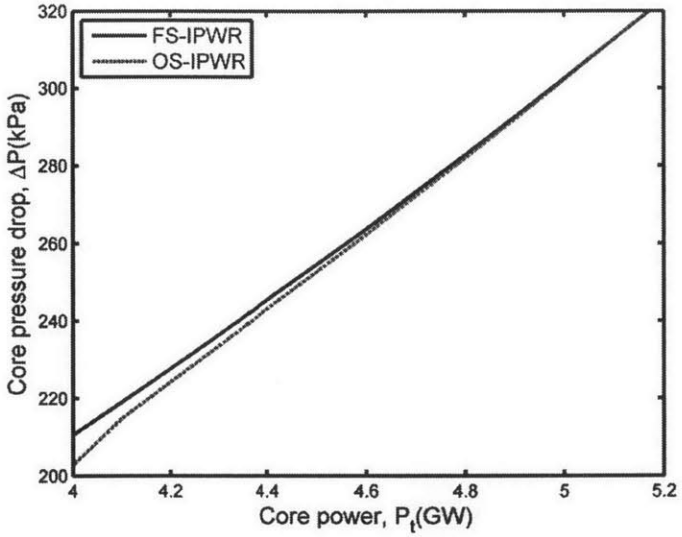

Figure 8-12: Pressure drop curves for the two designs: SO-IPWR and SF-IPWR

For the same core thermal power, a higher enthalpy rise would lower the required coolant flow rate, thus reduce the core pressure drop. These changes, however, can affect the DNBR profile in both directions:

- For a lower flow rate at the same heat flux, the DNBR values is lower because the CHF is lower. This will make the MDNBR constraint more limiting.

- For the same flow rate but lower inlet temperature, the CHF is higher (as it takes more heat to boil the same amount of fluid) therefore the DNBR values are higher. This will make this DNBR constraint less limiting.

To see these effects more clearly, consider the E-IPWR design at these two conditions for the thermal power of 4000 MWt (the maximum achivable power at reference conditions).

Figure 8-13 shows the MDNBR curves when the inlet temperature is kept at the reference condition (296.3^oC) while the core enthalpy rise is varying in a range from 195.2 to 250(kJ/kg). From the figure, it is confirmed that the DNBR values decrease as the enthalpy rise increases.

Figure 8-14 shows the DNBR curves for the E-IPWR design with different inlet

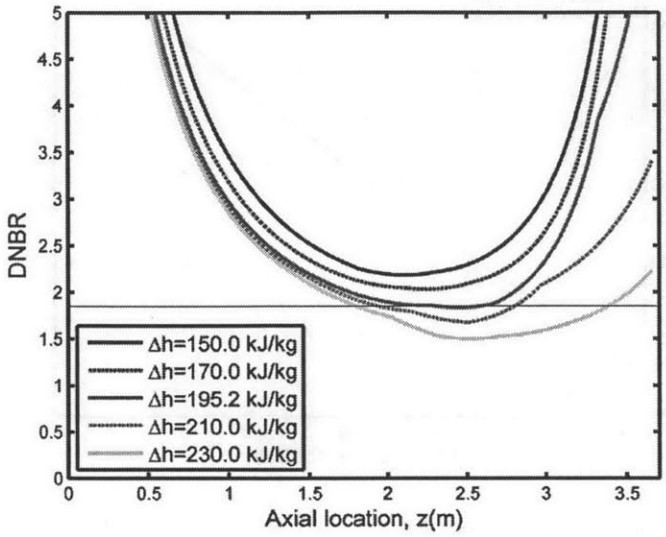

Figure 8-13: DNBR curves of the E-IPWR design with different enthalpy rises for T_{inlet}=296.3°C

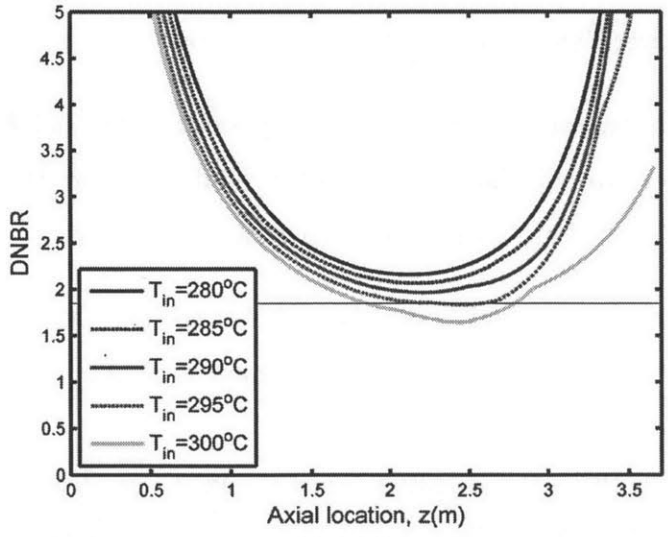

Figure 8-14: DNBR curves of the E-IPWR design with different inlet temperatures for Δh=195.2 kJ/kg

temperature (the enthalpy rise is held constant at $195.2kJ/kg$ - the reference condition). The DNBR values are indeed reduced as the inlet temperature increases.

Consider now the inlet temperature in the new PWR design AP1000[22]: $T_{in} = 280.4°C$. If the enthalpy rise were kept the same as for the reference core, the outlet temperature should be: $T_{out} = 316.2°C$. If the outlet temperature were kept the same at 326.8°C as for the reference core, the enthalpy rise would be 261.2kJ/kg. From the conclusions given above, it can be observed that:

- At $T_{out} = 316.2°C$: the enthalpy rise is the same as in the reference conditions. The DNBR values are expected to be higher than those in reference conditions because of the lower inlet temperature.
- As T_{out} increases, the enthalpy rise increases and the DNBR values start decreasing, although still higher than the values in reference conditions, until $T_{out} = T_c$ where T_c is some value to be determined

Therefore, given a new inlet temperature $T_{in} = 280.4°C$, if the outlet temperature is selected between $T_{out} = 316.2°C$ and T_c, the performance of the core will be better considering both the pressure drop and DNBR constraints: the pressure drop is lower and the DNBR values are higher. If the outlet temperature is selected between T_c and $T_{out} = 326.8°C$ (the reference outlet temperature), the pressure drop is reduced even more but the DNBR values will be lower than those in the reference conditions. These observations are confirmed and demonstrated in Figure 8-15 and Figure 8-16. The $T_c$value in this case is $324.5°C$ as observed in Figure 8-16.

Depending on the purpose of the design, the optimal outlet temperature can be chosen. If low pressure drop is in higher priority, T_{out} should be higher than T_c while if high MDNBR is more important, T_{out} should be lower than T_c. For the E-IPWR (and the reference core) where the power at reference conditions is limited by MDNBR, the new outlet temperature must be lower than T_c for the system to be operable. For IPWR designs with twisted-tapes, since MDNBR values can be improved, the value for $T_{out}$is not restricted.

Consider two values for the outlet temperature: $T_{o1} = 321.4°C$ (the value used in

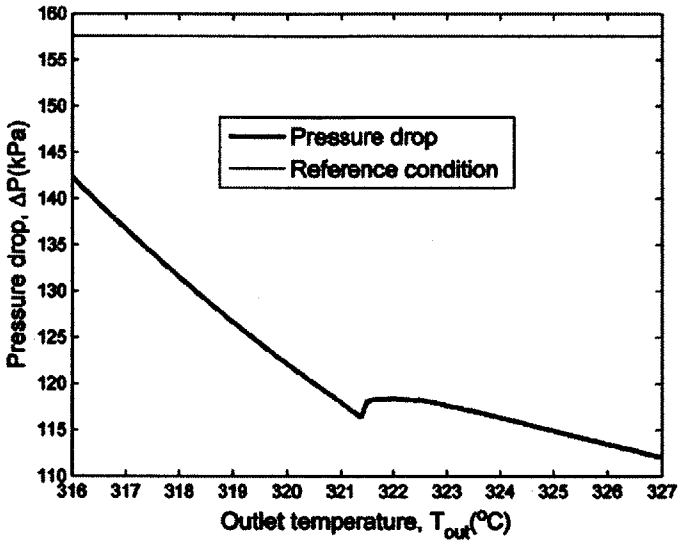

Figure 8-15: Core pressure drop vs. outlet temperature for the E-IPWR at 4000 MWt and T_{inlet}=280.4°C

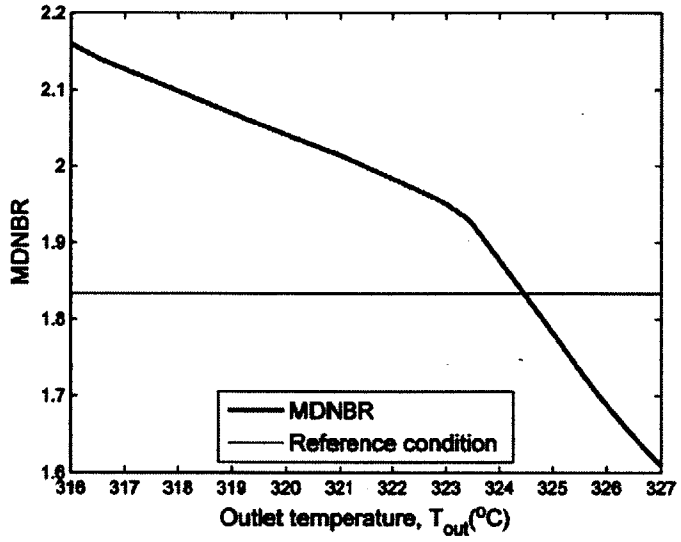

Figure 8-16: MDNBR vs. outlet temperature for the E-IPWR at 4000 MWt and T_{inlet}=280.4°C

the AP1000 design) and $T_{o2} = 326.8°C$ (the reference outlet temperature) (Assuming these temperatures are feasible. It should be noted, however, that a too high enthalpy rise may not be allowable due to mechanical design constraints).

T_{out}=321.4°C (AP1000 condition)

This is the condition used in the AP1000 design. Since the DNBR profile is improved, the E-IPWR and SF-IPWR are expect to perform better. Up to 5000 MWt, a second TT for each channel is not necessary. Therefore similar to the case with reference conditions, three designs selected for further evaluation in Chapter 9 for this temperature condition are: E-IPWR, SF-IPWR and F-IPWR

T_{out}=326.8°C (Higher enthalpy rise condition)

For this condition, the DNBR values are lower than those in the reference condition (at the same core power), therefore the E-IPWR is expected to perform worse (For 1.5x RCPs, the maximum achievable power is decreased from ~4000MWt in reference conditions to 3250MWt, limiting by MDNBR). However, it is still selected as the first design to be considered.

Since the DNBR values are lower in this outlet temperature condition, a single short twisted tape for each cooling channel may not be enough to maintain the DNBR values above the limit 1.85. Consider the SF-IPWR at power $P = 4500MWt$, the DNBR profile is showed in Figure 8-17.

It is showed in the figure that the DNBR curve drops closer to the DNBR limit at a position after the TT. Therefore as the power increase, the DNBR values can be lower than the limit at those two positions simultaneously. A second TT is needed in this case. Using the DNBR profile given in Figure 8-17, a new design is proposed for this condition: The first TT in the SF-IPWR is moved from $z = 1.5\ m$ to$z = 1.3\ m$ and a second TT is located at $z = 2.2\ m$. The acronym for this design is: MS-IPWR (multiple short twisted tapes IPWR).

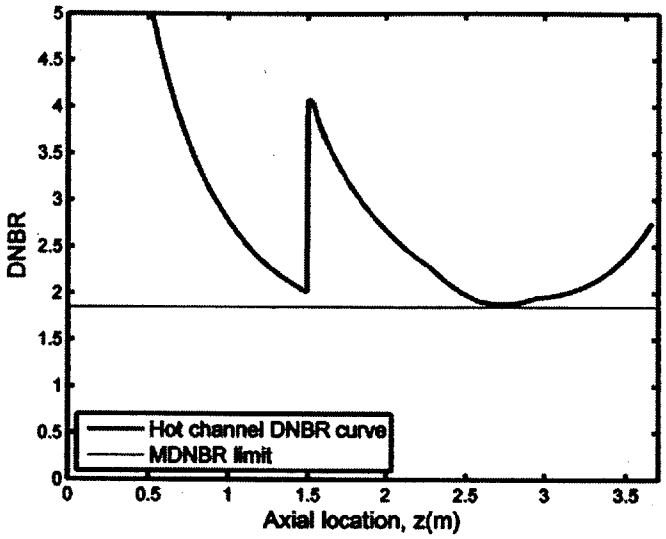

Figure 8-17: DNBR profile for the SF-IPWR at new outlet condition of 326.8°C, P=4500 MWt

8.4 Twisted tape choices

The performance of IPWR designs with twisted tapes is affected by the location of the TTs in the cooling channel as well as the properties of the twisted tapes. Given the axial location of TTs for the designs in the previous section, the effects of twisted tape properties (twist ratio, length...) on the core performance are investigated in this section.

8.4.1 SF-IPWR and MS-IPWR

Consider the SF-IPWR design with twisted tapes of 4 kinds:y = 2.5, 3.5, 5 and 10 (recall that y, the twist ratio, the the ratio between the length to complete a 180°turn and the tube diameter). Each TT has the same relative length, $N_{turn} = 1.5$. The core pressure drop and MDNBR curves of these configurations at reference temperature conditions as the power increases are showed in Figure 8-18 and 8-19

It is showed that the core pressure drop decreases as the twist ratio increases. At low power, the MDNBR performance of low y twisted-tapes are better but the difference decreases at higher power. For core power higher than $4000MW$, the

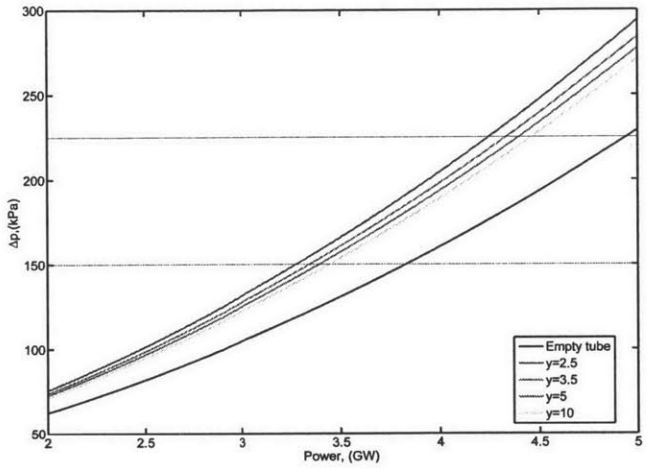

Figure 8-18: Core pressure drop of the SF-IPWR at the reference temperature conditons

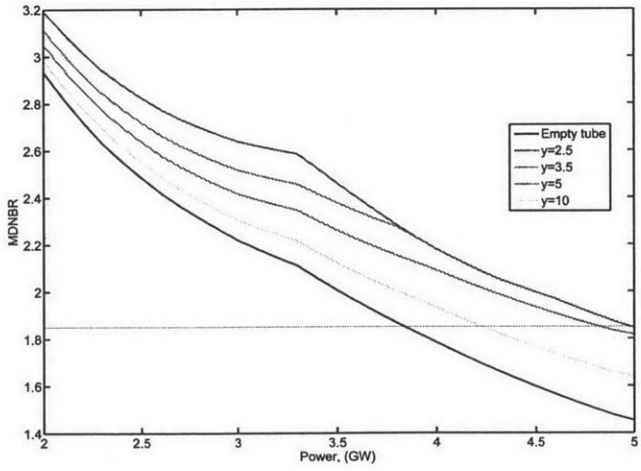

Figure 8-19: MDNBR of the SF-IPWR at the reference temperature conditons

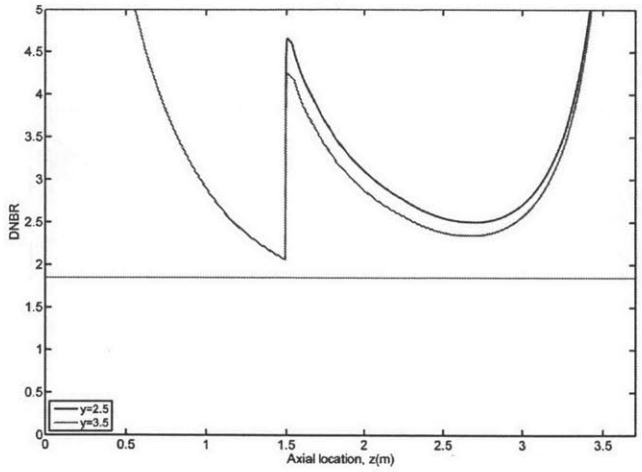

Figure 8-20: DNBR curves for the SF-IPWR different twist ratios at 5000 Mwt

MDNBR curves of $y = 2.5$ and 3.5 twisted tapes are almost identical. Considering both pressure drop and MDNBR, the twist ratio $y = 3.5$ is selected for the SF-IPWR design. Figure 8-20 demonstrates more clearly that the MDNBR values with y=2.5 and 3.5 are identical at high power.

Similarly, for the case with $T_{in} = 280.4^oC$, $T_{out} = 321.3^oC$ (the AP1000 conditions), the DNBR values are higher in general, therefore the performance gap between twisted tapes with y=2.5 and y=5 is reduced. As showed in Figure 8-21 , the performance of y=2.5 and y=5 are now identical for power higher than 4000MW. Twisted tape with y=5 is selected for the SF-IPWR in this case.

For the case with $T_{in} = 280.4^oC$, $T_{out} = 326.8^oC$, the MDNBR curves are showed in Figure 8-22. At high power, the performance of twisted tapes decreases significantly as y increases. Twisted tapes with y=2.5 should be used for both SF-IPWR and MS-IPWR.

8.4.2 F-IPWR

The pressure drop and MDNBR curves for the full length twisted tapes design F-IPWR are showed in Figure 8-23 and 8-24 (with $T_{in} = 280.4^oC$, $T_{out} = 326.8^oC$). It can be observed that twisted tapes with y=10 give lower pressure drop and are

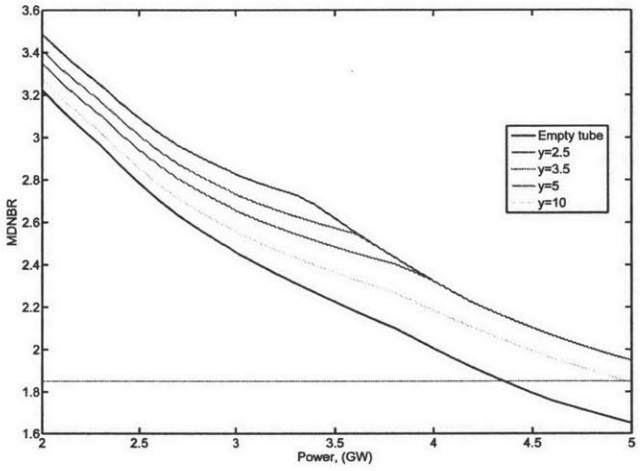

Figure 8-21: MDNBR of the SF-IPWR with the AP1000 temperature conditions

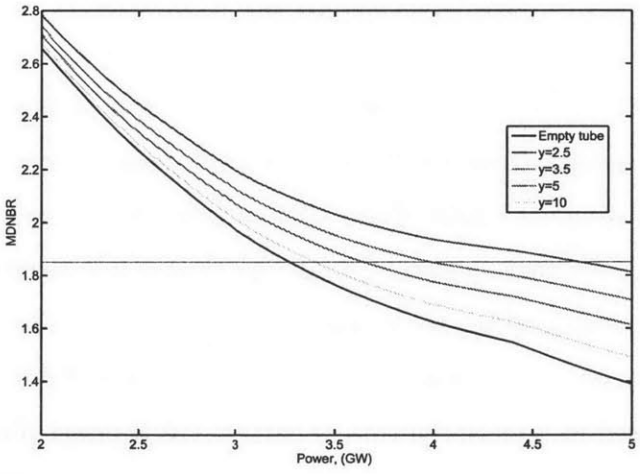

Figure 8-22: MDNBR of the SF-IPWR with T_{in}=280.4°C, T_{out}=326.8°C

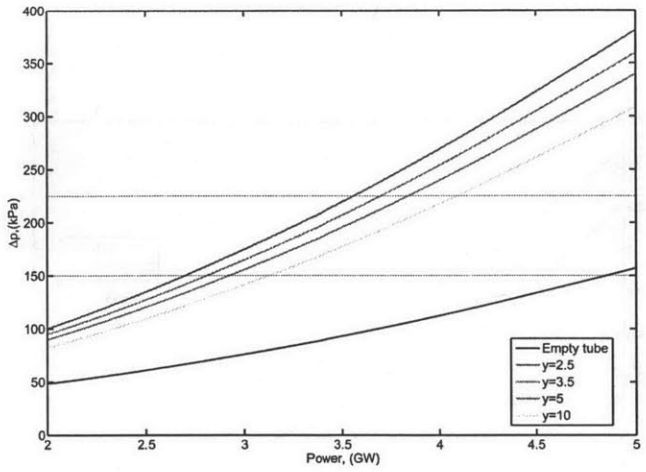

Figure 8-23: Pressure drop curves for the F-IPWR with various twist ratio values

good enough to keep the MDNBR well above the limit 1.85. For the cases with the reference temperature conditions or the temperature conditions in the AP1000 design, the MDNBR values are expected to be higher. Therefore with all three temperature, twisted tapes with twist ratio y=10 are chosen for the F-IPWR design.

8.5 Summary: Design choices

In this chapter, Ferroni cooling channel designs and new designs were investigated. For each inlet and enthalpy rise condition, inefficient designs were eliminated based on their DNB improvement. After these eliminations, the rest were selected to be evaluated further in the next chapter. The design choices selected for each inlet and outlet temperature condition set are summarized in Table 8.2. The first condition is used in the reference core and current typical PWRs, thus the IPWR design using this condition can be used to replace the core in current PWR power plants. The second condition, which will be used in the AP1000 and other new PWR designs, offers lower pressure drop and better MDNBR profile. With this condition, the maximum achievable power for the IPWR designs are expected to be higher. The last condition give a much higher enthalpy rise, and therefore much lower core pressure drop. While

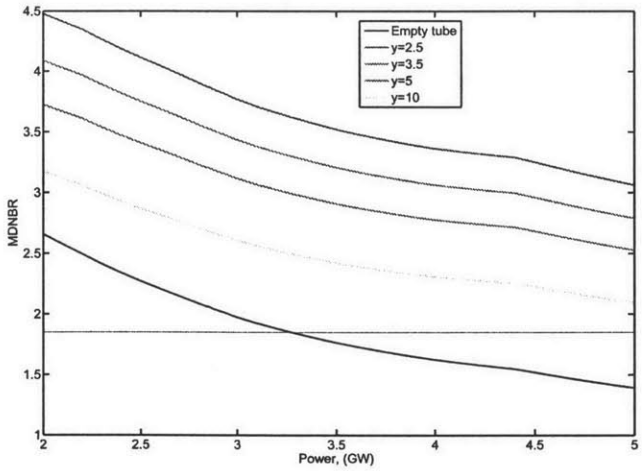

Figure 8-24: MDNBR curves for the F-IPWR design with various twist ratio values

it also worsens the MDNBR profile in the E-IPWR, the lower core pressure drop will allow more flexible TT insertion options.

Table 8.2: IPWR design choices for each temperature condition

	Reference conditions	AP1000 conditions	Higher enthalpy rise
T_{inlet}(°C)	293.1	280.4	280.4
T_{outlet}(°C)	326.8	321.3	326.8
Enthalpy rise (kJ/kg)	195.2	226.2	261.2
IPWR design choices	E-IPWR SF-IPWR with y=3.5 F-IPWR with y=10	E-IPWR SF-IPWR with y=5 F-IPWR with y=10	E-IPWR SF-IPWR with y=2.5 MS-IPWR with y=2.5 F-IPWR with y=10

Chapter 9

IPWR design selection

The IPWR designs selected in Chapter 8 are evaluated in this chapter to select the best IPWR design at each core inlet/outlet temperature condition. The Ferroni's selected geometry as listed in Table 8.1 will be used. As stated previously in Chapter 8, three temperature condition sets are considered:

- The reference condition: core inlet temperature 293.1^oC, outlet temperature 326.8^oC, enthalpy rise 195.2 kJ/kg
- The AP1000 condition: core inlet temperature 280.4^oC, outlet temperature 321.3^oC, enthalpy rise 226.2 kJ/kg
- Higher enthalpy rise condition: core inlet temperature 280.4^oC, outlet temperature 326.8^oC, enthalpy rise 261.2 kJ/kg

As a standard procedure used with the reference core, the inlet temperature will be increased conservatively by 3.2^oC in the steady state safety analysis for each design at each condition set.

Results show that the higher enthalpy rise condition causes the inside cladding temperature of the designs to exceed the limit value starting from low power levels (110% of the reference core power for the E-IPWR and lower than 100% for the designs with twisted tape). Therefore only the first two enthalpy condition sets (the reference and the AP1000 condition) are practical for the IPWR design with the

Table 9.1: Maximum achievable core power (%) for the designs

	REF core enthalpy rise condition				AP1000 core enthalpy rise condition			
Design	REF	E-IPWR	F-IPWR	SF-IPWR	REF	E-IPWR	F-IPWR	SF-IPWR
Max core power (%)	100	110.6	139.7	139.7	105.1	121.3	140.3	140.3
Limiting constraint	MDNBR	PD	T_{fuel}	T_{fuel}	MDNBR	MDNBR	T_{fuel}	T_{fuel}
Required RCP	1.0x	1.2x	2.7x	2.3x	<1.0x	<1.0x	1.7x	1.5x

selected geometries. The maximum achievable powers for the designs at these two conditions are summarized in Table 9.1. For both these conditions, the SF-IPWR can achieve the highest core power level, 139.7% and 140.3% of the reference core power, respectively assuming RCPs of power up to 3.0x are available. Using the AP1000 core enthalpy rise condition, the maximum core power of each design is slightly improved while the pumping power needed is lower. Overall, the SF-IPWR at the AP1000 condition which achieves the maximum core power of 140.3% of the reference core power, limited by the peak fuel temperature constraint, is the best design. Key geometry properties and operating parameters of the selected design are listed in Table 9.2. As used throughout the chapter, Ferroni's selected geometry (D_{ci} = 10.79 mm and t_{web} = 2.89 mm) is used in this SF-IPWR design. The detailed evaluations are presented below.

9.1 The reference condition

At this condition, the inlet temperature and core enthalpy rise are the same as in the reference core. As summarized in Table 8.2, three selected IPWR design choices for this condition are: E-IPWR, SF-IPWR and F-IPWR. The steady state operating parameters (pressure drop, MDNBR and temperatures) are calculated at different core thermal power levels. The thermal power level (measured by percentage compared to the reference power), the coolant flow rates and the core pressure drop provided by different pumping power at those flow rates are summarized in Table 9.3

Table 9.2: Geometry and operating parameters of the selected SF-IPWR design

Characteristic	Unit	Value
COOLING CHANNEL		
Total height	m	3.67
Inner diameter	mm	10.89
Fuel web thickness	mm	2.9
TWISTED TAPES		
Number per cooling channel	–	1
Location	m	1.5
Twist ratio	–	3.5
Length	mm	57.2
OPERATING CONDITION		
Nominal inlet temperature	^oC	280.4
Core outlet temperature	^oC	321.4
Average temperature rise in core	^oC	40.0
Enthalpy rise	kJ/kg	226.2
Core thermal power	MWt	4785.6
Coolant flow rate	kg/s	21157.0
Pumping power (4 loops)	MW	24.0

Table 9.3: Core power and coolant flow rate at different uprate levels

Uprate	Power (MWt)	Flow rate (kg/s)
102%	3479.2	17475.9
105%	3581.6	18349.7
110%	3752.1	19223.5
115%	3922.7	20097.3
120%	4093.2	20971.1
125%	4263.8	21844.9
130%	4434.3	22718.7
135%	4604.9	23592.5
140%	4775.4	24466.3
145%	4946.0	25340.1
150%	5116.5	26213.9

Table 9.4: Core pressure drop compared to pressure drop limits (kPa) at various RCP power ratings

	Pressure drop			Core pressure drop limit				
Uprate	E-IPWR	SF-IPWR	F-IPWR	1.0X	1.5X	2.0X	2.5X	3.0X
102%	148.8	177.8	276.6	233.6	454.6	747.2	1040.8	1333.5
105%	155.7	186.2	290.0	178.0	418.9	708.1	998.2	1287.5
110%	167.5	200.6	311.8	80.3	357.8	641.3	925.7	1209.2
115%	179.8	215.5	334.8	-	294.7	572.5	851.1	1128.8
120%	192.5	231.0	359.0	-	229.5	501.6	774.4	1046.5
125%	205.8	247.0	384.5	-	162.3	428.6	695.7	962.0
130%	219.4	263.5	409.8	-	92.0	352.3	613.2	873.5
135%	233.6	280.6	436.0	-	16.4	269.4	523.2	776.2
140%	248.2	298.2	462.7	-	-	180.3	425.8	670.6
145%	263.2	316.4	490.3	-	-	85.4	321.7	557.3
150%	278.7	335.0	520.4	-	-	-	211.2	436.7

Table 9.5: Maximum core power levels limited by pressure drop for each design at each RCP power level

Design	1.0x RCP	1.5x RCP	2.0x RCP	2.5x RCP	3.0x RCP
E-IPWR	106.0%	122.3%	136.7%	147.3%	U
SF-IPWR	104.6%	119.9%	134.4%	145.2%	U
F-IPWR	N	112.7%	127.2%	138.5%	147.2

N: the pump cannot deliver the required flow, U: the maximum power exceeds the considered power range (up to 150% the reference power)

9.1.1 Pressure drop

Five RCPs with different power levels are considered (1.0x, 1.5x, 2.0x, 2.5x and 3.0x) to provide different levels of core pressure drop limits. Core pressure drop of the designs at different core power levels, which are calculated using the updated Arment pressure drop correlation, and the corresponding pressure drop limits imposed by the RCPs are listed in Table 9.4 and shown in Figure 9-1

The E-IPWR has the lowest pressure drop as expected while inserting full length TTs nearly doubles the core pressure drop in the F-IPWR design and make it unoperable with the reference RCP. If 1.5x RCPs are used, the maximum allowable core power levels are 122%, 120% and 113% for the designs E-IPWR. SF-IPWR and F-IPWR, respectively, and so on. The maximum core power for each design at each pumping power, limited by pressure drop, is listed in Table 9.5.

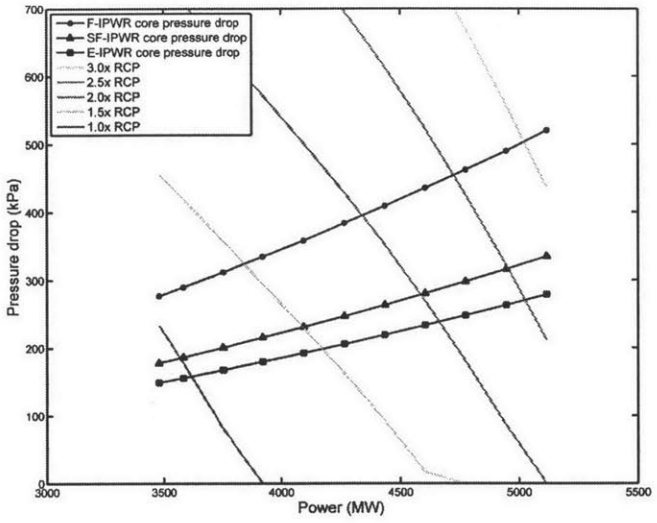

Figure 9-1: Pressure drop of various designs compared to the core pressure drop limits for various RCP power ratings

9.1.2 MDNBR

Table 9.6 and Figure 9-2 show the MDNBR values for the designs calculated by the Arment DNB correlation.

Given the MDNBR limit at 1.85, the E-IPWR power is limited by MDNBR at 3841.3 MWt (112% of the reference power) while the thermal power in the SF-IPWR and F-IPWR design can go up to more than 150% without violating the MDNBR constraint. In this case, a short length TT for each cooling channel as in the SF-IPWR is enough to keep the MDNBR values above the limit; full length TT's would not be necessary.

9.1.3 Fuel temperature

Table 9.7 and Figure 9-3 show the peak fuel temperature in the cores with different designs at different core power levels. The curves for the SF-IPWR and F-IPWR core are almost identical (the difference is only 0.1°C at each core power level) and only ~4°C higher than the design with no twisted tape, E-IPWR. The maximum core power levels limited by the peak fuel temperature constraint for the designs (E-IPWR,

Table 9.6: MDNBR for the designs at different core power levels

Uprate	E-IPWR	SF-IPWR	F-IPWR
102%	2.015	2.332	2.935
105%	1.965	2.294	2.883
110%	1.888	2.236	2.802
115%	1.816	2.185	2.726
120%	1.745	2.129	2.650
125%	1.680	2.075	2.578
130%	1.619	2.025	2.512
135%	1.563	1.979	2.450
140%	1.512	1.937	2.392
145%	1.463	1.898	2.337
150%	1.432	1.869	2.308

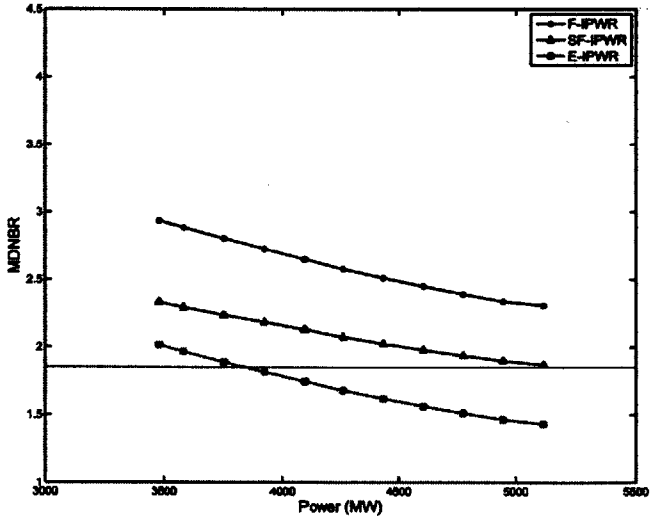

Figure 9-2: MDNBR for the designs at different power levels

Table 9.7: Peak fuel temperature (°C) at different core thermal power levels

Uprate	E-IPWR	SF-IPWR	F-IPWR
102%	564.0	568.1	568.2
105%	570.3	574.3	574.4
110%	580.8	584.6	584.7
115%	591.2	594.9	595.0
120%	601.7	605.3	605.4
125%	612.1	615.5	615.7
130%	622.5	625.9	626.0
135%	632.9	636.1	636.3
140%	643.2	646.4	646.6
145%	653.6	656.6	656.8
150%	663.9	666.9	667.0

SF-IPWR, F-IPWR) are 143.3%, 141.7% and 141.7%, respectively.

9.1.4 Peak inside cladding temperature

The peak inside cladding temperature for the designs are listed in Table 9.8. It can be observed that the existence of TTs inside the cooling channels has very little effect on the cladding temperature. For each core power level, the peak cladding temperature is increased by about 4°C for the F-IPWR and SF-IPWR designs. Also, the temperature increases only by 3-4°C as the core power increase from 102% to 150%. Given the limit at 370°C, the core power can get to 150% without having the cladding temperature exceed the limit value.

9.1.5 Summary

Using the results in the previous sections, the maximum achievable power for each design at each pumping power level can be determined.

E-IPWR

For the E-IPWR design with 1.0x RCP, the maximum core power level is 3616.3 MWt (106.0%) limited by the pressure drop constraint. The core can be uprated by using more powerful pumps. Using 1.5x RCP, the maximum power is 3814.3 MWt

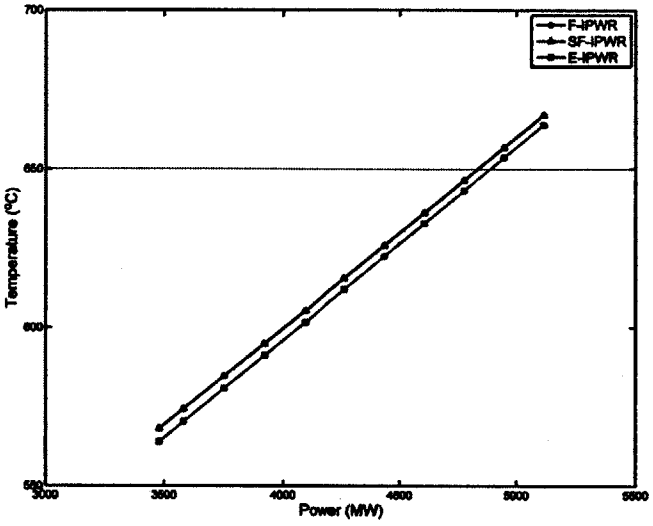

Figure 9-3: Peak fuel temperature at different core thermal power levels

Table 9.8: Steady state peak inside cladding temperature (°C) for the designs at different core power levels

Uprate	E-IPWR	SF-IPWR	F-IPWR
102%	363.2	367.7	367.4
105%	363.4	367.8	367.6
110%	363.9	368.1	367.9
115%	364.3	368.4	368.1
120%	364.7	368.7	368.4
125%	365.1	368.9	368.7
130%	365.4	369.2	369.0
135%	365.8	369.4	369.2
140%	366.1	369.7	369.4
145%	366.4	369.9	369.7
150%	366.7	370.1	369.9

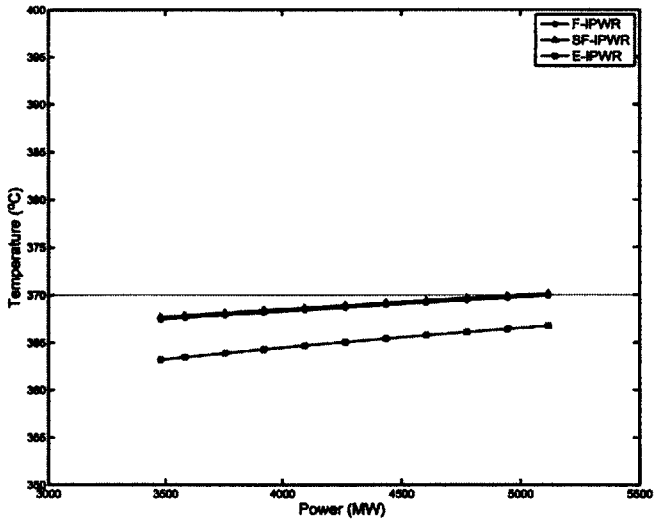

Figure 9-4: Steady state peak inside cladding temperature for the designs at different corepower levels

(111.8%), limited by the MDNBR constraint. This is the maximum achievable power for the design. Using more powerful RCPs would not increase the core power. Figure 9-5 shows the maximum achievable power for the E-IPWR core for each type of RCP. Note that for the 1.5X and higher power RCPs, the maximum core powers are the same at 3814.3 MWt (111.8%) due to the fact that the core power is limiting by the MDNBR constraint. The pumping power required to operate the core at 3814.3 MWt (111.8%) would be lower than the power given by the 1.5X and higher RCPs (optimally at the steady state, the core power is limiting by both the MNDBR and pressure drop constraints).

F-IPWR

For the F-IPWR design, the total RCS pressure drop is much higher than the reference pressure drop so that 1.0x RCPs cannot deliver the required coolant flow (only core power levels with in the range 102%-150% of the reference power are considered). With 1.5x RCPs, the maximum core power level is 3843.2 MWt, limited by pressure drop. For 2.0x and 2.5x RCPs, the values are 4337.8 and 4724.7 MWt, respectively,

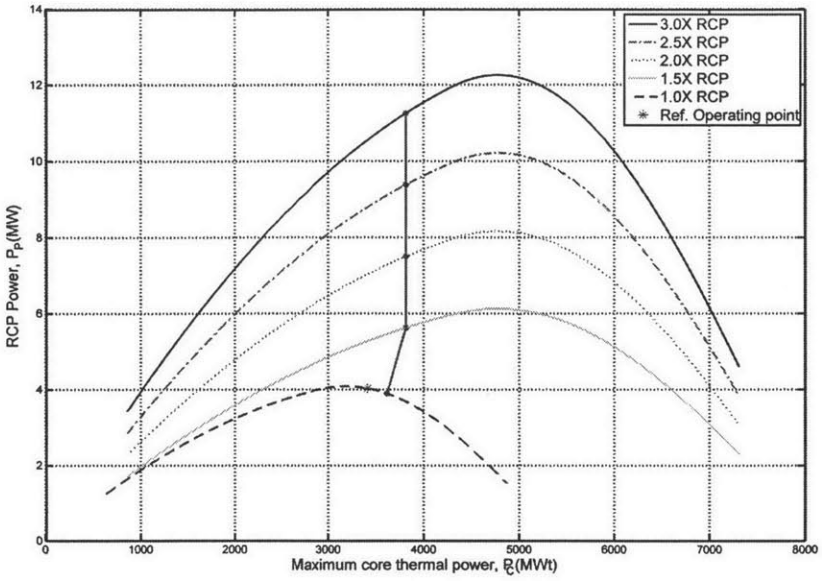

Figure 9-5: Maximum core power for the E-IPWR design for each type of RCP

still limited by pressure drop. Using 3.0x RCPs, the pumps can provide enough power to deliver the required flow for 5021.8 MWt but the maximum power for the core is only 4832.5 MWt, limited by the peak fuel temperature constraint. The maximum core thermal power for each RCP power level is shown in Figure 9-6

SF-IPWR

Similarly for the SF-IPWR design, the maximum achievable core power level if using 1.0x RCPs is 3568.4 MWt slightly lower than that of the E-IPWR design (3616.3 MWt). This is expected as the core power is limited by the pressure drop constraint while inserting TTs in the cooling channel increases core pressure drop. Using 1.5x RCPs, the maximum core power is 4090.2 MWt, still limited by pressure drop. The value for 2.0X RCPs is 4585.8 MWt. For the 2.5x RCPs (and 3.0x RCP), the pumps can deliver the coolant flow required for 4953 MWt (and higher) core power but the maximum achievable core power is 4832.5 MWt, limited by the peak fuel temperature constraint. Figure 9-7 summarizes the results for the SF-IPWR design.

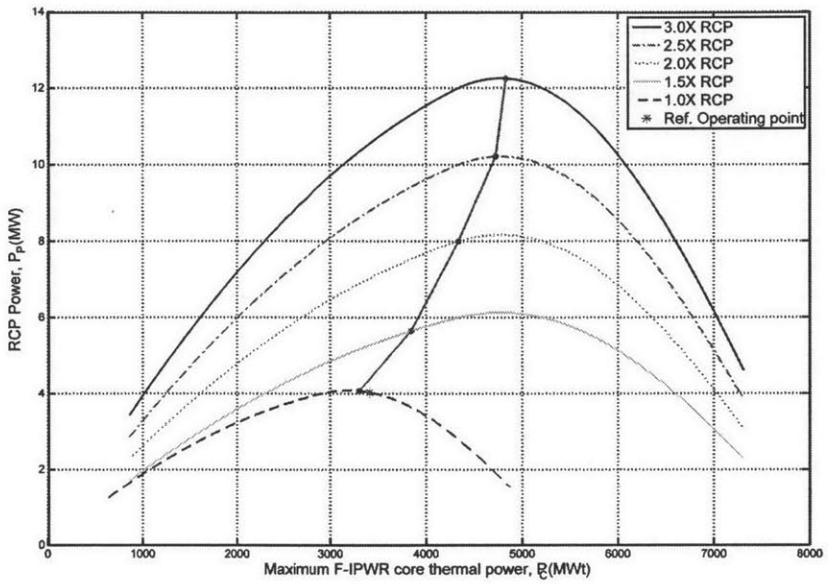

Figure 9-6: Maximum core power for the F-IPWR design for each type of RCP

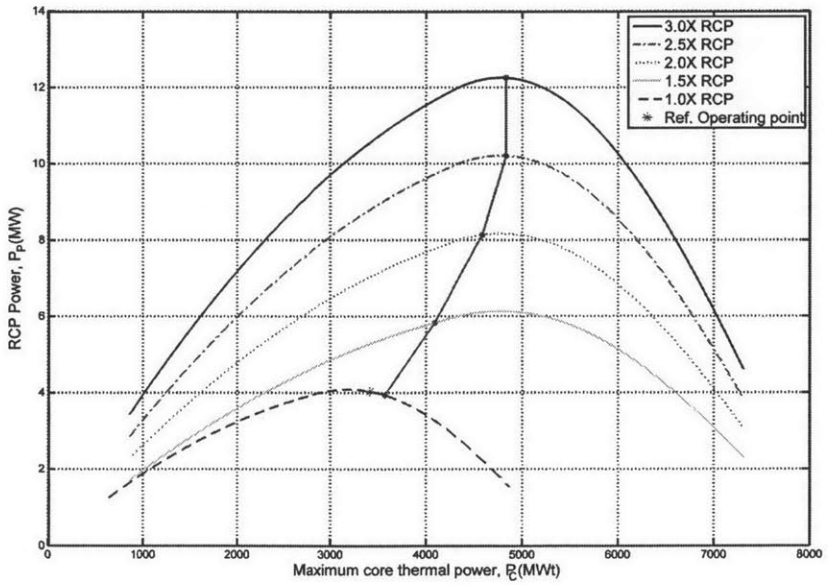

Figure 9-7: Maximum core power for the SF-IPWR design for each type of RCP

Table 9.9: Maximum increased core power (uprate level) limiting by each constraint for the designs

Design	1.0x RCP	1.5x RCP	2.0x RCP	2.5x RCP	3.0x RCP	MDNBR	T_1	T_2	T_3
REF	3.5%	19.6%	32.7%	44.4%	U	0.0	U	6.7%	NA
E-IPWR	4.0%	20.3%	34.7%	45.3%	U	10.6%	41.3%	NA	U
F-IPWR	N	10.7%	25.2%	36.5%	45.2%	U	39.7%	NA	U
SF-IPWR	2.6%	17.9%	32.4%	43.2%	U	U	39.7%	NA	U

N: the maximum core power is lower than the reference core power

NA: not applicable

U: the core power can go higher than 150% (50% uprate) of the reference power without violating the constraint

T_1: The maximum peak fuel temperature

T_2: The maximum average fuel temperature

T_3: The peak inside cladding temperature

Summary

Finally, the maximum core thermal power for the IPWR designs and the reference core limited by each pump power level and other constraints are summarized in Table 9.9 and Figure 9.9. Note that the analyses were performed at 2% more power (and +3.2°C higher inlet temperature). Therefore, the final maximum core power for each design at each condition is calculated by using the maximum core power given in the safety analysis minus 2% the reference core power. From Figure 9.9, it can be observed that the SF-IPWR is the best design for this condition with the maximum core power of 139.7%, limiting by the peak fuel temperature constraint. The pumping power needed is between 2.0x and 3.0x the reference condition.

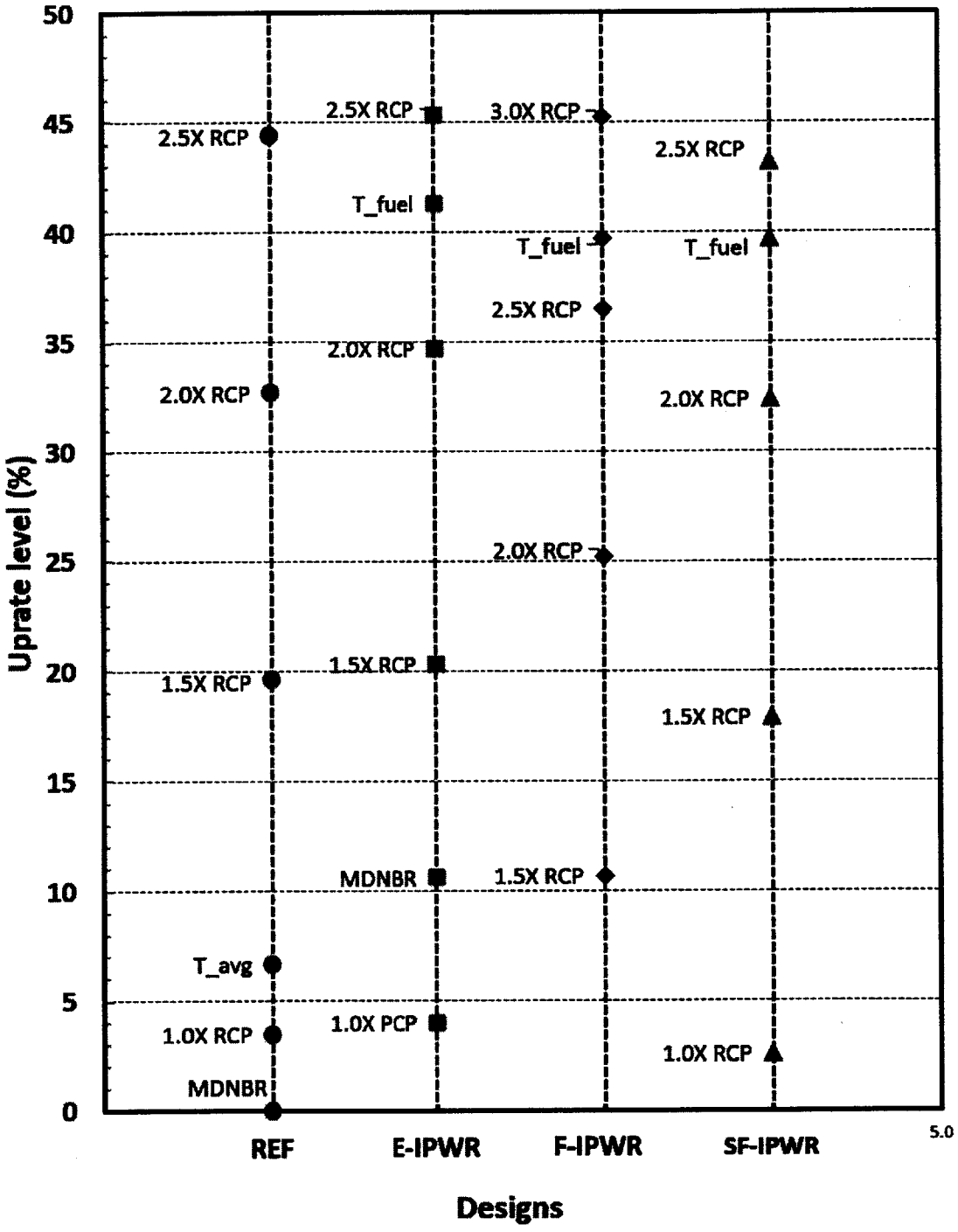

Figure 9-8: Maximum uprate levels (%) limiting by each constraint for the designs

9.2 The AP1000 condition

With this condition, the inlet temperature and the enthalpy rise in the AP1000 design are considered. The enthalpy rise is higher than that in the reference condition, therefore for the same core power level, the required flow rate is lower. As investigated in Section 8.3.2, for the same core power level, the pressure drop is lower and the MDNBR is higher than those values in the reference condition. The designs are expected to perform better in this condition. Three IPWR designs to be evaluated with this condition are: E-IPWR, SF-IPWR and F-IPWR. The core power levels to be considered and the coresponding required flow rate are listed in Table 9.10

Table 9.10: Core power levels and the required flow rates to be considered in the AP1000 condition

Uprate	Core power (MWt)	Flow rate (kg/s)
102%	3479.2	15381.1
105%	3581.6	15833.8
110%	3752.1	16587.5
115%	3922.7	17341.7
120%	4093.2	18095.5
125%	4263.8	18849.7
130%	4434.3	19603.4
135%	4604.9	20357.6
140%	4775.4	21111.4
145%	4946.0	21865.6
150%	5116.5	22619.4

9.2.1 Pressure drop

Core pressure drop and the limit values imposed by different power level RCPs for the three designs are listed in Table 9.11. The values are lower than those in the reference condition due to the lower coolant flow rate at each uprate level as expected. It can

Table 9.11: Core pressure drop and pressure drop limits (kPa) at different core power levels in the AP1000 condition

Uprate	E-IPWR	SF-IPWR	F-IPWR	1.0X	1.5X	2.0X	2.5X	3.0X
102%	116.5	138.6	211.8	508.0	659.9	981.9	1304.9	1626.8
105%	121.6	144.7	221.3	474.4	632.7	951.7	1271.6	1590.7
110%	130.2	155.4	238.6	412.8	586.1	900.2	1215.2	1529.2
115%	139.3	166.4	255.7	344.9	538.0	847.1	1157.2	1466.3
120%	148.6	177.8	273.3	271.2	488.5	792.6	1097.7	1401.9
125%	158.4	189.6	291.5	192.4	437.5	736.7	1036.8	1336.0
130%	168.4	201.9	310.2	108.9	385.0	679.2	974.4	1268.7
135%	178.7	214.5	330.6	21.4	331.0	620.3	910.5	1199.8
140%	189.5	227.5	350.5	-	275.6	559.9	845.2	1129.5
145%	200.5	240.8	370.9	-	218.6	498.1	778.3	1057.7
150%	211.8	254.6	391.8	-	160.3	434.7	710.0	984.5

Table 9.12: Maximum core power (MWt) for the designs limiting by pressure drop in the AP1000 condition

Design	1.0x RCP	1.5x RCP	2.0x RCP	2.5x RCP	3.0x RCP
E-IPWR	4325.9	4990.4	U	U	U
SF-IPWR	4268.7	4892.1	U	U	U
F-IPWR	4089.4	4605.7	U	U	U

also be observed that 2.0X RCPs can deliver the required flow rate for all three designs at the maximum uprate level considered (150%); higher power RCPs would not be necessary. Figure 9-9 shows the core pressure drop curves for the designs and the RCP curves for 1.0x, 1.5x and 2.0x RCPs. The exact maximum core power for each design limiting by each pump is listed in Table 9.12

9.2.2 MDNBR

Similarly, the results for MDNBR for the designs in this condition are listed in Table 9.13 and showed in Figure 9-10. For the E-IPWR, the maximum core power limited by the MDNBR constraint is 4204.4 MWt (123.3% of the reference core power) while the SF-IPWR and F-IPWR can achieve more than 150% uprate without having the MDNBR values below the limit.

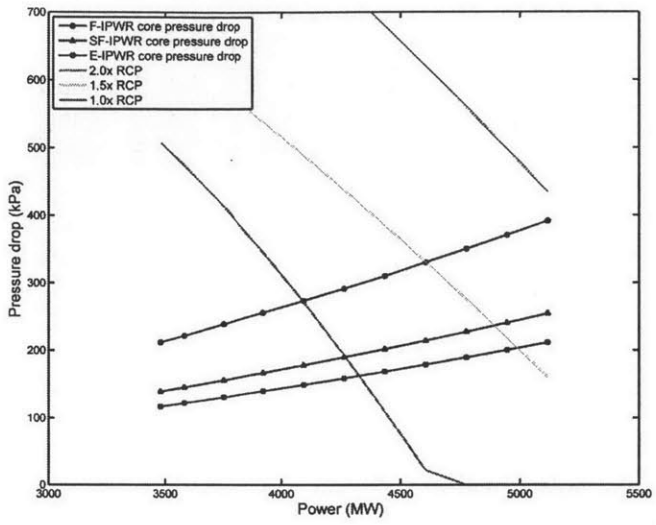

Figure 9-9: Pressure drop of various designs compared to the core pressure drop limits for various RCP power ratings for the AP 1000 core enthalpy rise condition

Table 9.13: MDNBR values for the designs in the AP1000 condition

Uprate	E-IPWR	SF-IPWR	F-IPWR
102%	2.148	2.360	2.981
105%	2.108	2.336	2.946
110%	2.046	2.301	2.892
115%	1.974	2.250	2.820
120%	1.897	2.190	2.739
125%	1.825	2.136	2.664
130%	1.759	2.086	2.594
135%	1.698	2.040	2.530
140%	1.649	1.991	2.481
145%	1.600	1.946	2.434
150%	1.553	1.904	2.386

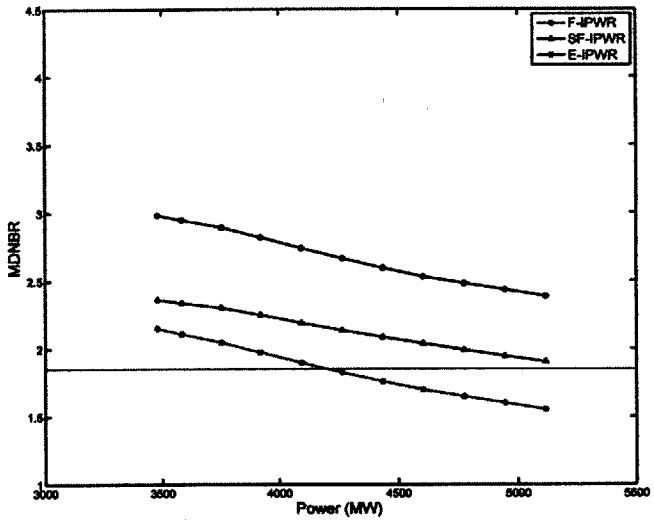

Figure 9-10: MDNBR curves for the designs in the AP1000 condition

9.2.3 Fuel temperature

The peak fuel temperature for the designs in this condition are listed in Table 9.14 and Figure 9-11. It is shown in Figure 9-11 that the curves for the SF-IPWR and F-IPWR are almost identical. Additionally, the temperature values are slightly reduced to lower than those in the reference condition. Not just the pressure drop and MDNBR are improved by using this condition, the fuel temperature is improved as well. The maximum core power levels for the three designs E-IPWR, SF-IPWR and F-IPWR limited by fuel temperature are 4920.8 MWt (144.3%), 4854.5 MWt (142.3%) and 4852.7 MWt (142.3%) , respectively.

9.2.4 Peak inside cladding temperature

The maximum inside cladding for the cooling channels of the designs at different core power levels are listed in Table 9.15. Consider uprate levels up to 150%, the temperatures for the E-IPWR are always below the limit (at 370°C). Those values for the SF-IPWR and F-IPWR slightly exceed the limit at 140% power but only by very small amounts (less than 0.5%) which are negligible. Therefore, it can be

Table 9.14: Peak fuel temperature (°C) at different core power levels in the AP1000 condition

Uprate	E-IPWR	SF-IPWR	F-IPWR
102%	561.6	566.8	566.8
105%	568.0	573.0	573.0
110%	578.5	583.4	583.4
115%	589.0	593.7	593.8
120%	599.4	604.1	604.1
125%	609.9	614.4	614.4
130%	620.3	624.7	624.8
135%	630.8	235.0	235.0
140%	641.1	645.3	645.3
145%	651.5	655.5	655.6
150%	661.9	665.8	665.9

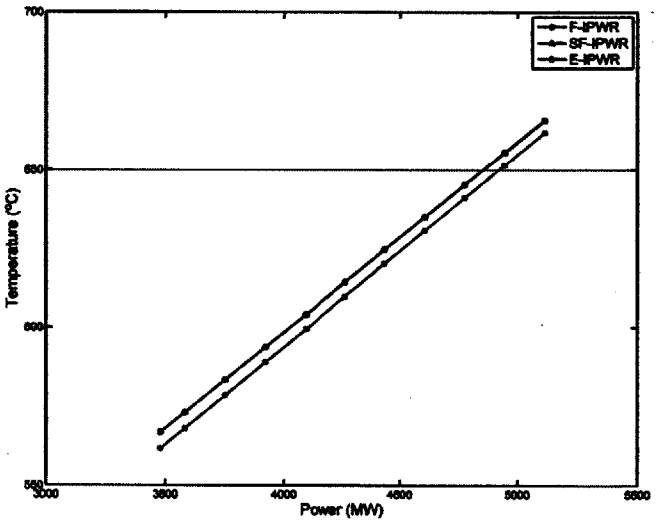

Figure 9-11: Peak fuel temperature at different core power levels in the AP1000 condition

Table 9.15: Maximum inside cladding temperature (°C) for the designs in the AP1000 condition

Uprate	E-IPWR	SF-IPWR	F-IPWR
102%	362.1	367.9	367.6
105%	362.4	368.1	367.8
110%	362.8	368.4	368.1
115%	363.3	368.7	368.4
120%	363.8	369.0	368.7
125%	364.2	369.3	369.0
130%	364.6	369.6	369.3
135%	365.0	369.9	369.6
140%	365.4	370.1	369.9
145%	365.8	370.4	370.1
150%	366.1	370.6	370.3

concluded that the cladding temperature values are always within the acceptable range for all three designs.

9.2.5 Summary

Similar to the method used with the reference condition, the overall maximum achievable core power for each design considering all four thermal hydraulic constraints can be determined using the results provided. The results are presented independently for each design and will be summarized at the end of this section.

E-IPWR

The core power level limited by MDNBR is 4204.4 MWt (123.3%), lower than the value limiting by pressure drop imposed by 1.0x RCPs. Therefore, the overall maximum achievable core power for the E-IPWR design is 123.3%. There is no need to use higher power RCPs in this case. This maximum core power is higher than the value in the reference condition (3616.3 MWt - 106.0%) because of the siginicantly lower core pressure drop. Figure 9-13 shows the maximum core thermal power at for each RCP power level.

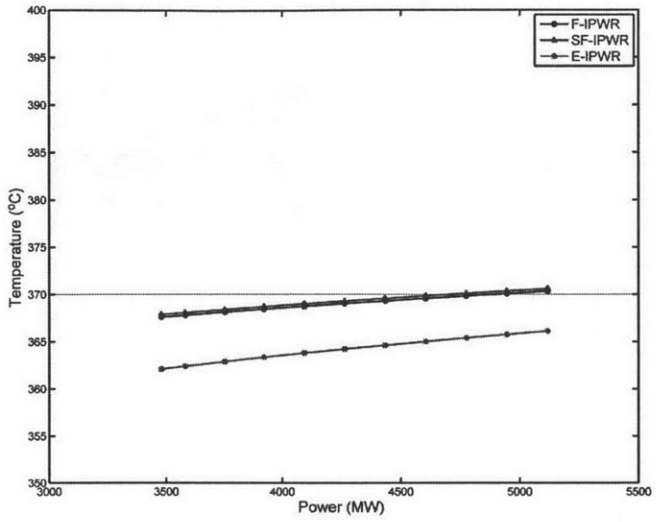

Figure 9-12: Maximum inside cladding temperature for the designs in the AP1000 condition

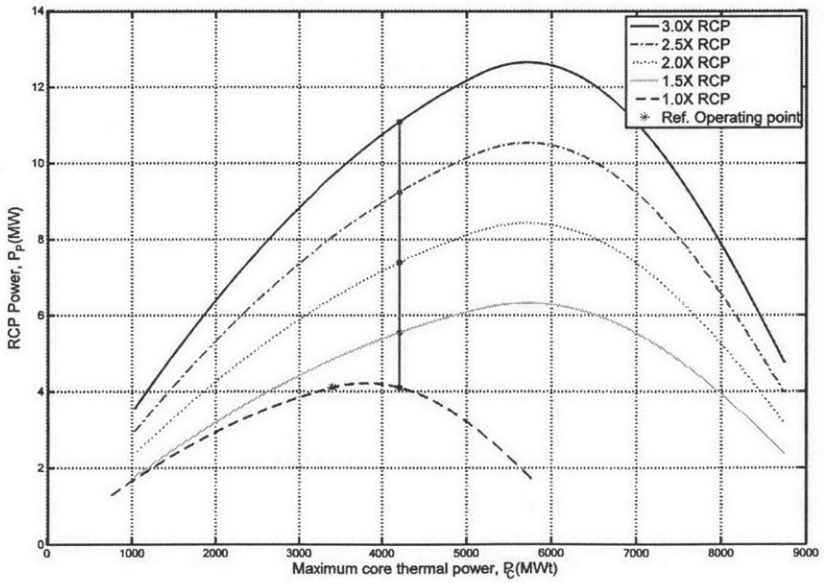

Figure 9-13: Maximum E-IPWR core thermal power in the AP1000 condition

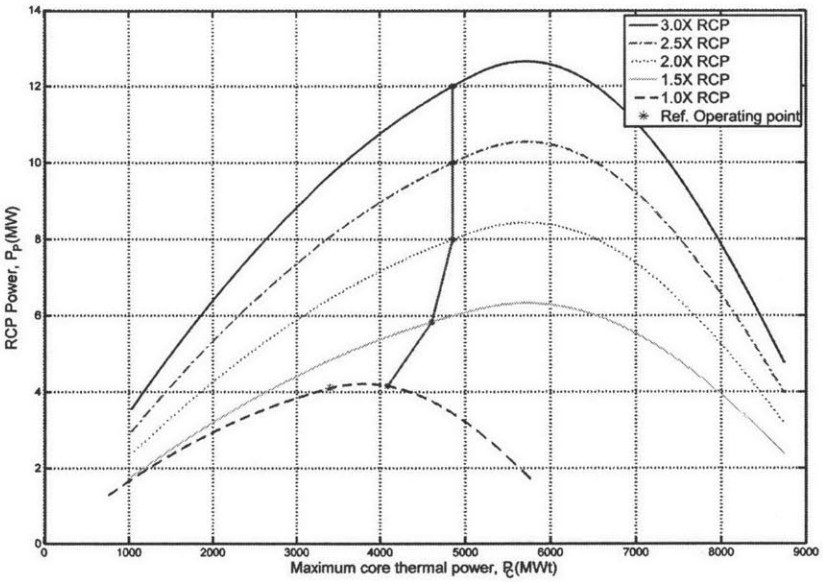

Figure 9-14: Maximum F-IPWR core thermal power in the AP1000 condition

F-IPWR

Consider the F-IPWR design in the 102-150% uprate range, the MDNBR and temperature values are always in their allowable ranges. The core power levels limited by 1.0x RCPs, 1.5x RCPs and fuel temperature are 119.9%, 135.0% and 142.3%, respectively while 2.0x or higher RCPs can deliver the required flow for more than 150% uprate. Therefore, using 1.0x RCPs, the maximum core power is 119.9%, limited by the pressure drop constraint. Similarly, that value for 1.5x RCPs is 135.0% MWt. Using 2.0x or higher power RCPs, the maximum core power is 142.3%, limited by the peak fuel temperature constraint. These results are shown in Figure 9-14

SF-IPWR

For the SF-IPWR design, the maximum core power limited by 1.0x RCPs, 1.5x RCPs and fuel temperature constraint are 125.1%, 143.4% and 142.3%, respectively while the MDNBR and cladding temperatures are always in the allowable range for core power lower than 150% the reference core power. Therefore, using 1.0x RCPs, the

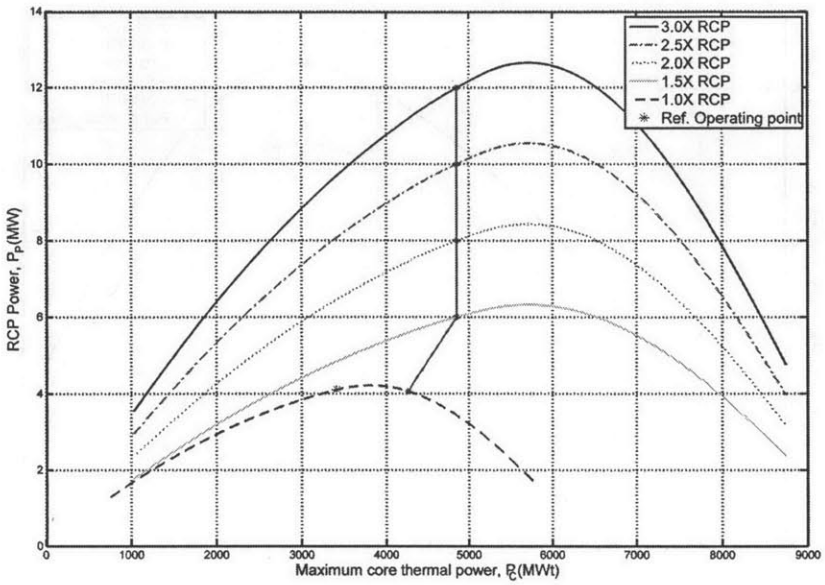

Figure 9-15: Maximum SF-IPWR core thermal power in the AP1000 condition

maximum core power is 125.1%, limited by pressure drop. Using 1.5x RCP, the maximum core power is now 142.3%, now limited by the peak fuel temperature constraint. Using higher power RCPs will not increase the maximum power for the design. These observations are shown in Figure 9-15

Summary

Finally, the maximum core power levels for the designs limiting by each thermal hydraulic design constraints are listed in Table 9.16. From the table it can be observed that the SF-IPWR outperforms the F-IPWR in every condition. And by using 1.5x or higher power RCPs, the SF-IPWR is the best design which gives a maximum core power of 4785.6 MWt (140.3% the reference core power). The results are illustrated in Figure 9-16

Table 9.16: Maximum core power increase (%) for the designs, limited by each design constraint in the AP1000 condition

Design	1.0x RCP	1.5x RCP	2.0x RCP	2.5x RCP	3.0x RCP	MDNBR	T_1	T_2	T_3
REF	24.7%	44.1%	U	U	U	5.1%	U	6.7	NA
E-IPWR	24.8%	44.3%	U	U	U	21.3%	U	NA	U
F-IPWR	17.9%	33.0%	U	U	U	U	40.3%	NA	U
SF-IPWR	23.1%	41.4%	U	U	U	U	40.3%	NA	U

N: the maximum core power is lower than the reference core power

NA: not applicable

U: the core power can go higher than 150% (50% uprate) of the reference power without violating the constraint

T_1: The maximum peak fuel temperature

T_2: The maximum average fuel temperature

T_3: The peak inside cladding temperature

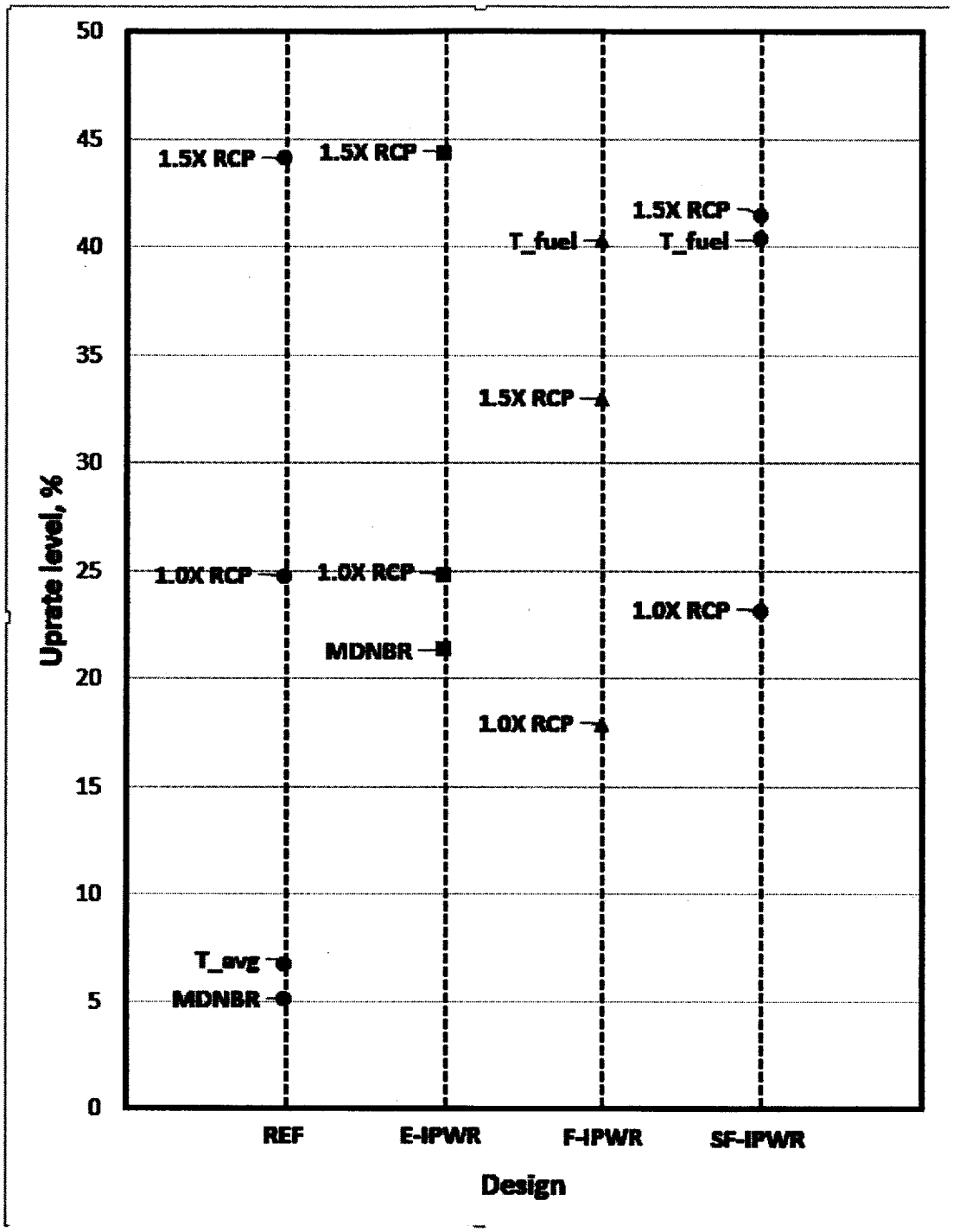

Figure 9-16: Maximum uprate levels for the designs, limited by each design constraint in the AP1000 condition

9.3 Higher enthalpy rise condition

With this condition, the enthalpy rise is even higher than that in the AP1000 condition. As analysised in Chapter 8, the required coolant flow rate is lower therefore the core pressure drop for each design is reduced significantly while the MDNBR profile is worsened. Four IPWR designs were selected for this condition, namely: E-IPWR, F-IPWR, SF-IPWR, and MS-IPWR as listed in Table 8.2. With the inlet temperature at 280.4°C and the enthalpy rise of 261.2 kJ/kg, the required flow rate at different core power levels are calculated and listed in Table 9.17

Table 9.17: Required flow rate at different core power levels with enthalpy rise 262.1 kJ/kg

Uprate	Core power (MWt)	Flow rate (kg/s)
102%	3479.2	13320.1
105%	3581.6	13712.1
110%	3752.1	14364.9
115%	3922.7	15018.0
120%	4093.2	15670.8
125%	4263.8	16323.9
130%	4434.3	16976.6
135%	4604.9	17629.8
140%	4775.4	18282.5
145%	4946.0	18935.7
150%	5116.5	19588.4

9.3.1 Pressure drop

The core pressure drop for the four designs in this condition are listed in Table 9.18. As expected, the core pressure drop values are lower than those in the lower enthalpy rise conditions while the pressure drop limit values are significantly increased. 1.5X RCPs can deliver the required flow rate for all four designs at up to 150%. There is

Table 9.18: Core pressure drop and the core pressure drop limits (kPa) for the designs with enthalpy rise 261.2 kJ/kg

Uprate	E-IPWR	SF-IPWR	MS-IPWR	F-IPWR	1.0X	1.5X
102%	105.3	127.2	139.9	192.6	644.3	775.6
105%	109.9	132.8	146.2	201.3	618.9	754.0
110%	117.7	142.5	157.0	216.2	575.6	717.2
115%	125.8	152.7	168.2	232.3	531.2	679.3
120%	134.2	163.2	179.9	248.3	484.4	640.2
125%	142.9	174.0	191.9	264.8	432.5	600.0
130%	152.0	185.2	204.3	281.8	375.7	558.7
135%	161.3	196.8	217.1	299.3	314.4	516.3
140%	170.9	208.8	230.3	317.2	249.0	472.8
145%	180.9	221.1	243.9	336.8	176.7	428.1
150%	191.1	233.8	257.9	355.8	107.0	382.4

no need to consider higher power RCPs.

9.3.2 MDNBR

The MDNBR values for the designs are listed in Table 9.19. The MDNBR profile of the designs are worsened in this case. For the E-IPWR and SF-IPWR designs, the MDNBR values are much lower that the maximum core power for each design is lower than the reference core. For the MS-IPWR and F-IPWR designs, the MDNBR values are on the same level and higher than the limit for the core power up to 150% the reference core power (the MS-IPWR has slightly higher MDNBR values) while the MS-IPWR gives significantly lower pressure drop. The MS-IPWR design is the best design up to this point.

9.3.3 Fuel temperature

The peak fuel temperatures for each design at different core power levels are listed in Table 9.20. The values are higher than those in the lower enthalpy rise condition. Therefore the maximum core powers limited by the peak fuel temperature constraint are lower than those with the reference and AP1000 condition.

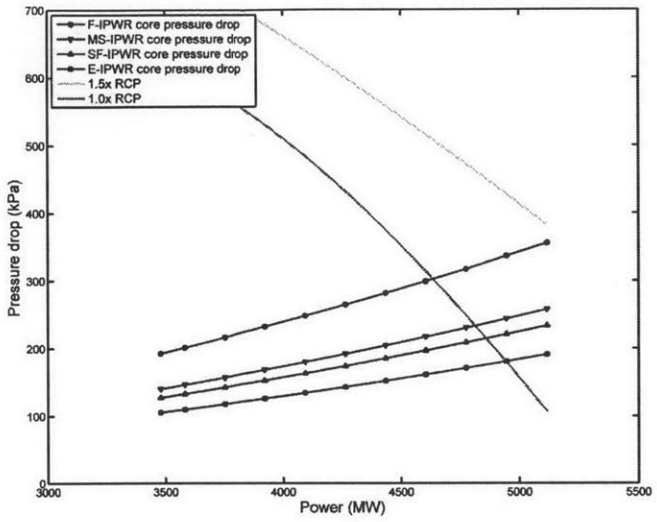

Figure 9-17: Pressure drop of various designs compared to the core pressure drop limits for various RCP power ratings with enthalpy rise 261.2 kJ/kg

Table 9.19: MDNBR for the designs with enthalpy rise 261.2 kJ/kg

Uprate	E-IPWR	SF-IPWR	MS-IPWR	F-IPWR
102%	1.663	1.885	2.324	2.284
105%	1.630	1.858	2.305	2.256
110%	1.583	1.821	2.277	2.217
115%	1.539	1.788	2.252	2.182
120%	1.503	1.762	2.226	2.155
125%	1.471	1.741	2.202	2.133
130%	1.440	1.724	2.177	2.110
135%	1.402	1.727	2.131	2.064
140%	1.362	1.728	2.088	2.022
145%	1.323	1.713	2.045	1.983
150%	1.288	1.695	1.997	1.946

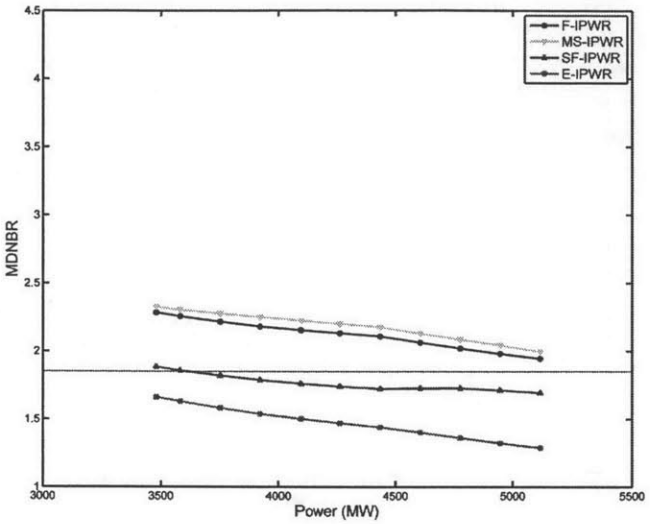

Figure 9-18: MDNBR for the designs with enthalpy rise 261.2 kJ/kg

Table 9.20: Peak fuel temperature (°C) for the designs with enthalpy rise 261.2 kJ/kg

Uprate	E-IPWR	SF-IPWR	MS-IPWR	F-IPWR
102%	567.2	576.1	576.4	576.3
105%	573.6	582.3	582.6	582.5
110%	584.2	592.6	592.9	592.9
115%	594.8	603.0	603.3	603.3
120%	605.5	613.3	613.7	613.7
125%	616.0	623.6	624.0	624.0
130%	627.6	633.9	634.3	634.4
135%	637.1	644.2	644.6	644.6
140%	647.7	654.5	654.9	654.9
145%	658.2	664.8	665.2	665.2
150%	668.6	675.0	675.5	675.5

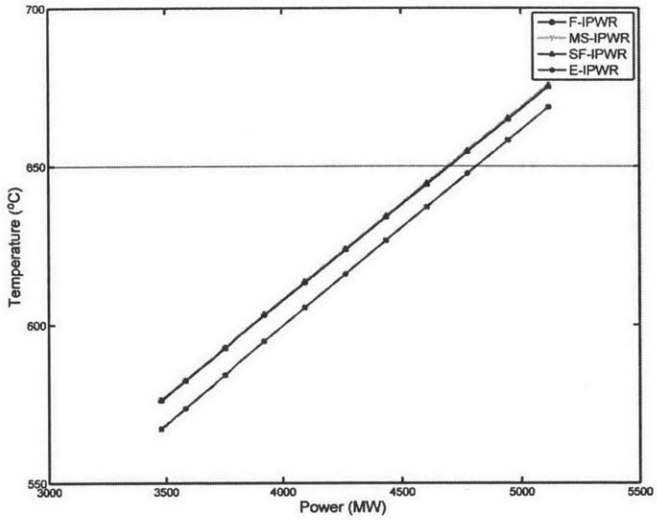

Figure 9-19: Peak fuel temperature for the designs with enthalpy rise 261.2 kJ/kg

9.3.4 Peak inside cladding temperature

Table 9.21 and Figure 9.21 show the result for peak inside cladding temperature for the design in this condition. As with the fuel temperature, the cladding temperature values are higher than those in the previous condition. For the E-IPWR, the cladding temperature goes beyond the limit for core power higher than 110% the reference condition. At 150% core power, the value for the E-IPWR design is less than 1% higher than the limit (370°C) while the values for the other three designs are about 3% higher than the limit.

9.3.5 Summary

Using this higher enthalpy rise condition, the pressure drops for the designs are reduced (improved) while the temperature profiles are worsened. As the cladding temperature exceeds the limit values for every core power level in the 100-150% range, the designs cannot work in this condition. Therefore unless more powerful pumps are not available, the designs perform better in the AP1000 condition. However, it can be observed that adding a second TT in the channels can be a solution when the

Table 9.21: Maximum inside cladding temperature (°C) for the design with enthalpy rise 261.2 kJ/kg

Uprate	E-IPWR	SF-IPWR	MS-IPWR	F-IPWR
102%	368.8	377.8	376.9	377.5
105%	369.2	378.0	377.1	377.8
110%	369.8	378.4	377.4	378.1
115%	370.4	378.8	377.8	378.5
120%	371.0	379.1	378.1	378.8
125%	371.6	379.4	378.4	379.2
130%	372.1	379.8	378.7	379.5
135%	372.6	380.1	379.0	379.8
140%	373.1	380.4	379.2	380.1
145%	373.6	380.7	379.5	380.4
150%	374.0	381.0	379.8	380.7

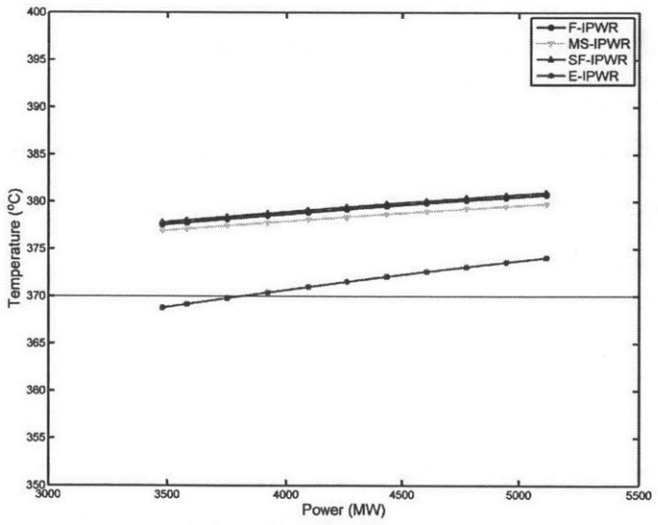

Figure 9-20: Maximum inside cladding temperature for the design with enthalpy rise 261.2 kJ/kg

SF-IPWR design cannot maintain the MDNBR above the limit value. This problem occurs for designs with very high enthalpy rise as considered above or designs with different geometry (different combination of cooling channel inside diameter and fuel web thickness) when the MDNBR value at some location downstream from the first TT drops below the DNBR value at the TT. A second TT is needed for each channel and the MS-IPWR must be used to replace the SF-IPWR.

Chapter 10

Conclusions and future work

10.1 Summary

10.1.1 PWR designs

In Chapter 7, possible uprating options for the reference PWR design using higher power RCPs were investigated. The results showed that for the same inlet and outlet temperature condition, the MDNBR value decreased as the core power increased although the coolant flow rate also increased proportional to the core power increase. Since the MDNBR limit was fixed at the reference value, the core could not achieve higher power than its reference power. Therefore to increase the PWR core power, the DNB performance needs to be improved. For the investigations in Chapter 7, since the geometry of the PWR was fixed, the only option to improve the DNB profile was to reduce the coolant inlet temperature while maintaining the coolant flow rate level. For this condition, the inlet temperature and the enthalpy rise of the PWR AP1000 design were used. The result showed that the DNB profile was indeed improved and the core power could be uprated. The maximum power for the reference PWR core at the AP1000 condition was 105% reference power. This was not much an increase and higher power RCPs were not necessary.

There is another option to uprate the PWR core power, which is to improve the DNB profile by redesigning the core geometry. An investigation of uprating PWRs

Table 10.1: IPWR design choices investigated in Chapter 8

Design choices		Twisted tape properties
Ferroni's	E-IPWR	No twisted tape
	H-IPWR	Long TT in the top 1.6m, y=2.5
	S-IPWR	3 short TTs at z=2.07, 2.54 and 3.08m; y=2.5
Nguyen's (this thesis)	F-IPWR	Full length twisted tape, y=10
	SO-IPWR	One short TT at its optimal location, y=2.5 to 5
	SF-IPWR	One short TT at z=1.5m, y=2.5 to 5
	MS-IPWR	Two short TTs at z=1.3m and 2.2m, y=2.5

using this option was performed by Shuffler at al.[23]. The result showed that by redesigning the core geometry and using more but smaller diameter fuel rods, the PWR can be uprated to up to 126.8% of the reference power. Although the authors used a different PWR as the reference core with the reference power at 3800 MWt, the uprate level for PWRs of the size of the Seabrook PWR can be expected to be on the same level.

10.1.2 IPWR designs

Similarly, the IPWR design has the same problems. The maximum power of the Ferroni E-IPWR is 4078 MWt or 119.6% of the reference design power, limited by the MDNBR constraint. To get to higher core power, the DNB profile of the core needs to be improved (and higher power RCPs may be needed to deliver the increased coolant flow rate). Inserting twisted tapes as swirl flow promoters in the cooling channel is an option. Ferroni (2010) investigated two different cooling channel designs with twisted tapes, namely: H-IPWR and S-IPWR. However, based on the performance of these three design, the E-IPWR was still selected as the best design. The Ferroni IPWR designs and new designs with twisted tapes are summarized in Table 10.1. For all cases, the channel diameter and fuel web thickness were maintained constant at D_{ci}=10.79 mm and t_{web}=2.89 mm.

In Chapter 8, the three Ferroni IPWR designs were re-investigated using updated pressure drop and DNB correlations developed by Arment (2012) [7]. The results showed that for two cooling channel designs with twisted tapes (H-IPWR and S-

IPWR) the DNB improvement was minor while the pressure drop increase was significant, which were the reasons that made these two designs perform poorer than the E-IPWR. Based on the DNB profiles, new channel designs, SO-IPWR, SF-IPWR, MS-IPWR and F-IPWR, were proposed to effectively improve the MDNBR while keeping the core pressure drop small.

The SO-IPWR design uses one twisted tape in each cooling channel at its optimal location which changes as the core thermal power for each channel varies. This made the design impractical while also its performance was not really better than the SF-IPWR (similar design except that the twisted tape location is fixed at z=1.5m in the channel). Therefore the SF-IPWR was selected as the better design and the SO-IPWR was eliminated.

The MS-IPWR uses two twisted tapes in each cooling channel to keep the MDNBR above the limit value when one TT is not enough. For the core power within the range 100-150% of the reference power, this only occurs when the enthalpy rise is so high that the required flow rate is significantly lower than that in the reference condition which results in a worse DNB profile. Therefore, the MS-IPWR was selected only for the higher enthalpy rise condition.

The F-IPWR was also investigated due to the fact that it may be easier to manufacture the fuel assembly with full length twisted tapes. The full length twisted tape in each cooling channel, however, significantly increases the pressure drop accross the channel. Much higher pumping power is needed to operate a F-IPWR core which leads to a poorer performance of the F-IPWR design compared to the SO-IPWR and SF-IPWR designs.

Also in Chapter 8, for each new design in each enthalpy rise condition, a higher twist ratio was shown to increase the DNB improvement while reducing the pressure drop increased by the presence of the twisted tape. Considering the trade-off between these effects on DNB and pressure drop, an optimal twist ratio was selected for each design as listed in Table 10.1 as based on the extensive results reported in Table 8.2.

The prefered designs E-IPWR, F-IPWR, SF-IPWR and MS-IPWR were evaluated further in Chapter 9. The assembly geometry selected by Ferroni (2010) (D_{ci} =

$10.79mm$ and $t_{web} = 2.89mm$) was used. For these new designs, as the core power increased, the required coolant flow rate also increased which would then resulted in higher RCS pressure loss (the core pressure drop and therefore the RCS pressure loss were further increased by the presence of twist tapes in the cooling channels). Hence, higher power RCPs are needed for these "uprated" IPWRs. For the investigations of Chapter 9, RCPs of power up to 3.0 times the reference RCP were assumed to be available. The characteristics of these higher power RCPs were presented in Chapter 6. The results of Chapter 9 showed that for both the reference and the AP1000 condition, the SF-IPWR gave the highest power and required the least pumping power (among designs with twisted tapes). Therefore, the SF-IPWR design with the AP1000 enthalpy conditions and 1.5x RCP was selected as the optimal IPWR design.

10.2 Conclusions

As investigated in Chapter 8 and Chapter 9 , the SF-IPWR was selected as the best IPWR design. At the AP1000 core enthalpy rise condition, the SF-IPWR design with the Ferroni selected geometry can operate with 1.5x RCP at the thermal power up to 140.3% of the reference power (3411 MWt), limited by the fuel temperature design constraint. Also, as analyzed by Ferroni (2010), the effect of short length twisted tapes on quenching time in LOCA reflood is negligible. Figure VIII-10 in his thesis [1] plotted the inside cladding temperatures of the E-IPWR (empty cooling channel) design and S-IPWR design (3 short twisted tapes in each cooling channel) vs. time in case of a LOCA. The S-IPWR quenching time is higher by about 10%. With the selected SF-IPWR design using only one twisted tape per channel, the quenching time increase is expected to be less significant.

Since there is no option to significantly reduce the fuel temperature when the geometry of the system is fixed, the only way to achieve further higher core power is to change the cooling channel diameter and fuel web thickness combination. These are the two key characteristics of Ferroni's selected geometry, in which the cooling channel inner diameter $D_{ci} = 10.79mm$ and the fuel web thickness $t_{web} = 2.89mm$.

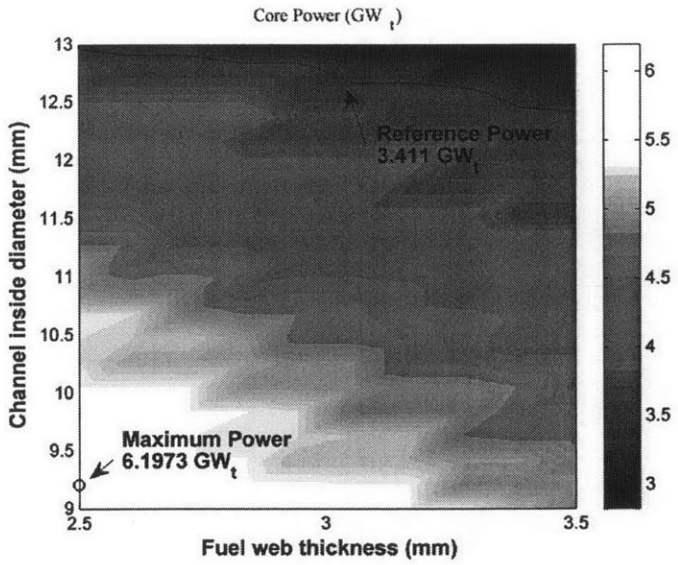

Figure 10-1: Core power map for the SF-IPWR using 3.0x RCPs at the AP1000 enthalpy conditions

By varying these two parameter, the new geometries offer the possibility to reduce the steady state fuel temperature and therefore allow the SF-IPWR design to operate at even higher thermal power.

To investigate this option of further uprating the IPWR core, the updated Ferroni code was used to calculated the maximum achievable core power of the SF-IPWR design using 3.0x RCPs at the AP1000 core enthalpy rise conditions for different core geometry with the channel inner diameter, D_{ci},varying from 9 to 13 mm and the fuel web thickness, t_{web}, varies from 2.5 to 3.5 mm.. The results are shown as the power and limiting parameter maps in Figure 10-1 and 10-2.

From the power and limiting constraint maps, the maximum core power for the SF-IPWR design is 6197.3 MWt (181.7% the reference core power), achieved by decreasing D_{ci} from 10.89 to 9.2 mm and t_{web} from 2.89 to 2.5 mm, the maximum achievable of the SF-IPWR significantly increases from 140.3% to 181.7%, limited by the pressure drop constraint. This result confirms the possibility of an optimal geometry for the SF-IPWR design which will further increase the core power of the design. However, as investigated by Ferroni (2010)[1], the use of smaller diameter cooling channels would increase the inside cladding temperature in case of a loss-of-

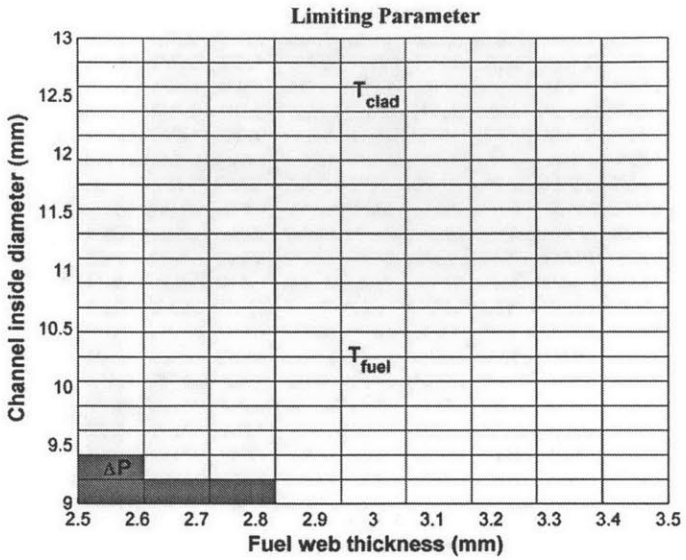

Figure 10-2: Limiting constraint map for the SF-IPWR using 3.0x RCPs at the AP1000 enthalpy conditions

coolant accident. Figure VIII-8 in Ferroni's thesis[1] illustrates that reduction of Dci from 12mm to 9mm increase the quenching time by about 100s, from about 380s to 480s. Nevertheless 9 mm inside diameter for the cooling channels may still be considered acceptable .

10.3 Future work

10.3.1 Pressure drop and DNB tests

While the pressure drop and DNB correlations selected and developed by Arment were compared to those of Ferroni (2010) and some experimental data, test results are still needed to further validate and confirm their goodness. This section outlines major points of the pressure drop and DNB tests which should be conducted in the future.

Pressure drop tests

The Arment pressure drop correlation gives options to predict the pressure drop across cooling channels or pipes with both pure axial flow and swirl flow (generated by a long twisted tape, one or multiple short length twsited tapes). It covers the range of the flow from single-phase liquid to two-phase annular flow. The flow is heated by either uniform or (chopped) cosine heat flux. . A more comprehensive test at heated conditions would be useful to confirm the goodness of the correlation for application to IPWR design conditions:

- Empty channels (pure axial flow)
- Channels with full length twisted tapes (swirl flow)
- One short length twisted tape per channel (swirl flow with decay regions). The position of the twisted tape can be changed to cover different range of the flow.
- Channels with multiple short length twisted tapes

As mentioned, similar but isothermal pressure drop tests were conducted by Ferroni (2010) [1] at MIT for the cases with empty channels, full length twisted tapes and multiple short length twisted tapes (at specific fixed locations). The equipment for those tests can be reused as a starting point for this comprehensive test. For simplification, a uniform heat flux should be used. The system pressure may not necessary be 15.0 MPa (as in the cases with IPWR designs) but should be as close as possible. In particular the two phase region characteristic of an IPWR channel at full power needs to be tested.

DNB tests

Due to the lack of CHF data for (decaying) swirl flow generated by a long twisted tape or multiple short length twisted tapes, a comprehensive DNB test is also necessary. The same setup for the pressure drop tests presented above could be used in this case. Furthermore, the pressure drop and DNB tests should be conducted simultaneously

for the sake of time efficiency as well as conditioning consistency. As CHF predictions by the base DNB correlation (Groeneveld[17]) depend significantly on the heat flux profile, a chopped cosine heat flux should be use to simulate the condition of IPWR cooling channels at the operating conditions

10.3.2 Analyses

Reactor coolant pumps

For the studies performed in this thesis, more powerful pumps were assumed to be available in the near future and were modeled based on typical WEC pumps with the assumption that the same technology (which leads to similar characteristic curve) is used for the new RCPs. In the future, however, an analysis based on pump characteristic of the current state of technology should be performed to model high power RCPs more accurately.

Safety analyses

The designs in this thesis were evaluated using the five design constraints in steady state conditions and the transient LOCA performance was assessed using Ferroni's Figure VIII-10[1]. While the results of these studies can be used to eliminate inappropriate designs, they cannot ensure the selected design can operate safely in full reactor conditions. Therefore, more thermal hydraulic and mechanical safety analyses in steady state, transient and accident conditions should be also be performed. Specifically, the core performance analysis for the complete loss of flow accident (CLOFA) needs to be first performed.

Geometry

As analyzed in Section 10.2, choosing a new assembly geometry allows the design to achieve even higher core power. To select the optimal geometry for the SF-IPWR, further safety analyses in steady state and also in a LOCA need to be performed.

Appendix A

Assessment of the difference between Ferroni's and Arment's pressure drop predictions

Results in Chapter 4 showed that the difference between Ferroni's and Arment's pressure drop predictions is quite significant, even just for a simple empty channel case (axial flow with no twisted tape). This appendix takes a closer look at these correlations to determine the factor causing them to give divergent pressure drop predictions.

Consider Ferroni's selected E-IPWR core (31603 cooling channels with $D_{ci} = 10.79mm$, $t_{web} = 2.89mm$) operating at 4.0 GW at the reference enthalpy rise condition ($\Delta h = 195.2kJ/kg$). With these conditions, the mass flow rate through each channel can be calculated as:

$$\dot{m} = \frac{4.0GW}{31603 \times 195.2kJ/kg} = 0.648kg/s$$

The equilibrium quality and pressure loss factor predicted by the two correlations are calculated and plotted in Figures A-1 and A-2, respectively. Figure A-1 shows that the flow in the channel can be consider mostly single phase. In the single phase region, the acceleration loss predictions are the same between the two correlations

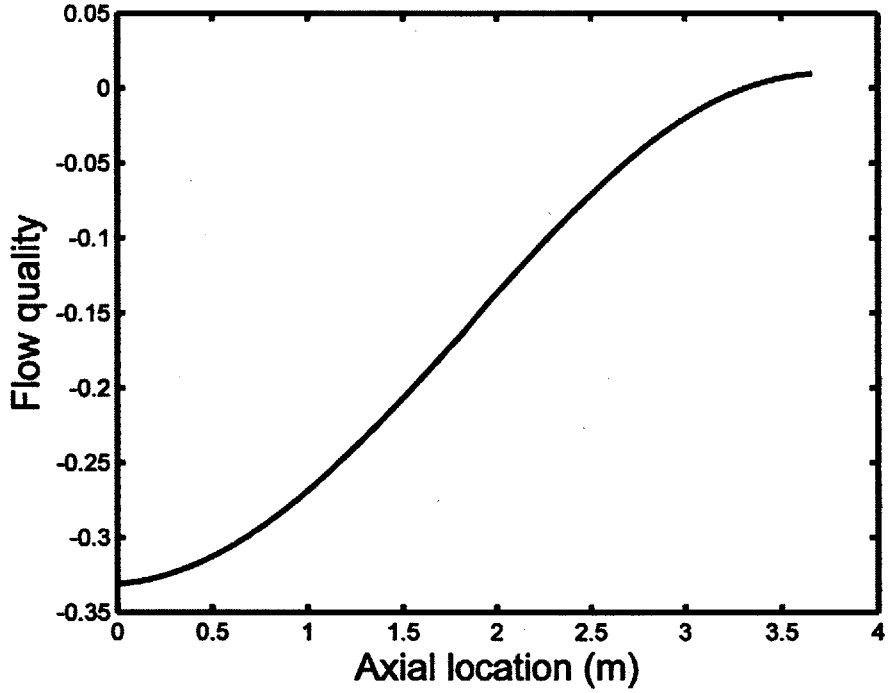

Figure A-1: Equilibrium quality in a hot channel with D_{ci}=10.79mm, flow rate 0.648 kg/s and core power 4.0GW

and so are the gravity losses. The difference between the two correlations is caused by the friction loss factor in the single phase region.

To see this single phase difference more clearly, the core power is lowered to 1.0GW while keeping the flow rate the same (0.648kg/s for each channel). The flow in each channel is now pure subcooled liquid, as shown in Figure A-3. Similar to the result at core power of 4.0GW, the only difference between the two correlations in this condition is caused by the friction loss factors since the distance between the two fiction loss curves increases continuously with axial location.. The detailed results are shown in Figure A-4.

To explore more in the two phase region, the core power is increased to 6.0GW while the mass flow rate is kept at 0.648 kg/s per channel. The flow in the upper half of each channel is now two phase as shown in Figure A-5. The pressure drop prediction results are shown in Figure A-6. As for the other two cases, in the single phase region only the friction losses are different between the two correlations. In

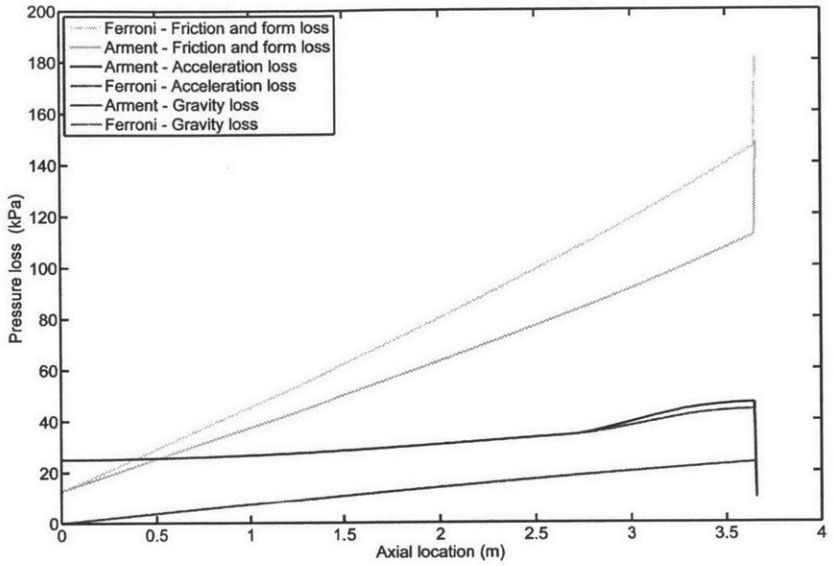

Figure A-2: Pressure drop predictions by Ferroni's and Arment's correlations for the channel with D_{ci}=10.79mm, flow rate 0.648 kg/s and core power 4.0GW (gravity loss curves overlap)

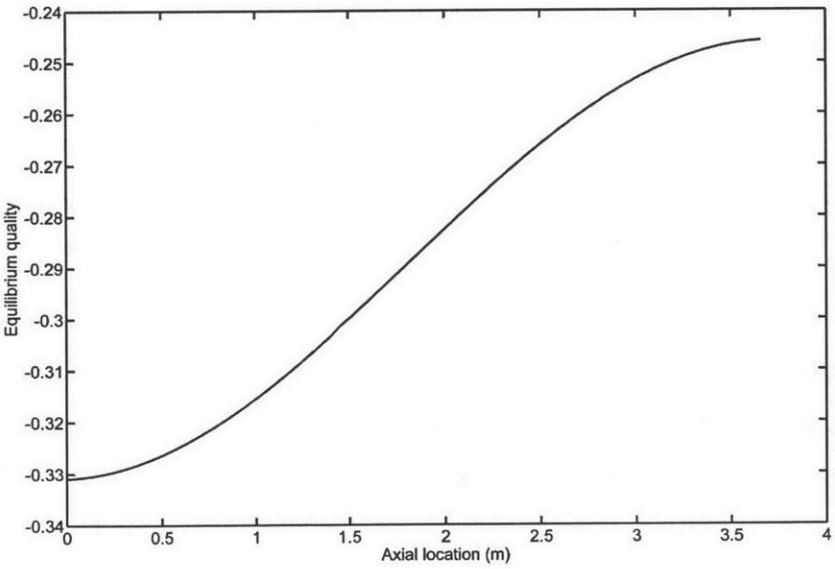

Figure A-3: Equilibrium quality in a hot channel with D_{ci}=10.79mm, flow rate 0.648 kg/s and core power 1.0GW

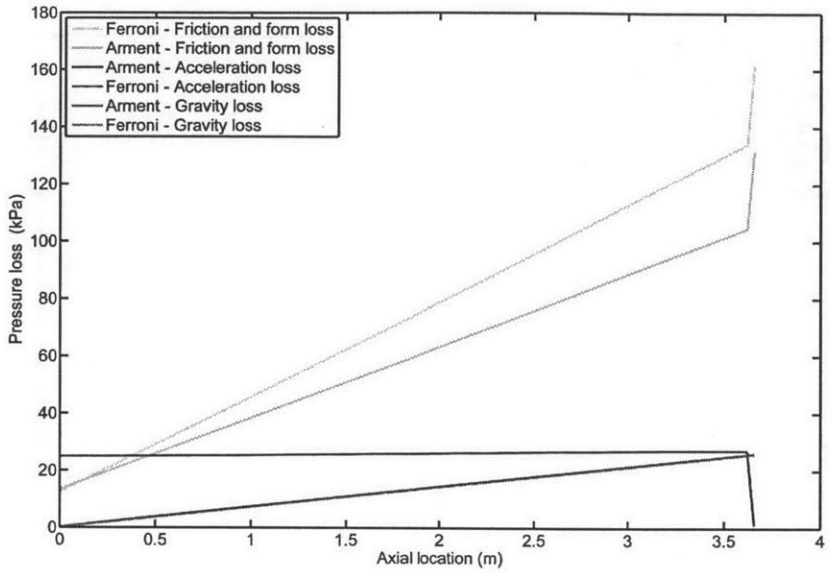

Figure A-4: Pressure drop predictions by Ferroni's and Arment's correlations for the channel with D_{ci}=10.79mm, flow rate 0.648 kg/s and core power 1.0GW (gravity loss curves overlap)

the two phase region, the two gravity loss curves are identical while the difference between the two acceleration curves is still negligible. The difference between the two phase friction factor losses is insignificant as well in this case since the distance between the two friction loss curves is almost the same through the whole region of two phase flow, i.e for axial location greater than about 2m.

Finally, these results show that the difference between the pressure drop predictions by these two correlations is caused by the friction factors in the single phase region. To calculate the friction loss, Ferroni uses Eqn. 4.8 which accounts for the surface roughness of the channels while Arment uses Eqn. 4.14 which ignores the channel roughness. The difference between these two friction factor formulas yields the divergent predictions by the two correlations.

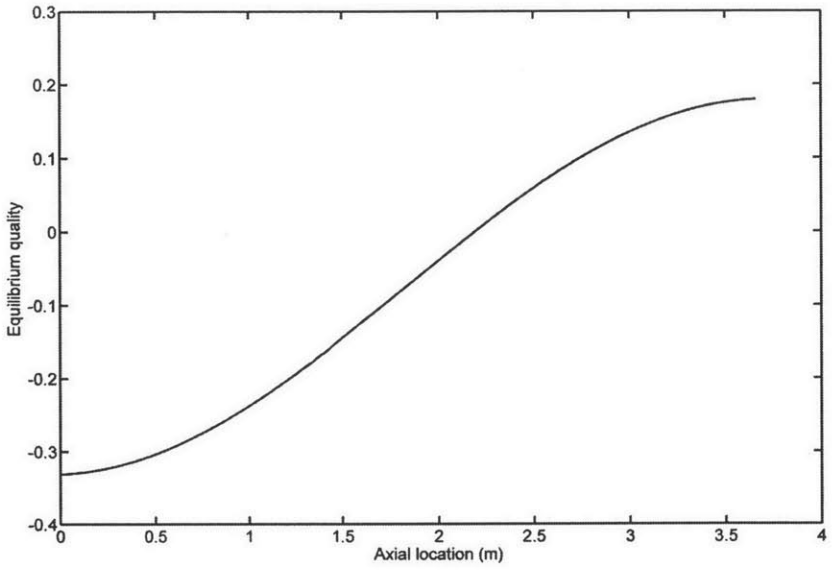

Figure A-5: Equilibrium quality in a hot channel with D_{ci}=10.79mm, flow rate 0.648 kg/s and core power 6.0GW

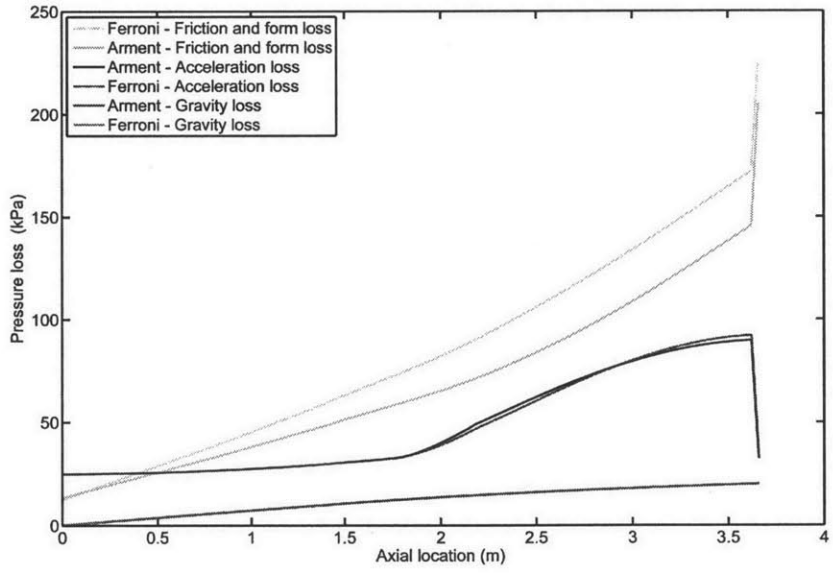

Figure A-6: Pressure drop predictions by Ferroni's and Arment's correlations for the channel with D_{ci}=10.79mm, flow rate 0.648 kg/s and core power 6.0GW (gravity loss curves overlap)

Appendix B

MATLAB Codes

This chapter presents the supplemental MATLAB scripts written during this study by the author of this thesis. These codes consist of two parts:

- RCP codes (#1): Containing the codes used to plot the characteristic and power curves of the typical and higher power RCP and also the core pressure drop imposed by those RCPs.
- Channel analysis codes (#2): Containing channel analysis codes written by Ferroni(2010) and Arment(2012) but modified and updated to be compatible to each other.

Please note that these two (#1 and #2) are just supplemental codes that require the full IPWR code (#3), written by Ferroni (2010), updated during this study (as described in Chapter 3) to work. All these code sets are submitted along with this thesis and will be available at the MIT NSE library.

RCP codes:

```
function [dp_co] = dP_limit(Pth,P,Tc,ent_rise,f_r,h_r)
% This function calculate the core pressure drop limit imposed by a RCP
%Pth: Thermal power in W
%P: Operating pressure in MPa
%Tc: Cool leg temperature, in oC
%Th: Hot leg temperature, in oC
%f_r: Flow increase factor
%h_r: Total head increase factor

% Created by Tat Nghia Nguyen, MIT'14 |nghiant@mit.edu

P=10*P; %Pressure in bars
h_out=XSteam('h_pT',P,Tc)+ent_rise*1e-3;
Th=XSteam('T_ph',P,h_out);
Ta=(Tc+Th)/2;
rho_c=XSteam('rho_pT',P,Tc);
rho_h=XSteam('rho_pT',P,Th);
rho_a=XSteam('rho_pT',P,Ta);
mdot=Pth/ent_rise;
Q=mdot/(4*rho_c);
%%%%%%%%%%%%%%%%%%%%
X=1:0.01:8.5;
Y=X;
for i=401:length(X)
    Y(i)=RCP_total_head(X(i));
end
for j=1:400;
k=401-j;
Y(k)=interp1(X(k+1:length(X)),Y(k+1:length(X)),X(k),'linear','extrap');
end

X=f_r*X;
Y=h_r*Y;
deltah=bsearch(X,Q,Y);
k=[0.939498 0.330773 0.548069 0.059101];
rho=[rho_a rho_c rho_a rho_h];
dp_pu=rho_c*9.81*deltah/1000;
dp_ot=0.5*mdot^2*sum(k./rho)/1000;
dp_co=dp_pu-dp_ot;
if dp_co<=0;
    dp_co=0.01;
end
end
```

```
% This files is used to plot the characteristic and power curves for the
% typical and higher power RCPs

% Created by Tat Nghia Nguyen, MIT'14 |nghiant@mit.edu
```

```
clear all
close all
clc

pos=[60 60 1357 910];
set(0, 'DefaultFigurePosition', pos);
set(0,'DefaultAxesFontName', 'Helvetica')
set(0,'DefaultAxesFontSize', 12)
addpath('C:\Users\TatNghia\Desktop\P2Codes\Plotting_supp');

X=1:0.01:8.5;
Y=X;
for i=401:length(X)
    Y(i)=RCP_total_head(X(i));
end
for j=1:400;
k=401-j;
Y(k)=interp1(X(k+1:length(X)),Y(k+1:length(X)),X(k),'linear','extrap');
end

Q=X;
h=Y;

Q1=1.5*Q;
h1=1*h;

Q2=1.5*Q;
h2=1.333*h;

Q3=1.5*Q;
h3=1.667*h;

Q4=1.5*Q;
h4=2*h;

ent_rise=195.2e3;
Tc=293;
rho_c=XSteam('rho_pT',155.1,Tc);
Q_r=3411e6/(4*ent_rise*rho_c);
h_r=bsearch(Q,Q_r,h);

figure(1)
plot(Q4,h4,'k-','LineWidth',2)
hold on
plot(Q3,h3,'m-.','LineWidth',2)
plot(Q2,h2,'r:','LineWidth',2)
plot(Q1,h1,'g-','LineWidth',2)
plot(Q,h,'b--','LineWidth',2)
axis([3 11 0 300])
xlabel('\fontsize{16}Flow rate, Q(m^3/s)')
ylabel('\fontsize{16}Total head, \Deltah(m)')
legend('\fontsize{16}\fontsize{16}3.0x power RCP','\fontsize{16}2.5x power
RCP','\fontsize{16}2.0x power RCP','\fontsize{16}1.5x power
RCP','\fontsize{16}Typical RCP')
plot(Q_r,h_r,'r*','MarkerSize',10)
```

```
text(1.02*Q_r,1.02*h_r,'Ref. Operating point','FontSize', 16)
grid on
plotfixer_paper
export_fig('Headcurve','-tif','-nocrop','-transparent','-r150')
hold off

figure(2)
plot(Q4*(4*ent_rise*rho_c)*1e-6,c*h4.*Q4*1e-6,'k-','LineWidth',2)
hold on
plot(Q3*(4*ent_rise*rho_c)*1e-6,c*h3.*Q3*1e-6,'m-.','LineWidth',2)
plot(Q2*(4*ent_rise*rho_c)*1e-6,c*h2.*Q2*1e-6,'r:','LineWidth',2)
plot(Q1*(4*ent_rise*rho_c)*1e-6,c*h1.*Q1*1e-6,'g-','LineWidth',2)
plot(Q*(4*ent_rise*rho_c)*1e-6,c*h.*Q*1e-6,'b--','LineWidth',2)
xlabel('\fontsize{16}Maximum core thermal power, P_C(MWt)')
ylabel('\fontsize{16}RCP Power, P_P(MW)')
grid on
plot(Q_r*(4*ent_rise*rho_c)*1e-6,c*Q_r*h_r*1e-6,'r*','MarkerSize',10)
legend('\fontsize{16}3.0X RCP','\fontsize{16}2.5X RCP','\fontsize{16}2.0X
RCP','\fontsize{16}1.5X RCP','\fontsize{16}Typical RCP')
text(1.02*Q_r*(4*ent_rise*rho_c)*1e-6,1.02*c*Q_r*h_r*1e-6,'Ref. Operating
point','FontSize', 16)
% plot(Q_s*(4*ent_rise*rho_c)*1e-6,P_s*1e-6,'r.-
','LineWidth',2,'MarkerSize',20)
% axis([3000 7000 1 14])
plotfixer_paper
export_fig('Powercurve','-tif','-nocrop','-transparent','-r150')
hold off
```

Channel analysis codes:

```
function
[deltap,MDNBR,MDNBR_z,LDNBR_z,Tci,Tbulk]=T_channel_study(Q,Dci,Ncells,Tin,en
t_rise,byp_fraction,Hot_channel_fraction,Nnodes,design,tt_z,y)
%Channel analysis code writen by Tyrell Arment (2012)
%Modified by Tat Nghia Nguyen to make it compatible with the Ferroni IPWR
%code

comp.N_nodes=Nnodes;          %number of computational nodes
comp.it_limit=20;           %iteration limit
comp.epsilon=1e-4;          %convergence criteria for iterative processes
%Geometry
geom.L_h=3.6576;                                %heated length [m]
geom.z=linspace(0,geom.L_h,comp.N_nodes);   %z-position vector [m]
geom.D_rod=Dci;                               %pipe diameter [m]
geom.D_h=geom.D_rod;                          %tube diameter [m]
geom.squiggle=1.5e-6;                         %pipe roughness [m]
geom.rough_flag=0;                            %DO NOT USE
                                              %uses rough friction factor = 1
```

```
                                                %, Blasius = 0 for swirl decay
%Operations
Qcore=Q;
power_inc=1.515; %multiplies channel power to find max power for the channel
oper.Q_pin=power_inc*Qcore/Ncells;                %total channel power [W]
oper.Press=15.51e6;                              %operating pressure [Pa]
oper.T_in=Tin-273.16;                               %Inlet temperature [C]
%Inlet enthalpy [J/kg]
oper.h_in=XSteam('h_pT',oper.Press/1e5,oper.T_in)*1000;
oper.delta_h=ent_rise;
oper.m_core = Q/oper.delta_h;
oper.m_dot=oper.m_core*(1-byp_fraction)/Ncells;      %mass flow rate [kg/s]
oper.G=Hot_channel_fraction*oper.m_dot/(pi/4*geom.D_rod^2);      %mass flux
[kg/m^2-s]
oper.P_bar=oper.Press*1e-5;                    %system pressure [bar]
oper.flux_shape=1;
%neutron flux shape, 0 = bottom peaked, 1 = chopped cosine
oper.axialpeak=1.515;        %axial peaking factor for chopped cosine shape
oper.radialpeak=1.515;     %radial peaking factor used only for total power
%Saturated properties
sat.rho_f=XSteam('rhoL_p',oper.P_bar);          %sat liquid density [kg/m^3]
sat.rho_g=XSteam('rhoV_p',oper.P_bar);          %sat vapor density [kg/m^3]
sat.h_f=XSteam('hL_p',oper.P_bar)*1000;         %sat liquid enthalpy [J/kg]
sat.h_g=XSteam('hV_p',oper.P_bar)*1000;         %sat vapor enthalpy [J/kg]
sat.h_fg=sat.h_g-sat.h_f;                       %heat of vaporization [J/kg]
sat.T_sat=XSteam('Tsat_p',oper.P_bar);          %saturation temperature [C]
sat.mu_f=XSteam('my_ph',oper.P_bar,sat.h_f/1000*0.99);
%sat liquid viscosity [N-s/m^2]
sat.mu_g=XSteam('my_ph',oper.P_bar,sat.h_g/1000*1.01);
%sat vapor viscosity [N-s/m^2]
sat.k_f=XSteam('tcL_p',oper.P_bar);%sat liquid thermal conductivity [W/m-K]
sat.cp_f=XSteam('CpL_p',oper.P_bar)*1000;%sat liquid specific heat [J/kg-K]
sat.Pr_f=sat.cp_f*sat.mu_f/sat.k_f;       %sat liquid prandtl number
%Twisted tape info
tape_info.y_TTs=y*ones(1,length(tt_z));                  %twist ratio of
each SLTT
tape_info.N_TTs=length(tape_info.y_TTs);     %number of twisted tapes
tape_info.N_turns=1.5*ones(1,length(tt_z));      %number of 360-deg rotations
for each SLTT
tape_info.FLTT=design;                            %0 = MSLTT; 1 = FLTT; 2 =
empty;3 long twisted-tape
tape_info.z_TTs=tt_z;                    %z-location of each SLTT
tape_info.t_TT=5e-4;                           %twisted tape thickness [m]

%*************************************************************************
%***********************   START COMPUTATIONS   **************************
%*************************************************************************

%initialize
oper.incip_index=comp.N_nodes;  %node of boiling incipience
oper.dep_index=comp.N_nodes;    %node of bubble departure
oper.sat_index=comp.N_nodes;    %first node where x_eq>0

%%%%%%%%%%%%%%%%%%%%%%%%%%%%%%%%%%%%%%%%%%%%%%%%%%%%%%%%%%%%%%%%%%%%%%%%%%%
%Flow properties
[oper]=flow_props(comp,geom,oper,sat);
```

```
%Effective Twist Ratio and form pressure drop due to twisted tapes
[oper]=Decay(oper,geom,comp,tape_info);
%Wall temperature if the entire pipe was in axial flow
[oper]=T_wall(comp,geom,oper,sat,tape_info);
%Pressure drop
[oper]=P_drop(comp,geom,oper,sat);
dP_tot=oper.Press-oper.Pz(comp.N_nodes);
deltap=dP_tot/1000;
%Critical Heat Flux correlation
[CHF,~]=Arment_TTCHF(comp,geom,oper,sat);
DNBR=CHF./oper.q_dp_z;
MDNBR=min(DNBR);
MDNBR_z=geom.z(find(DNBR==MDNBR));
LDNBR_z=geom.z(find(DNBR<=1.85)-1);
if isempty(LDNBR_z)
    LDNBR_z=MDNBR_z;
end
LDNBR_z=LDNBR_z(1);
%Core Sizing and Total Power
N_chan=Ferroni_chan(geom);
Tci=oper.T_wall+273.16;
Tbulk=oper.T_bulk+273.16;
end
```

```
function
[deltap,Tco_max,mchfr,mchfr_z,Tci_maxx,Tco_maxx,Tf_maxx,max_vel,N_TT]=channe
l_study_multiple(Nrev,TT_spacing,Dcin,TT_thickness,Tin,PF_tot,Qcore,ent_rise
,byp_fraction,Ncells,LHGR_avg,LHGR_max,y_mult,mult_TT_start_z,N_nodes,L_extr
,roughn,what_sub_corr,what_multip,...

subc_reg,pcrit,Dcout,what_CHF_free,what_CHF_TT,bundle_flag,Dfuel,Pitch,Hot_c
hannel_fraction,loopindex,Tdesign,Ttt_z,Ty)

%Channel analysis code written by Ferroni(2010)
%Modified by Tat Nghia Nguyen to include the new Arment pressure drop and
%DNB correlations

global roughness Reynolds k_entrance k_exit p grav H_core_heated
H_core_total rhog rhof C_Katto L_over_D rho_ratio kLM kfuel
global Tsat hf hg hfg rhof rhog muf mug kcool_f kcool_g Cpf Cpg sigmaa hin

%%%%%%%%%%%%%%%%%%%%%%%%%%%%%%%%%%%%%%%%%%%%%%%%%%%%%%%%%%%%%%%%%%%%%%%%%%%%
%%%%%%%%%%%%%%%%%%%%%%%%%%%%%%%%%%%%%%%%%%%%%%%%%%%%%%%%%%%%%%%
%
```

```
%                             ELABORATION OF INPUT DATA TO GET INTERMEDIATE
INPUT DATA
%
%%%%%%%%%%%%%%%%%%%%%%%%%%%%%%%%%%%%%%%%%%%%%%%%%%%%%%%%%%%%%%%%%%%%%%%%%%%%
%%%%%%%%%%%%%%%%%%%%%%%%%%%%%%%%%%%%%%%%%%%%%%%%%%%%%%%%
% geometric data calculations
roughness=roughn;
Dcin=Dcin/1000;                                   %conversion of Dci to
meters
Dcout=Dcout/1000;                                 %conversion of Dco to
meters
Pitch=Pitch/1000;
Dfuel=Dfuel/1000;
P_over_Df=Pitch/Dfuel;                            %P over Dfuel to be entered
in the eq.annulus correction factor
Df_eq_an=Pitch*sqrt(2*sqrt(3)/pi);                %eq. annulus external
diameter (m)

TT_thickness=TT_thickness/1000;                   %conversion of TT_thickness
to meters
Aflow_empty=pi*0.25*Dcin^2;                       %empty channel flow area
(m2)
Aflow_TT=Aflow_empty-Dcin*TT_thickness;           %flow area where TTs are
present (m2)
Aratio=Aflow_TT/Aflow_empty;

Prf=Cpf*muf/kcool_f;                            %saturated liquid Prandtl
number

% flow rate calculations
m_core=Qcore/ent_rise;                          %core flow rate (kg/s)
m_channel=m_core*(1-byp_fraction)/Ncells;       %flow rate through hot
channel (kg/s)
G_empty=m_channel*Hot_channel_fraction/Aflow_empty;                   %mass
flux in empty channel (kg/s m2)

% twisted-tape related parameters
y_mult=4.5;
TT_twist_angle=90-(180/pi)*atan(pi/(2*y_mult));     %TT twist angle
(degrees) (angle between the TT edge profile and the horizontal)
TT_180pitch=y_mult*Dcin;                            %TT half pitch (m)
TT_length=Nrev*2*TT_180pitch;                       %length of each TT (m)

N_TT=1;

%axial nodalization of the heated length
z=linspace(0,H_core_total,N_nodes);
TT_length_nod=TT_length/(z(2)-z(1));                %TT length expressed in
number of axial zones
swirl_decay_length_nod=(TT_spacing*Dcin)/(z(2)-z(1));    %swirl decay region
expressed in number of axial zones

%identification of the axial elevations at which the center of each TT is
located
z_TT=[1.9];
```

```
%identification of the axial position index corresponding to the center of
each TT
for w=1:N_TT
    for k=1:N_nodes
        diffe(k)=abs(z_TT(w)-z(k));
    end
    z_index_TT(w)=find(diffe==min(diffe));          %index corresponding to
the axial position of the centre of each TT
end

%assignment of the right values to the "TT_yes_or_no_phys" array
TT_yes_or_no_phys=zeros(1,N_nodes);                 %initialization of a
vector containing N_nodes positions coinciding with the axial nodalization.
1 means that TT is present, 0 that it is not
for w=1:N_TT
    for k=round(z_index_TT(w)-
0.5*TT_length_nod):(z_index_TT(w)+0.5*TT_length_nod)
        TT_yes_or_no_phys(k)=1;
    end
end

[deltap,MDNBR,MDNBR_z,LDNBR_z,Tci,Tbulk]=T_channel_study(Qcore,Dcin,Ncells,T
in,ent_rise,byp_fraction,Hot_channel_fraction,N_nodes,Tdesign,Ttt_z,Ty);
% % display('Done step 1')
% % LDNBR_z
%
[deltap,MDNBR,MDNBR_z,LDNBR_z,Tci,Tbulk]=T_channel_study(Qcore,Dcin,Ncells,T
in,byp_fraction,Hot_channel_fraction,N_nodes,loopindex,3,2.07);
% %0 = MSLTT; 1 = FLTT; 2 = empty

LHGR=zeros(1,N_nodes);
heat_flux=zeros(1,N_nodes);
rhom=zeros(1,N_nodes);
for k=1:N_nodes
    if (z(k)<0.5*(H_core_total-H_core_heated) || z(k)>(H_core_total-
0.5*(H_core_total-H_core_heated)));
        LHGR(k)=0;
        power_z(k)=0;
    else
        [LHGR(k),
power_z(k)]=Ax_profile(LHGR_max,H_core_heated,L_extr,z(k));        %LHGR at
elevation z(k) (W/m) and power produced up to that elevation (W)
    end
    heat_flux(k)=LHGR(k)/(pi*Dcin);
%heat flux at tube inner wall (W/m2)
    rhom(k)=Densityl_15MPa(Tbulk(k));
end
%%%%%%%%%%%%%%%%%%%%%%%%%%%%%%%%%%%%%%%%%%%%%%%%%%%%%%%%%%%%%%%%%%%%%%%%%%%%
%%%%%%%%%%%%%%%%%%%%%%%%%%%%%%%%%%%%%%%%%%%%%%%%%%%%%%%%%%%%%%%%%%%%%%%%%%%%
%%%%%

%CALCULATION OF TEMPERATURE OF: CLADDING OUTSIDE SURFACE, FUEL INSIDE
SURFACE AND HOT SPOT IN THE FUEL
for k=1:N_nodes
```

```
    deltaT_corr(k)=(LHGR(k)/18300)*(7.04525*P_over_Df^4-
61.7191*P_over_Df^3+199.264*P_over_Df^2-282.679*P_over_Df+155.226);
    err_Tc_ave=10;                                  %initial value for the error
in average clad T calculation
    correction=20;

    while abs(err_Tc_ave)>2
        Tc_ave_tent=Tci(k)+correction;              %tentative value for
clad average temperature at axial elevation "k"
        [kclad, Cpclad]=ZrNb_prop(Tc_ave_tent);   %cladding thermal
conductivity (W/m K) and specific heat (J/kg K)
        Tco_tent=Tci(k)+(LHGR(k)/(2*pi*kclad))*log(Dcout/Dcin);
        Tc_ave=0.5*(Tci(k)+Tco_tent);
        err_Tc_ave=Tc_ave-Tc_ave_tent;
        if err_Tc_ave<0
            correction=correction-1;
        else
            correction=correction+1;
        end
    end
    Tco(k)=Tco_tent;
    Tfi(k)=Tco(k)+LHGR(k)*(Dfuel-Dcout)/(pi*kLM*(Dfuel+Dcout));
    Tf_hot(k)=Tfi(k)+(LHGR(k)/(2*pi*kfuel*0.25*(Df_eq_an^2-
Dfuel^2)))*(0.25*Df_eq_an^2*log(Df_eq_an/Dfuel)-(1/8)*(Df_eq_an^2-
Dfuel^2))+deltaT_corr(k);
    velocity(k)=G_empty/rhom(k);
end

Tci_max=max(Tci);
Tco_max=max(Tco);
Tf_max=max(Tf_hot);
Tci_maxx=Tci_max-273.16;
Tco_maxx=Tco_max-273.16;
Tf_maxx=Tf_max-273.16;

max_vel=max(velocity);
mchfr_z=MDNBR_z;                                    %location of MCHFR (m)
mchfr=MDNBR;                                      %MCHFR
end
```

The full IPWR code (#3) is too lengthy to be listed here. Readers who are interested should contact Rachel Morton, *Manager, Computer Facilities,* RM 24-106, Department of Nuclear Science & Engineering, MIT.

Bibliography

[1] P. Ferroni. *An Inverted Hydride-fueled Pressurized Water Reactor Concept.* PhD thesis, Department of Nuclear Science & Engineering, Massachusetts Institute of Technology, 2010.

[2] USNRC Technical Training Center. *Pressurized Water Reactor (PWR) Systems*, 06 2003.

[3] N. E. Todreas and P. Ferroni. Enhancing reactor core thermal performance through Inverted Fuel Design. In *The 13th International Topical Meeting on Nuclear Reactor Thermal Hydraulics*, 2009.

[4] *Seabrook Station Updated Final Safety Analysis Report*, revision 11 edition, 2008.

[5] P. R. Rubiolo, L. E. Conway, L. Oriani, et al. Advanced Power Ultra-Uprates of Existing Plants. Technical report, U. S. Department of Energy, 2006.

[6] J.A. Malen, N.E. Todreas, P. Hejzlar, P. Ferroni, and A. Bergles. Thermal hydraulic design of a hydride-fueled inverted PWR core. *Nuclear Engineering and Design*, 239:1471–1480, 2009.

[7] T. W. Arment. Departure from Nucleate Boiling and Pressure Drop Prediction for Tubes Containing Multiple Short-Length Twisted-Tape Swirl Promoters. Master's thesis, Department of Nuclear Science & Engineering, Massachusetts Institute of Technology, 2012.

[8] J.M. Cuta, A.S. Koontz, C.W. Stewart, S.D. Montgomery, and K.K. Nomura. *VIPRE-01: A Thermal Hydraulic Code for Reactor Cores. Volume 2: User's Manual*, revision 2 edition, 1985.

[9] L.K.H. Leung, D.C. Groeneveld, A. Teyssedou, and F. Aubé. Pressure drops for steam and water flow in heated tubes. *Nuclear Engineering and Design*, 235:53–65, 2005.

[10] D. G. Reddy and Sreepada S. R. Two-phase friction factor multiplier correlation for high-pressure steam-water flow. Research Project 813 NP-2522, Columbia University for Electric Power Research Institute, 1982.

[11] S.W. Churchill. Empirical expressions for the shear stress in turbulent flow in commercial pipe. *AIChE Journal*, 19, No. 2:375–376, 1973.

[12] R.M. Manglik and A.E. Bergles. Heat transfer and pressure drop correlations for twisted-tape inserts in isothermal tubes: Part II - Transition and turbulent flows. *Transactions of the ASME*, 115:890–896, 1993.

[13] N. E. Todreas and M. S. Kazimi. *Nuclear Systems Volume I: Thermal Hydraulic Fundamentals*, volume 1. CRC Press Taylor & Francis Group, 2nd edition, 2012.

[14] W.R. Gambill, R.D. Bundy, and R.W. Wansbrough. Heat transfer, burnout, and pressure drop for water in swirl flow through tubes with internal twisted tapes. *Chemical Engineering Progress, Symposium Series*, 57:127–137, 1961.

[15] F.T. Kanizawa, R.S. Hernandes, A.A.U. Moraes, and G. Ribatski. A new correlation for single and two-phase flow pressure drop in round tubes with twisted-tape inserts. *Brazillian Society of Mechanical Science and Engineering*, 33:243–250, 2011.

[16] H.Y. Wu, H.E. Cheng, R.J. Shuai, and Q.T Zhou. An analytical model for decaying swirl flow and heat transfer inside a tube. *ASME Journal of Heat Transfer*, 122:204–208, 2000.

[17] D. C. Groeneveld, J. Q. Shan, Vasic A. Z, et al. The 2006 CHF look-up table. *Nuclear Engineering and Design*, 237:1909–1922, 2007.

[18] M.K. Jensen. A correlation for predicting the critical heat flux condition with twisted-tape generators. *International Journal of Heat and Mass Transfer*, 27:2171–2173, 1984.

[19] Y. Katto. Critical heat flux of forced convection boiling in uniformly heated vertical tubes (correlation for CHF in HP-regime and determination of CHF-regime map). *International Journal of Heat and Mass Transfer*, 23:1573–1580, 1980.

[20] F. Kreith and O.K. Sonju. The decay of a turbulent swirl in a pipe. *Journal of Fluid Mechanics*, 22:257–271, 1965.

[21] A.H. Algifri, R.K. Bhardwaj, and Y.V.N. Rao. Prediction of the decay process in turbulent swirl flow. *Proc. Insts. Mech. Engineers*, 201:279–283, 1987.

[22] *AP1000 Design Control Document*, 15th edition, 2007.

[23] C. Shuffler, J. Trant, J. Malen, and N. E. Todreas. Thermal hydraulic analysis for grid supported pressurized water reactor cores. *Nuclear Engineering and Design*, 239:1442–1460, 2009.